From Single-Crystals to High-Throughput: Concepts for Rational Perovskite Photovoltaics Research

THÈSE N^{O} 8686 (2018)

PRÉSENTÉE LE 20 JUILLET 2018

À LA FACULTÉ DES SCIENCES DE BASE
LABORATOIRE DES SCIENCES PHOTOMOLÉCULAIRES
PROGRAMME DOCTORAL EN CHIMIE ET GÉNIE CHIMIQUE

ÉCOLE POLYTECHNIQUE FÉDÉRALE DE LAUSANNE

POUR L'OBTENTION DU GRADE DE DOCTEUR ÈS SCIENCES

PAR

Jeannette Medina KADRO

acceptée sur proposition du jury:

Prof. G. Laurenczy, président du jury
Prof. U. A. Hagfeldt, directeur de thèse
Dr T. Baikie, rapporteur
Prof. R. Andriessen, rapporteur
Dr E. Horvath, rapporteur

ÉCOLE POLYTECHNIQUE
FÉDÉRALE DE LAUSANNE
Suisse
2018

Résumé

L'efficacité de la conversion lumineuse en électricité des cellules solaires au perovskites a subi une augmentation spectaculaire. Depuis les premiers travaux de recherche en 2009, des milliers de publications scientifiques ont été publiées, traitant de leurs propriétés opto-électroniques spectaculaires, des différentes architectures de cellules solaires possibles, de l'optimisation de leur composition et de leurs possibles applications.

Au cours de ce travail, j'ai décidé de traiter plusieurs domaines d'intérêt, en me concentrant sur certains aspects de recherche appliquée.

Le premier chapitre décrit un nouveau processus rapide et efficace de produire des mono-cristaux de pérovskite, utilisant un minimum d'équipement. Ce procédé à base de solution permet la fabrication de larges cristaux en quelques minutes, en chauffant une solution de précurseurs à certaines températures. Simple et efficace, il m'a permit de préparer une large quantité de pérovskite stoechiométrique, utilisé comme précurseur dans la déposition de couches minces de pérovskites par évaporation thermique. La rapide sublimation des cristaux de perovskites permet de déposer des couches minces à stoechiométrie précise, sans devoir recourir à une approche à deux sources thermiques, largement moins reproductible.

Un autre projet traité dans cette thèse est le développement de méthodes de recherche à haut-débit, permettant le dépistage rapide de nouvelles compositions prometteuses. Des librairies combinatoires ont été préparées par évaporation thermique au cours de mes travaux de recherche. Similairement, des processus d'impression de pérovskites en solution par effet piézo ainsi que des résultats préliminaires sont présentés dans le dernier chapitre.

Une large partie de cette thèse traite de la fin de vie et du recyclage des modules solaires au perovskites. Un processus sélectif, rapide et efficace a été développé pour désassembler la cellule solaire en ces différents composants, permettant de les réutiliser et ainsi de réduire les coûts de fabrication ainsi que l'empreinte carbone des cellules aux pérovskites. S'en suit une discussion détaillée des défis technologiques, environnementaux et régulatoires de la fin de vie de tels panneaux photovoltaïques.

Zusammenfassung

Die Wirkungsgrade von Perowskitsolarzellen sind in den letzten Jahren stark angestiegen. Vermultlich ist die Verbesserung der Effizienzen der schnellste je dagewesene Anstieg im gesamten Forschungsgebiet der Photovoltaik. Seit sie 2009 zum ersten mal in einer wissenschaftlichen Veröffentlichung erwähnt wurden, sind tausende Artikel zu ihren einmaligen Eigenschaften erschienen. Vermultich existieren heute hunderte verschiedene Solarzellenvariationen in hunderten Laboren weltweit.

In dieser Arbeit versuche ich, mehrene verschiedene praktische Aspekte der Perowskitsolarzellenforschung zu untersuchen.

Im ersten Kapitel wird ein neuartiges Verfahren zur einfachen und schnellen Synthese von Einkristallen beschrieben. Dieses Verfahren erlaubt es, mit minimalem Materialeinsatz, grosse Mengen hochwertiger Einkristalle verschiedener Zusammensetzungen innerhalb weniger Minuten heruzstellen. Dies erlaubte es mir, Einkristalle als Sublimationsmaterial in einem weiteren neuartigen Vakuumaufdampfverfahren zu verwenden.

Thermal Flash Vacuum Deposition genannt, vereinfacht diese Abwandlung traditioneller Vakuumbeschichtungsprozesse die Optimierung und praktische Umsetzung der normalerweise komplizierten Prozesskontrolle bei der Aufbringung ultradünner Perowskitschichten. Die Vakuumaufdampfung wurde eingesetzt, um erstmals kombinatorische Probenmatrizen für sog. High Throughput Verfahren zur Materialanalyse herzustellen.

Zwei weitere Kapitel widmen sich der Entsorgung und dem Recyclen zukünftiger Perowskitsolarmodule. Wichtige Aspekte zur Wertstoffrückgewinnung werden diskutiert.

Abstract

Perovskite solar cells have undergone increase in power-conversion efficiencies at an unprecedented pace. Since their emergence in academic research in 2009, thousands of scientific papers have been published on their unique properties, variations cell architectures, material composition optimization and potential applications.
In the course of this work, I attempted to cover multiple topics and focussed on applied research aspects.
The first chapter describes a novel, rapid process for the growth of hybrid perovskite single crystals. Using minimal equipment and growth times, the solution-based process allows the fabrication of freestanding single crystals within minutes by heating stoichiometric precursor solutions. This efficient, simple process allowed me to produce single crystals in large amounts which, in turn, enabled me to develop a vacuum deposition technique for the preparation of perovskite thin films. Using rapid thermal flash vacuum deposition, thin films could be prepared with short deposition times and minimal manual sample preparation. The use of single crystals as sublimation precursors ensured stoichiometry of the deposit without the need for the challenging, precise control of multiple thermal sources.
Another project covered in this thesis aimed to develop methods for high-throughput perovskite material screening or high-throughput research. Combinatorial libraries for the screening of perovskite compositions for optoelectronic applications were prepared by the vacuum deposition process also developed in the course of my PhD. Inkjet printing was also identified as suitable process and preliminary results are included in the last chapter of the thesis.
The end-of-life and recycling of perovskite solar cells are covered in two chapters. A simple, highly selective dismantling process using orthogonal solvents is developed to reverse-engineer full solar cell devices and successful re-use of important device components is demonstrated. A detailed discussion of technological, environmental and regulatory challenges for the end-of-life management of perovskite solar panels is included as chapter three.

Keywords: photovoltaics, perovskite solar cells, single crystals, PV end-of-life, vacuum deposition, inkjet printing, high-throughput research, recycling, EU directives, device libraries

Acknowledgement

I owe a debt of gratitude to many colleagues, friends, strangers, funding agencies and family.

In no particular order I would like to thank-

Prof. ***Anders Hagfeldt****, for convincing me to move to Switzerland and do a PhD at EPFL. Particularly for not attempting to micro-manage, allowing an amazing degree of freedom, never asking too many questions and for letting me travel so much!*

*Prof. Maria Elisabeth "****Maibi****" Michel-Beyerle, for simply being an inspiration, in science and life. I wouldn't be pursuing a PhD if it hadn't been for her support, patience and late-night discussions.* ***Heidi Francelet****- for being simply the single best most powerful person at LSPM. Without you, we'd all be lost and bankrupt. Thanks a lot for all the chats, jokes and also for watering my flowers occasionally. Prof.* ***Michael Grätzel*** *for always having an open door (when in the country).* ***Hannah Gardner*** *for hosting me in Singapore several times during research visits and conferences and for always having an ear for me.* ***Hui-Seon Kim****,* ***Yasemin Saygili****,* ***Jiyoun Seo****,* ***Natalie Flores*** *and* ***Jessica Flach*** *for being amazing colleagues. Without all the dinners, coffees, hikes, runs, lunches and all the support in the lab this PhD would really have been no fun at all. Thanks girls!* ***Prof. Arie Zaban*** *for having me as a guest in his amazing laboratory at Bar Ilan University. It was inspiring, motivating and eye-opening in many ways****.*** ***Prof. Aram Amassian*** *for inviting me to his lab in KAUST. Visiting this very special place has changed my view on many things and the research facilities were breath-taking.* ***All my other collaborators in Saudi Arabia, Israel, Singapore, Japan, Germany, Sweden and EPFL****. There are too many to list here but I appreciate having met all of them.* ***Kurt Schenk*** *for all his help with anything related to X-rays and for never giving up on trying to teach me crystallography. It must have taken so much patience!*

Norman*, for always being there.*

About this Thesis

This thesis is made up of five main chapters, three of which are adaptations of published articles. A brief section on the background of this work summarizes the most important developments in the field, followed by separate sections explaining the motivation and background of the individual chapters. The main chapters are arranged chronologically, starting with the oldest work and finishing with chapter six which shows results from an ongoing project that will be taken over by a new PhD student. Chapters one to three have been adapted from the original manuscripts in language, presentation of figures, format, and content. Where applicable, unpublished data have been included or figures from the original supporting information have been added into the main text to improve readability. The annex contains data obtained from single-crystal XRD, X-ray fluorescence, details of the jet-setup for inkjet printing, and other information that may be interesting to anyone attempting to reproduce measurements or experiments. Experimental methods are presented in separate sections included in respective chapters with only relevant and unique processes are described in detail. Unless otherwise indicated, experiments and measurements have been performed by myself at various facilities at the EPFL. Permissions to reproduce figures have been obtained where required.

Abbreviations

ACN	Acetonitrile
CB	Chlorobenzene
CL	Cathodoluminescence
DLS	Dynamic light scattering
DOD	Drop-on-demand
EoL	End-of-Life
EtOH	Ethanol
FALB/FALI	Formamidinium lead bromide/iodide
FTO	Fluorine-doped tin oxide
HTR	High-throughput research
IJP	Inkjet printing
IPA	2-propanol
ITO	Indium-doped tin oxide
jV	Current-voltage
LCA	Life-cycle assessment
MABr	CH_3NH_3Br
MAI	CH_3NH_3I
MALB	Methyl ammonium lead bromide, $CH_3NH_3PbBr_3$
MALI	Methyl ammonium lead iodide, $CH_3NH_3PbI_3$
MAX	CH_3NH_3X, x=Br, Cl, I
MeOH	Methanol
Mono-Si	Monocrystalline silicon
MPP	Maximum power point
PCE	Power conversion efficiency
PhCl	Chloroform
PL	Photoluminescence
PSC	Perovskite solar cell
PVD	Physical vapour deposition
RoHS	Restriction of hazardous substances
TFVD	Thermal Flash Vapour Deposition
WEEE	Waste electronic and electric equipment
XRD	X-ray diffraction
XRF	X-ray fluorescence

Content

Figures

1 Introduction

1.1 Background

The world's population has never grown faster and never consumed more energy. For more than a century, coal, oil, natural gas, and other variations of fossil fuels have allowed extremely rapid technological development in many parts of the world. The industrial revolution has changed the way billions of people live more than any other disruptive event in modern human history by re-shaping societies to promote urbanization and allow more people than ever to gain access to education, healthcare, and mobility.. While manufacturing technology evolved rapidly, the sources that have powered the planet's factories and cities since the emergence of the steam engine have not. While the inherent finite nature of fossil fuels has been of concern since the oil price shock of the 19XXs, consequences of their excessive use has now come to pose one of humankind's largest challenges to be addressed. Leaving aside impact on the climate, the excessive use of coal in particular has led to more immediate, unprecedented environmental impacts in particularly rapidly developing countries such as China and India. Consequences of climate change are already impacting life of populations and governments are seeking (?) solutions to limit further increase in emissions of greenhouse gases and mitigate already irreversible effects.

Many governments have implemented or are in the process of developing national strategies to reduce their greenhouse gas emissions following international agreements including the original Kyoto Protocol and its successors as well as the recent Paris Climate Agreement. Gradual transition from traditional energy sources towards renewable energy sources are key to achieving set goals. Recently, Germany, as Europe's largest producer of industrial goods, has implemented a national strategy for its renewable energy transition ("Energiewende").

Deployment of photovoltaic (PV) installations has been growing at unprecedented rates since the beginning of the century. In 2017, global installed PV capacity exceeds 330GW. By 2050, the global

installed capacity is expected to exceed 20TW. Photovoltaic installations require minimal maintenance and can be rapidly deployed.

In addition to allowing industrialized countries to gain independence from fossil fuel imports and reduce CO_2 emissions, PV panels can be installed in remote locations to allow populations without access to a centralized grid to use electrical appliances.

1.2 Perovskite Solar Cells

Organic-inorganic perovskite materials have attracted a lot of attention over the past years for use in photovoltaic and other optoelectronic devices owing to their unique properties. Research in this class of materials goes back far into the 20th century[1,2], and academics as well as large industrial corporations, including technology leaders such as IBM[3–6], have been intrigued by their unique properties and simple preparation. Still, it was not until 2009 that a member of this class of materials was used for solar energy harvesting[7]. The first functioning PV device reported incorporated the perovskite $CH_3NH_3PbI_3$ as the absorber material, replacing the dye in a classical dye-sensitized solar cell configuration. Although the device architecture in Kojima et al.'s work was far from optimum due to rapid dissolution of the perovskite material by the liquid electrolyte and low power conversion efficiency , it led to further research into the matter[8]. Elimination of the liquid electrolyte in a solid-state architecture allowed power conversion efficiencies to increase dramatically and perovskite solar cells to rapidly become a subject of intense research and debate[9–13] Many excellent reviews have been published detailing milestone developments in the field as well as highlighting potential and shortcomings of the materials involved and are available to the interested reader[14–21]. Today, certified lab-scale power-conversion efficiencies of perovskite solar cells (PSCs) reportedly exceed 20%[22] and first attempts at industrialization of the technology are being undertaken[23].

While the extremely rapid evolution of PSC technology is undeniably unprecedented in photovoltaics, the chemical composition of the most efficient absorber materials of this class to date has also been the subject of scepticism. Aside from their inherent sensitivity to moisture, the most efficient materials today contain lead. Attempts to eliminate the heavy metal have been undertaken but lead-free alternatives do not yet pose real alternatives in terms of either processability or photovoltaic properties[24–26]. This fact, coupled with the solubility of the employed $CH_3NH_3X_x$- absorbers has led to intense debates about the safety and sustainability of potential large-scale PSC installations and their production. Important

potential markets including the European Union, the United States, China and Japan have all passed legislations restricting the use and disposal of heavy metals. [27] A detailed discussion on regulatory limitations can be found in chapter four.

1.3 Aim and Scope of this Thesis

The aim of the projects leading to this thesis is to

- establish scalable processes that can lead to rational approach to perovskite exploration
- find simple ways to produce necessary precursors
- introduce processes for combinatorial, high throughput research
- reduce the human factor in device preparation
- assess end of life, which is necessary for sustainable technology to be compatible with EU directives

PSC research today mostly relies on manual labour to produce thin films for optical characterization, solar cell devices, and other samples. This approach has undoubtedly led to impressive developments and advances in the field but also requires large amounts of man-hours. The reliance on manual tasks further complicates knowledge or skill transfer within a research institution or between research partners. Several parameters such as the angle between a pipette and a substrate, the speed at which a liquid is expelled from a syringe, or the force used to press two items together can hardly be quantified by the experimentalist, making reproducibility challenging to achieve.

Leaving aside issues related to reproducibility, the time spent on acquiring the necessary skill set for producing efficient PSC devices reproducibly does not contribute to the generation of new information and knowledge. In the typical academic perovskite PV research group, highly educated personnel frequently spend large amounts of time optimizing processes to cover a large parameter space. The aim of the work presented in this thesis was to find new approaches to PSC research that decrease the human factor in sample preparation as much as possible and allow for high degrees of automation. Two approaches to the fabrication of compositional libraries for materials screening are introduced; one

solution based and one vapour deposition process. A rapid, simple route to the fabrication of single crystals of $CH_3NH_3PbX_3$ for use in fundamental characterization and as precursor for vacuum deposition is developed.

Considering the practical aspects of PSC research in industry and academia, one frequently overlooked aspect is the end-of-life of the potential technology and the associated challenges. While awareness of the finite nature of fossil fuels is a main driver for the development and deployment of PV technology, the raw materials involved in the manufacturing of PV panels are also of finite nature. PSC panels based on today's most efficient formulations contain valuable components whose availability potentially limits the rapid expansion of the technology. End-of-life management of waste electronic and electrical equipment falls under regulations in important markets such as the EU, and assessment of challenges ahead is the topic of two chapters in this thesis.

The following sections detail motivation and scope of the individual chapters.

1.3.1 Chapter 1

Single crystals represent the most-ordered, best-defined form of a crystalline material. They find applications in commercial devices such as mono-crystalline silicon solar cells, as well as in fundamental academic research. Many advanced fundamental characterization techniques, such as synchrotron or neutron diffraction measurements, rely on high-quality single crystals to deliver the best results.

For research into optoelectronic devices and materials, such as the hybrid perovskites considered promising for PV applications, the use of single crystals in some measurements theoretically allows for a better de-coupling of sample morphology and measured signal. In PSC research, a frequently discussed topic is the role of grain boundaries of the crystalline perovskite layer on recombination, emission, electron and/or exciton lifetimes, diffusion lengths, and other key material or device parameters[28–31]. Performing measurements of lifetimes, diffusion lengths, emission yield, etc. on single crystals would finally allow assessment of the characteristics of the bulk material without having to take grain boundary effects into consideration. Aside from this, a reduction in the number of interfaces that have to be considered should simplify interpretation.

Growing single crystals is in many cases a time-consuming task. While processes as diverse as solvent evaporation, vapour-induced crystallization, the Czochralski process, use of Bridgeman furnaces, a most common method for soluble materials is based on simply achieving supersaturation by cooling of a concentrated solution. This classic method relying on the positive temperature coefficient of the target material's solubility has been described for hybrid perovskites and leads to the growth of freestanding single crystals. [1,32]

The first chapter of this thesis describes a novel, very simple process that allows for the growth of large, freestanding crystals of $CH_3NH_3PbX_3$ and variations thereof. Previously unreported, the particularity of this process lies in that a highly concentrated, stoichiometric solution of PbX_2 and MAX is heated rather than cooled to achieve crystal growth. The mechanism behind this uncommon phenomenon described here has become the subject of discussion of numerous publications by other research groups but has not yet been fully understood.[33]

The process developed can deliver high yields of crystalline material in very short growth times. These high material yields and minimal requirements for equipment and experimental preparation made it feasible to use single crystals as precursors to another novel preparation method described in detail in chapter four. The crystals were used as precursors in vacuum deposition of thin films and combinatorial libraries. Their small surface-to-volume ratio made them easy to handle, dose, and also ensured a comparatively long shelf-life of up to two years. Inherent stoichiometry eliminated several weighing steps and ensured proper ratios even during complex handling in a large glovebox environment where electrostatic forces can make dosing challenging. A further advantage of having a precursor that is not a fine powder is that potential losses, induced during pumping of the vacuum chamber, do not influence the stoichiometry of the material left in evaporation crucibles. Without a simple, reproducible process for the fabrication of the required crystalline precursor, the work presented in this thesis on combinatorial, high-throughput research methods would not have been possible.

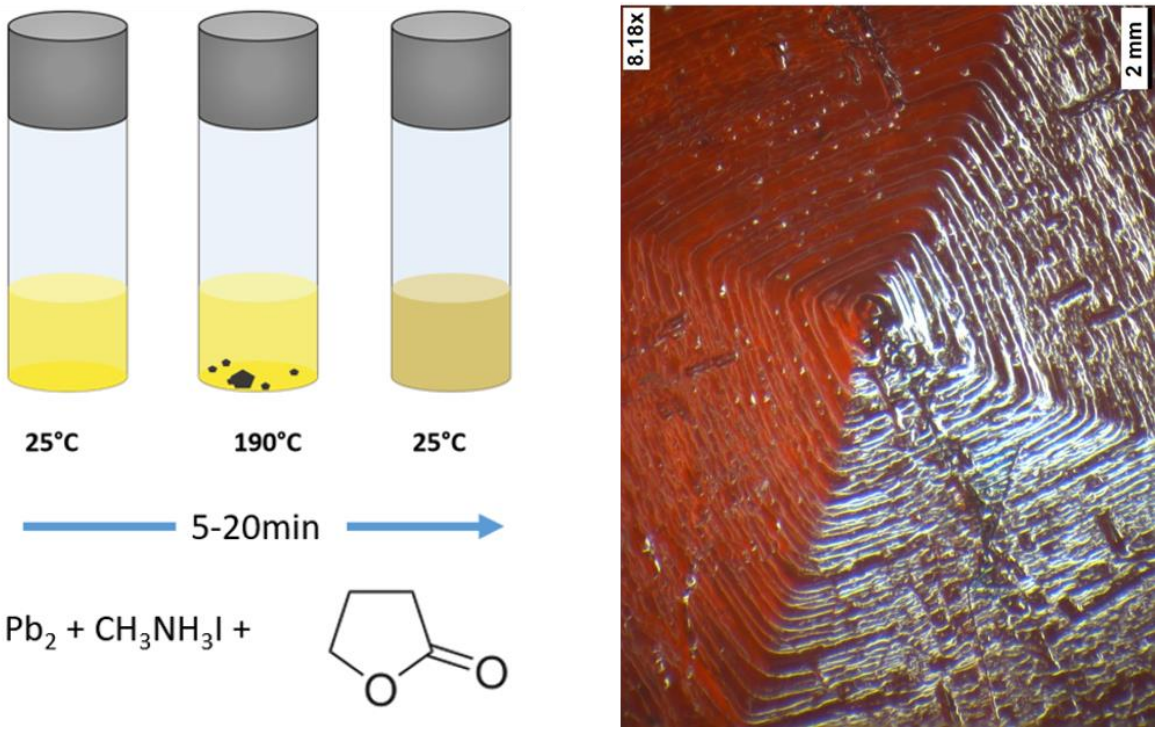

Figure 1 schematic of single crystal growth process and optical microscopy image of surface of $CH_3NH_3PbBr_{3-x}I_x$ crystal

1.3.2 Chapter 2

The work summarized in this chapter describes a wet-chemical process for the partial recycling of PSC devices that allows direct re-use of the most valuable components. While the commercialization attempts at PSC are still in an embryonic state, life-cycle analyses have been carried out on hypothetically industrially produced panels as well as on lab-scale fabrication processes. Results and conclusions of published analyses vary, but overall available studies conclude that the fluorine-doped tin oxide (FTO) coated glass substrate with its TiO_2 coating contributes significantly to most investigated impact categories. The mass of a PSC device today is heavily dominated by the substrate with active layers making up less than 1% of the device mass and volume. FTO is also likely to dominate the material cost of a PSC. TiO_2 sintering adds to the necessary process energy. Re-use of these valuable components could potentially decrease the energy-payback time (EPBT), reduce the environmental impact of PSC production, and save valuable resources such as tin and flat glass. A process that allows recovery of the substrate/superstrate is likely particularly desirable for patterned substrates.

The work presented in this chapter describes a simple, highly selective wet-chemical process allowing for the recovery of the TiO_2 coated FTO substrates. Possibilities for recovery of other components are also discussed.

1.3.3 Chapter 3

This chapter is based on a review article and discusses regulatory, technological, economic and ecological implications for the end-of-life (EoL) of PSC devices. While the growth in installed PV capacity worldwide is generally regarded as a positive development on the way to a more sustainable world economy, the lifespans of PV panels are not endless. Eventually, the 222GW capacity installed to date will have to be taken down at the end of their life cycle. While the most important portion of installed capacity is expected to operate for at least another 20 years, solutions to deal with waste PV panels should be developed before the issue becomes pressing. Figure 2 shows predictions by the International Renewable Energy Agency (IRENA) for installed capacity and end-of-life PV panels from 2020-2050.

The predictions highlight that EoL PV panels are likely to represent a significant portion of waste electric and electronic equipment (WEEE) by the middle of the century. Today global cumulative PV waste only represents a tiny fraction of approximately 0.1% of all WEEE, but owing to increased deployed capacity predicted it is expected to exceed 10% in 2050.

.

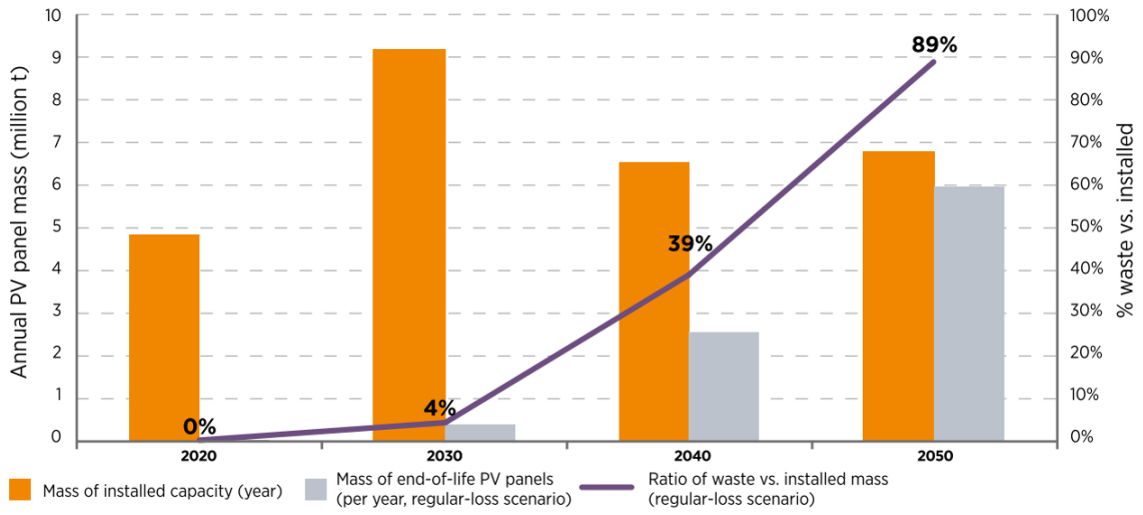

Figure 2predictions for annually installed and end-of-life PV panels 2020-2050 (IRENA)[34]

Managing a large amount of waste panels undoubtedly represents a challenge for all institutions involved, including manufacturers, municipal waste management institutions, and legislators. The EU has passed PV-specific waste regulations which will be discussed in more detail in this chapter. Aside from challenges associated to potential hazardous components contained in PSC devices, the chapter focuses on possibilities for value recovery and decreased resource depletion through re-use of panel components basic regulatory aspects.

> "[…] this directive should not prevent the development of renewable energy technologies that have no negative impact on health and the environment and that are sustainable and economically viable. Exemptions from the substitution requirement should be permitted if substitution is not possible from the scientific and technical point of view, taking specific account of the situation of SMEs or if the negative environmental, health and consumer safety impacts caused by substitution are likely to outweigh the environmental, health and consumer safety benefits of the substitution or the reliability of substitutes is not ensured […]".
>
> -Excerpt from Directive 2011/65/EU

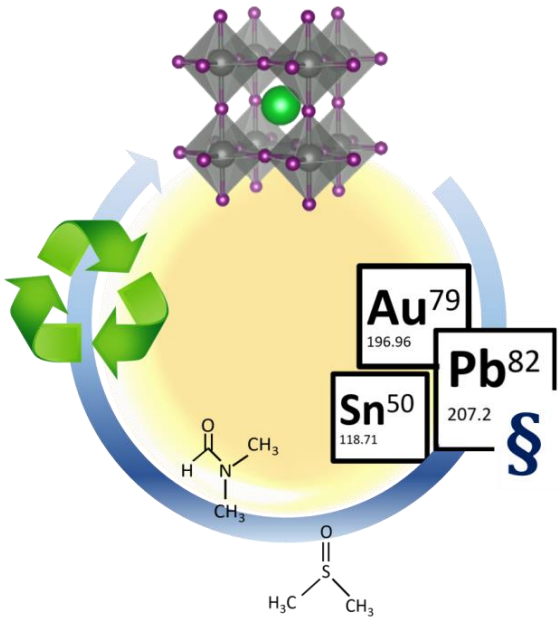

Figure 3 graphical abstract of review paper this chapter is based on (Joule1,129-46, September 2017)

1.3.4 Chapter 4

This chapter introduces two new concepts for a more rational approach to PSC research. First, a new, rapid, and simple vacuum deposition process for the fabrication of perovskite thin films is introduced. The new deposition process eliminates practical issues frequently encountered in vapour deposition of this hybrid material arising from starkly differing sublimation temperatures of MAX and PbX_2. Typically, the two powder precursors are sublimed in separate crucibles and left to form the perovskite phase on a substrate. Precise control over the two sublimation rates is crucial in order to achieve defined ratios of the two. Particularly the control of deposition rates of MAX can be highly challenging due to its low sublimation point and the often poor linearity of source control in low temperature regimes. The process developed during the course of this thesis relies on perovskite single crystals as precursor materials for the vacuum deposition, therefore eliminating the need for separate temperature control, precise weighing, and problematic behaviour of MAX powders in the deposition chambers. Deposition on organic flexible substrates is also possible by using a cold-wall reactor.

Most importantly, this single-source process allowed for the preparation of compositional perovskite libraries for high-throughput research for the first time. By using two different single halide perovskite precursors in two separate crucibles, large samples with compositional gradients could be produced. The vacuum deposition method introduced here allows for a high degree of automation and requires minimal human-machine interactions, hence de-coupling the outcome of performed experiments from the manual skills of the experimentalist to a maximum. Such an approach should lead to better reproducibility within a research group and also between institutions as it greatly facilitates knowledge transfer.

Combinatorial (material) research originally has found its main applications so far in the pharmaceutical industry and in high-throughput screening of catalysts, but has also been successfully used to screen oxides for photovoltaic applications[35–39]. By using high-throughput (HTR) combinatorial methods, very large numbers of compositions can be evaluated in short periods of time, particularly when coupled with appropriate characterization methods. While optimum parameters may still have to be found in more manual experiments, combinatorial HTR methods will allow significant narrowing down of an available parameter space and will ideally save large amounts of man-hours, resources and, funding while still delivering high-quality data. The large numbers of individual experiments that can be performed on a

single library also decreases the likelihood of false positive results and decreases the effect of systematic errors.

Halide perovskites lend themselves to combinatorial materials science not only due to the broad interest they have received in solar and LED research since 2012, but also due to the simplicity of tuning their properties. The fact that one of the most important parameters for optoelectronic materials, the bandgap, can be tuned by systematically varying the halide and/or cation of the material makes hybrid perovskites well-suited for studies that explore this parameter space[40–42]. In addition, the materials are relatively simple to prepare and changes in halide composition and/or cation do not greatly influence other processing parameters (annealing temperature, solvent compatibility etc.)

This chapter introduces a simple method for the fabrication of PSC combinatorial libraries and presents some preliminary solar cell characterization based on the presented methods. The project was in collaboration with Prof. Arie Zaban's group at Bar Ilan University, Israel. They measured jV characteristics of the libraries fabricated at EPFL and allowed me to visit their facilities to get more insight into the practicalities of library-based PV research.

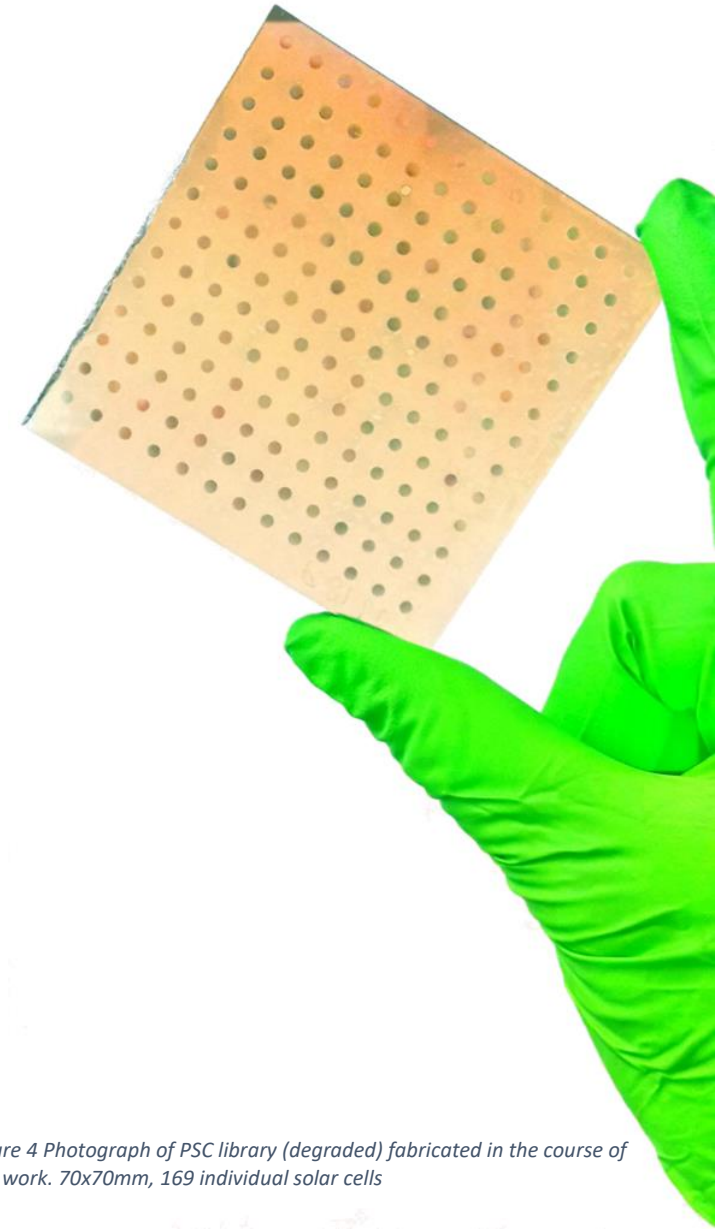

Figure 4 Photograph of PSC library (degraded) fabricated in the course of this work. 70x70mm, 169 individual solar cells

1.3.5 Chapter 5

This last chapter discusses inkjet printing as another scalable, industry-compatible fabrication process for perovskite thin films. Inkjet printing is widely used industrially for a large range of applications and has also been introduced for printing perovskite layers in academic research. The goal of this project is to ultimately use inkjet printing to fabricate compositional libraries analogous to those discussed in chapter four. As solution processing is frequently considered a strength of hybrid perovskite materials, this project aims to develop and optimize a process that can be used in high-throughput research to investigate solvent effects as well. Challenges in perovskite inkjet printing are discussed and preliminary results presented. This chapter does not represent a completed project and its main aim is to aid future group members in setting up inkjet printing experiments.

2 Facile route to freestanding $CH_3NH_3PbI_3$ crystals using inverse solubility

This chapter is an adaptation of the article "Facile route to freestanding $CH_3NH_3PbI_3$ crystals using inverse solubility", by Jeannette M. Kadro[11], Kazuteru Nonomura[1], David Gachet[2], Michael Grätzel[3], Anders Hagfeldt[1*]

published in Scientific Reports 30 June 2015, 5:11654

DOI: 10.1038/srep11654

[1] 1 Laboratory for Photomolecular Science, Institute of Chemical Sciences and Engineering, EPFL, CH-1015 Lausanne, Switzerland

2 Attolight AG, EPFL Innovation Park, Bâtiment D, CH-1015 Lausanne, Switzerland

3 Laboratory for photonics and interfaces, Institute of Chemical Sciences and Engineering, EPFL, CH-1015 Lausanne, Switzerland

Abstract

$CH_3NH_3PbI_3$ was found to exhibit inverse solubility at high temperatures in γ-butyrolactone. Making use of this unusual, so far unreported phenomenon, we present a facile method for the growth of freestanding crystals of $CH_3NH_3PbI_3$ and related materials from solution without addition of any capping agents or seed particles. Large, strongly faceted crystals could be grown within minutes. This finding may aid in understanding the crystallization process of $CH_3NH_3PbI_3$ from solution that may lead to improved morphological control of film deposition for a range of device architectures. Our process offers a facile and rapid route to large, freestanding crystals for use in a broad range of characterization techniques.

2.1 Introduction

Since the first peer-reviewed publications of metalorgano halide perovskite based solar cells in 2009[7], research in materials of this family has undergone immense revival. They unite a broad range of suitable characteristics including long-range charge diffusion[43], high extinction coefficient as well as ease of fabrication[44]. With solar-to-energy conversion efficiencies now exceeding 20%[45], some already regard them as possible competitors to the well-established silicon technology[46,47]. Despite the undisputable impressive developments in conversion efficiencies for laboratory scale devices since the first reports, many non-trivial issues including long-term device stability and reproducibility, material degradation, toxicity of the water-soluble lead halide, and the establishment of reliable device testing protocols remain yet to be solved[15]. Much effort has been invested into the optimization of deposition conditions for thin films for application in solar cells with processes ranging from simple one-step solution deposition over sequential deposition processes[11,48] to vapor based processes[12,49].

In most reported solution growth methods for freestanding crystals, supersaturation is achieved by cooling saturated solutions or by the addition of poor solvents[1,2]. To the best of our knowledge, none of the reported protocols for the formation of $CH_3NH_3PbI_3$ structures, including thin films as well as freestanding products, rely on inverse solubility. We report a facile method for rapid growth of large, freestanding crystals of $CH_3NH_3PbI_3$ from a solution of γ-butyrolactone (GBL) through heating at unconventionally high temperatures. To our knowledge, the possibility of formation of crystalline $CH_3NH_3PbI_3$ from solution in a good solvent without additives has not been reported.

Several methods for the growth of freestanding crystals of $CH_3NH_3PbI_3$ from solution have been reported[50]. Commonly, growing large freestanding crystals in solution is a slow process but Yang et al. [51] have demonstrated a simple and efficient method for growth of $CH_3NH_3PbI_3$ via sequential solution growth method. Their process allowed for the formation of crystals of a range of habits and sizes. Recently, Kollek et.al. have reported a novel single-precursor route for the preparation of a range of nanostructures including porous, shape-anisotropic single crystals via crystal-to-crystal transformation[52].

Studies of important physical properties such as thermal conductivity or Hall Effect commonly have to rely on freestanding structures rather than thin films[53]. Reported formations of $CH_3NH_3PbX_3$ (x=Cl, Br, I) include

nanowires[54], size-controlled cuboids on mesoporous substrates[55], freestanding crystals[1,2,51] and freestanding nanoparticles[52,56].

Our findings show that crystal growth can be achieved through heating rather than cooling a concentrated solution containing only two precursor salts, indicating negative temperature dependence of the solubility of $CH_3NH_3PbI_3$. The solution composition we use to grow freestanding crystals has been commonly used for spin coating $CH_3NH_3PbI_3$ to fabricate crystalline thin films as components in solar cell devices [9,57,58]

2.2 Results and Discussion

PbI_2 and CH_3NH_3I were used as precursors and γ-butyrolactone (GBL) was used as solvent. No additives such as capping agents, stabilizers or seeding particles were used. Both salts were dissolved in GBL at 1:1 molar ratio. The powders were dissolved under vigorous stirring on a hotplate set at 100°C until clear solutions were obtained. To grow crystals, the temperature of the hotplate was rapidly increased to 190°C and held at that temperature until formation of crystals of desired dimensions was achieved. For concentrations stable at room temperature, crystals were found to start forming when the solution temperature exceeded 135°C. Detailed experimental procedures are available in the methods section.

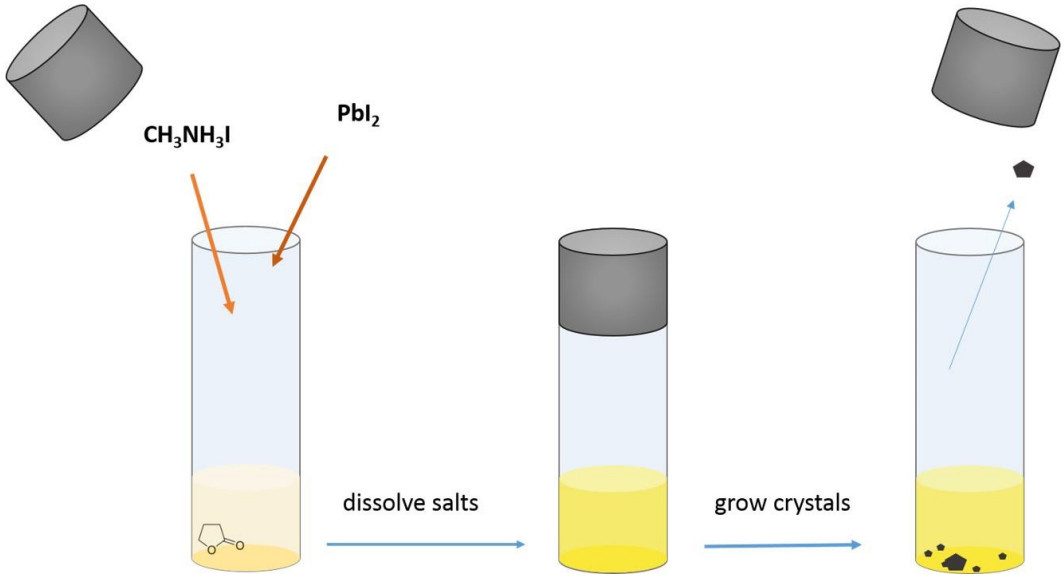

Figure 5 Schematic of the simple crystal growth setup for $CH_3NH_3PbI_3$ single crystals

Large crystals of ca. 1mm length could be grown within minutes at precursor concentrations of 0.9M $CH_3NH_3PbI_3$. Crystal formation occurred in solutions with equimolar ratio of the two precursor salts as well as for solutions with as much as 70% excess of CH_3NH_3I. No crystal growth occurred in solutions with higher excess of CH_3NH_3I. Addition of excess quantities of CH_3NH_3I was found to lead to the formation of large numbers of small crystals while addition of excess amounts of PbI_2 aided the formation of small numbers of larger crystals when identical heating rates were used.

The process is outlined schematically in Figure 5. Crystals were recovered from the hot growth solutions and dried carefully before storage in anhydrous chlorobenzene, hexane or dichloromethane. Upon removal of the growth vessel from the hot plate, the crystals dissolve rapidly in the solution upon cooling. Small crystals are easily dissolved upon removal from the hot growth solution as the liquid film remaining on their surface cools down rapidly and supersaturation at the interface is no longer maintained. Trials replacing GBL partially or completely with *N, N*-dimethylformamide (DMF) or dimethylsulfoxide (DMSO) were unsuccessful[2].

Figure 6a shows a photograph of $CH_3NH_3PbI_3$ crystals freshly grown from a 0.9M equimolar precursor solution within 25min. The surface of the freshly grown crystals is black and glossy and appears smooth to the eye. After exposure to ambient air, degradation leads to the formation of a yellow phase on the surfaces within days. [1,59]

All crystals were strongly faceted but varied in habit. Crystals mostly formed as rhombic dodecahedra or rhombo-hexagonal dodecahedra. Such faceting is consistent with the *I4/mcm* space group reported for this material grown from different routes[59].

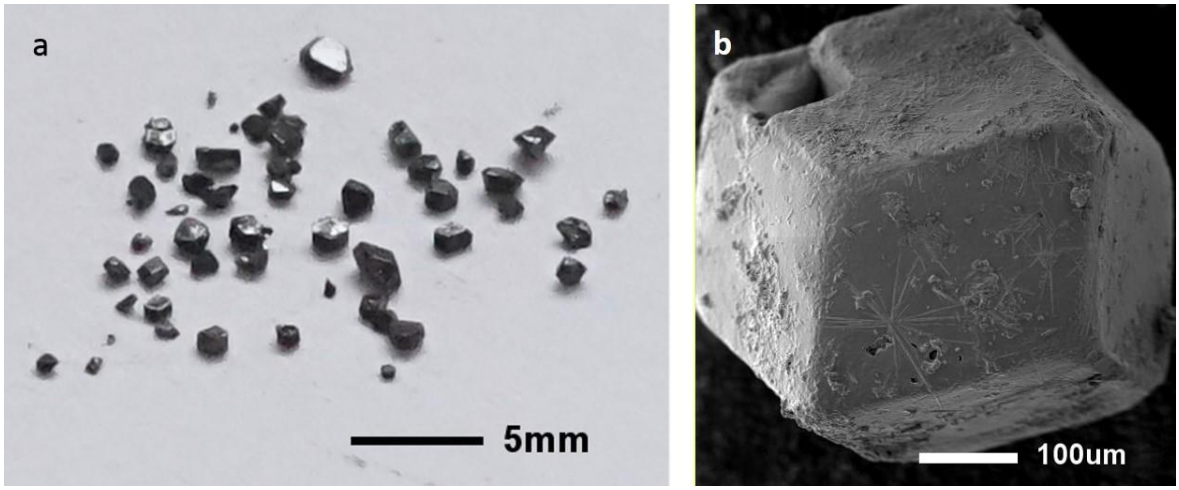

Figure 6 a) typical batch of $CH_3NH_3PbI_3$ crystals, b) secondary electron image of crystal used for CL

The micrograph in Figure 6b shows a typical crystal of ca. 500µm diameter grown from 0.9M precursor solution. Elongated needle-like structures on the surface indicate the beginning of degradation due to

[2] For a more detailed discussion please see following sections

exposure to humidity during storage. The surface of the crystal is not entirely smooth and may have been attacked by the storage solvent. Star-like dendrite formations are typical for DMF induced degradation. Remarkably, without exception, the solid material produced by this process was found to form strongly faceted crystals rather than shapeless formations. Even fast heating regimes of >10°C/min resulted in formation of strongly faceted crystals. Larger crystals typically exhibit strong distortions, probably the result of preferential growth of favored facets due to space constraint. Optimized experimental geometry may enable growth of undistorted large crystals.

Figure 7b shows photoluminescence (PL) and cathodoluminescence (CL) spectra of $CH_3NH_3PbI_3$ grown with our process. PL spectra were collected on finely ground particles suspended in chloroform and CL spectra on a single point on the surface, indicated by cross-hairs in a). PL spectra show a single emission peak at 775nm after excitation at 480nm. Peaks for both PL and CL almost coincide and are well within the range of expected values for the reported band gap ranging around 1.5eV of tetragonal $CH_3NH_3PbI_3$.[50,51]

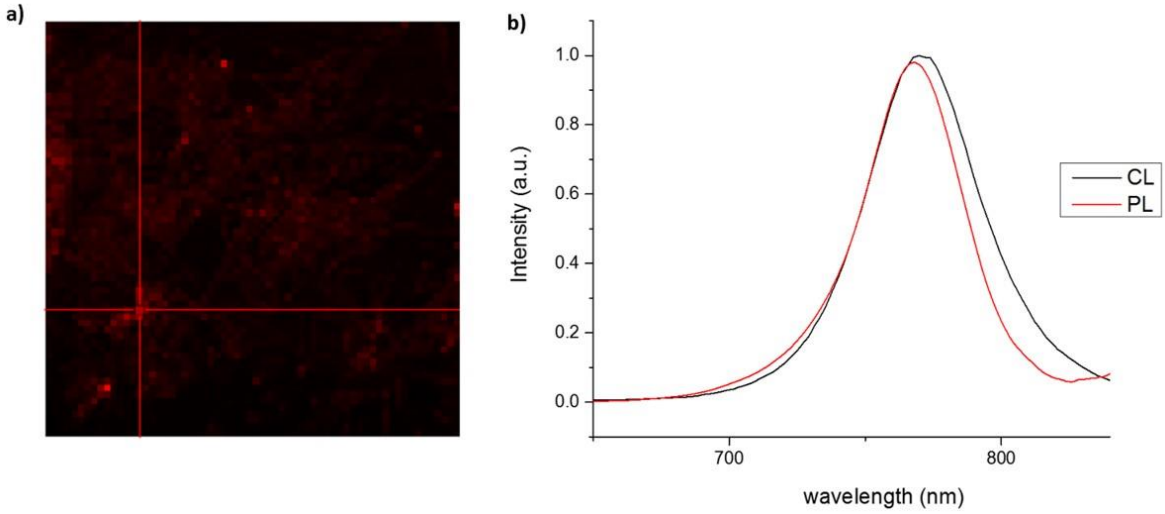

Figure 7 a) CL hyperspectral map of surface of crystal seen in figure (0), b) CL and PL spectra of same sample

To assess the crystallinity of the material further, XRD patterns were collected on a finely ground powder prepared by the same process (Figure 8). $CH_3NH_3PbI_3$ has a cubic $Pm\bar{3}m$ high temperature phase with phase transition from its *I4mcm* tetragonal room temperature phase occurring around 56°C at atmospheric pressure[59]. Whether the crystals form as pseudo cubic crystals in the hot solution and then

undergo a phase transition to the tetragonal phase after cooling to room temperature remains to be investigated.

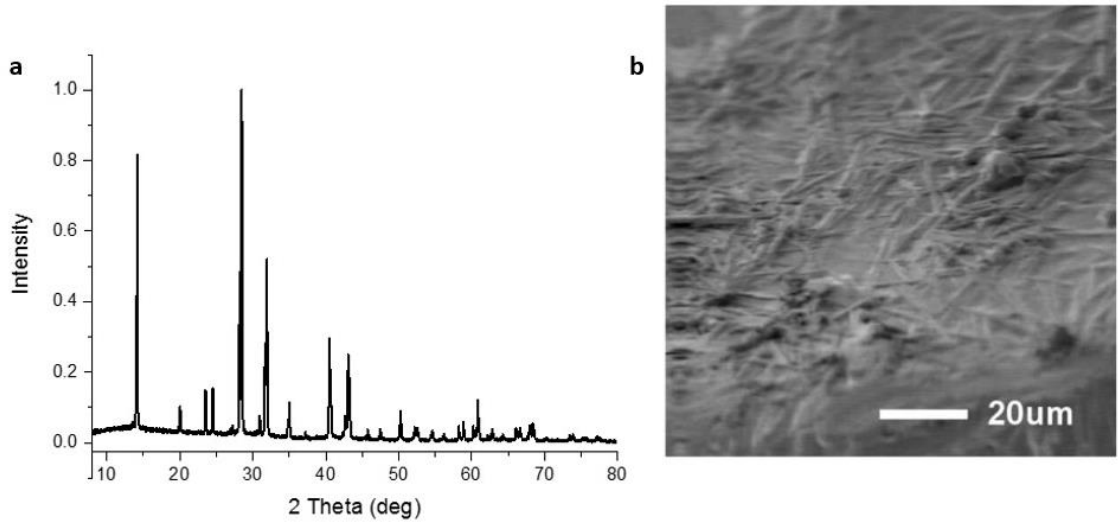

Figure 8 PXRD pattern of manually ground crystals and micrograph of crystal surface after 1 week exposure to ambient air

Commonly, crystals of this type of material are grown by cooling solutions to achieve supersaturation[1,50]. Methods recently reported relying on a sequential approach to the formation of $CH_3NH_3PbI_3$ freestanding crystals through controlled addition of PbI_2 crystals to a solution of CH_3NH_3I or anti-solvent vapor based methods rely on decreased solubility of the target material in the growth medium[13,51] To the best of our knowledge, neither $CH_3NH_3PbI_3$, nor other metalorgano halide perovskites are known to be able to crystallize in their own solvents at elevated temperatures. Such crystallization requires negative temperature dependence of the solubility. Figure 9a shows the temperature dependence of the onset of crystallization in PbI_2-MAI-GBL equimolar precursors.

Broadly speaking, nucleation in supersaturated solutions can be divided into homogeneous and heterogeneous nucleation[60,61]. For our case, the nature of the nucleation remains under investigation. When fast heating rates were employed, crystals were found to form at the bottom of the growth vessel while when the temperature was raised slowly (<5°C/min) they appeared to be forming floating in the bulk of the solution and only sink to the bottom of the vial after reaching a certain critical size. We thus

assume that crystal formation at the bottom of the growth vessel is not primarily due to crystals forming at surface flaws of the vessel but that in fast heating regimes nucleation temperature is only attained in a small solution volume close to the heat source. Slow heating regimes lead to a more uniform distribution of temperature in the growth solution. As the heat is conveyed to the growth vessel from a hotplate below, we assume large temperature differences in the growth solution.

Figure 9 b) shows optical absorption spectra of 0.9M solutions collected before and after crystallization and dissolution as schematically shown in Figure 5. Shape and onset of the spectra are practically identical, demonstrating the reversibility of the process. The higher absorption of the solution after crystallization and dissolution of the crystals likely stems from a slight increase of concentration due to solvent loss under heating.

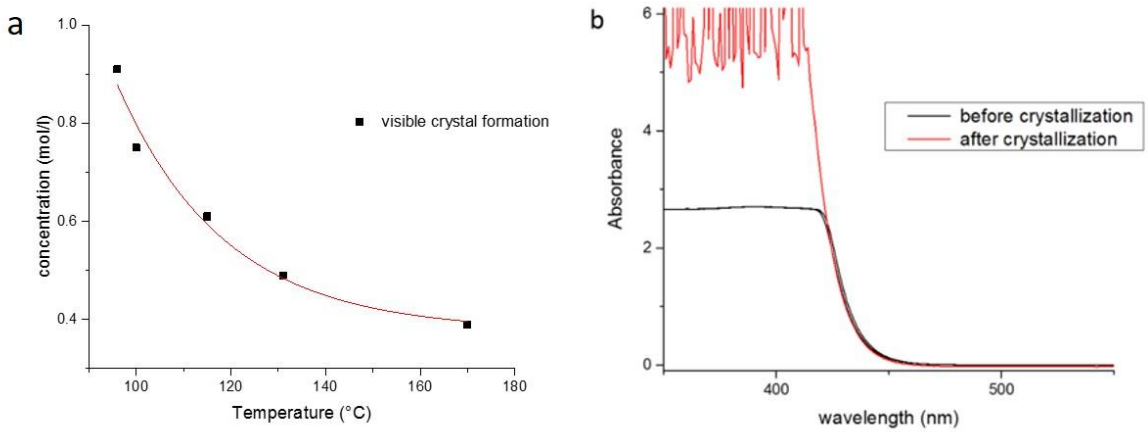

Figure 9 Onset of visible crystallization with respect to temperature and absorption characteristics of 0.9M growth precursor before and after heating to crystallization temperature

As the experiments were performed in ambient conditions, it has to be assumed that the hygroscopic solvent was not water-free. The high temperatures the liquid was subjected to might lead to small bubbles escaping from the solution which in turn may induce cavity nucleation. To minimize the effect of collapsing bubbles stemming from boiling water content, freshly distilled GBL was used to grow crystals in a nitrogen glovebox under water-free conditions; this was not found to affect the crystallization temperature.

Cavitation induced nucleation cannot be ruled out to be a contributing process for this solution-based growth considering the temperature range used, but the observation that crystallization is not delayed in conditions where the effect should be minimal indicates that it is likely not the primary nucleation process taking place.

Both observations by naked eye as well as absorption monitoring of the growth precursor during heating reveal changes is the liquid's color. While bright yellow at room temperature, the liquid gradually darkens and, under prolonged heating, can be observed to turn to deep dark red and finally deep brown, similar to the color of Iodine solutions at high concentrations. To quantify the changes observed by onlookers and to assess whether the observed darkening of the precursor is due to simply higher optical density or the consequence of an actual change in absorption onset, a small volume of precursor liquid was sandwiched between two cover glasses, mounted on a heating state of an optical microscope and its absorption characteristics recorded through an optical fiber.

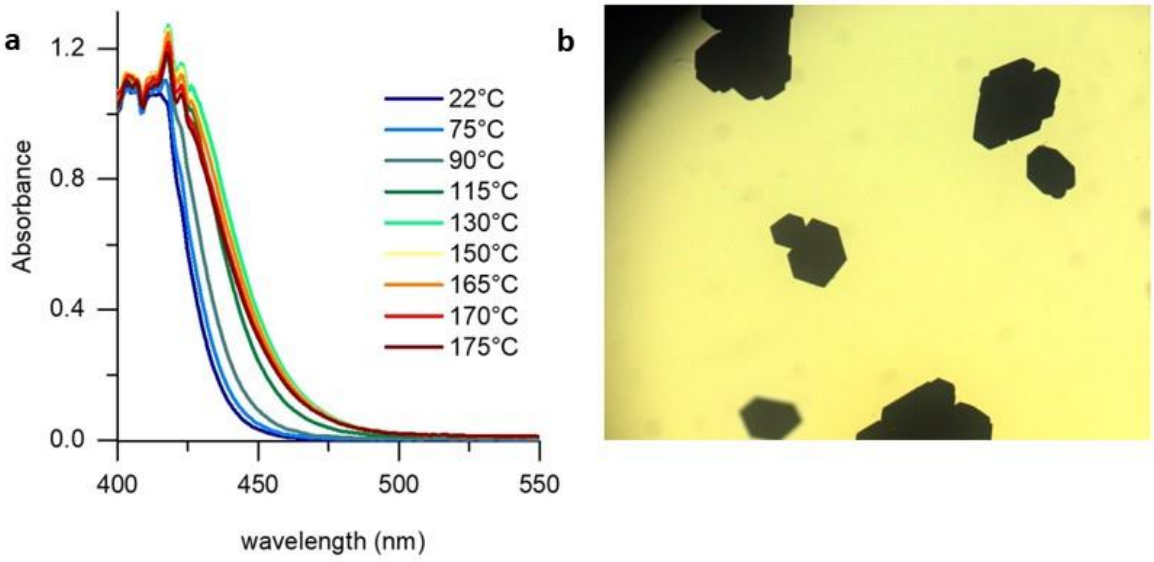

Figure 10 Temperature dependent absorption spectra of $CH_3NH_3PbI_3$-GBL precursor, measured on 20µml liquid between two microscope slides and brightfield micrograph taken of the same solution at 140°C once crystals had formed

Results show a gradual shift in absorption onset from 440nm at RT to a maximum of 460 at 130°, where first crystals can be distinguished. Further heating leading to increased formation of crystals is accompanied by a slight back-shift in absorption onset. Figure 10 b shows a micrograph collected on the

sample subjected to heating and absorption measurements at 140°C. Strongly faceted formations are clearly visible against the yellow background solution.

Growth precursors were found to exhibit Tyndall effects when a red laser beam passed through the solution as it was heated to induce crystal formation, shown in Figure 11b. The effect could clearly be observed at all temperatures from 25°C to 140°C, confirming that particles are present at all stages. At least a portion of the particles are large enough to easily be seen by the unaided eye as the beam passes through the liquid. The term "solution" should therefore be used with caution when referring to this type of $CH_3NH_3PbI_3$ precursor as it is apparent that they actually constitute of a dispersant in a solution. Similar observations have been reported by Yan et.al, attributing the dispersant to the formation of soft colloidal frameworks .[62]

Precursors filtered through 0.05µm PTFE syringe filters did no longer produce crystals upon heating unless the initial concentration was above 1M.

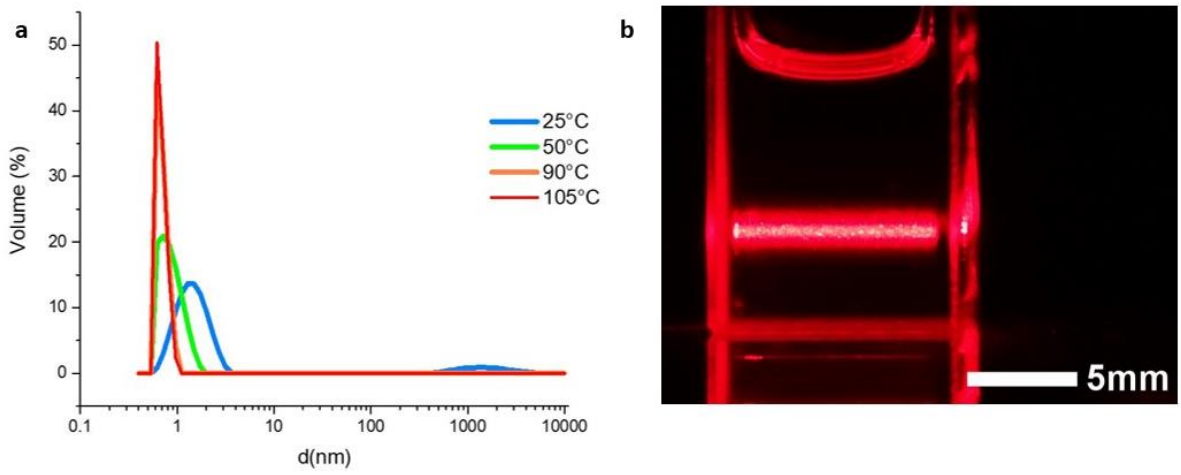

Figure 11 a) Results of Dynamic Light Scattering experiments on heated precursor and b) Tyndall effect on 0.9M solution with 660nm LASER

Temperature-dependent dynamic light scattering (DLS) experimetns were carried out on 1.1M growth precursors[3]. Calculations were performed assuming ideal, non-interacting, spherical particles. The results

[3] Data collected at KAUST

presented in Figure 11a can only be seen as qualitative indications as too many optical parameters, such as the refractive index of the particle and its reflective properties are unknown. The data, however, clearly shows alterations in detected particle sizes as well as disctribution. While two fractions of particles can be distinguished at room temperature, by raising the solution temperature to only 50°C, the larger particle fraction appears to be absent while the smaller particle fraction's size distribution is narrowed. Data from 90°C and 105°C coincides, showing an even more narrow particle size distribution as well as a startly increased particle volume. It should be noted that some fractions of very large particles responsible for the encountered Tyndall effect are out of range of the DLS technique.

2.3 Related Unpublished Results

Aside from $CH_3NH_3PbI_3$, single crystals of a range of variations of $MAPbX_3$ could be successfully prepared using the method outlined in the previous sections. Minor modifications to the heating regime as well as solvents had to be made to prepare a wide range of crystals.

Figure 12 below shows the Bromide-based analogue to Figure 5a, i.e. the temperature-concentration dependence of onset of visible crystallization in an equimolar hot $CH_3NH_3PbBr_3$ precursor liquid. It was found that overall crystallization of the bromide-based material occurred at lower temperatures than the iodide analogue. $PbBr_2$ is poorly soluble in GBL and no crystallization occurred in GBL based liquids. Dimethylformamide was used as solvent for all experiments in this chapter that were based on $PbBr_2$.

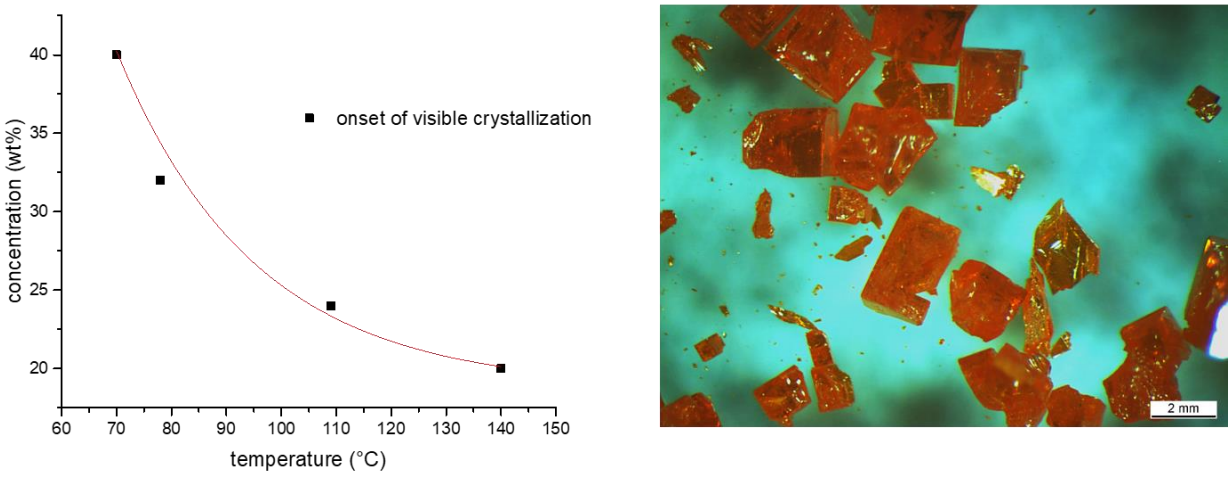

Figure 12 Onset of visible crystallization of $CH_3NH_3PbBr_3$ in DMF, optical microscopy brightfield image of crytals recovered

Growths rendered a high yield of freestanding, deep orange cubic crystals. Yields of min. 25% were reached for fast heating regimes with 50° C/h. Photoluminescence and single-crystal XRD were used to confirm the material as $CH_3NH_3PbBr_3$ (Figure 14).

Formamidinium lead iodide could be prepared by the described method as well. Figure 13a below shows the onset of crystallization in heated solution for an equimolar FAI-PbI_2-GBL precursor with the corresponding curve for $CH_3NH_3PbI_3$ for comparison. The onset of crystallization occurred at lower temperatures for $FAPbI_3$ at all compositions. The middle panel shows the photoluminescence measured on a selected black crystal and panel c) shows a photograph of freshly grown crystals. The black crystals rapidly decay to the yellow γ-phase and could not be examined in single crystal XRD due to too many incompatibilities. The strongly red-shifted PL peaking at 825nm and the characteristic decay points to the recovered material being indeed formamidinium iodide.

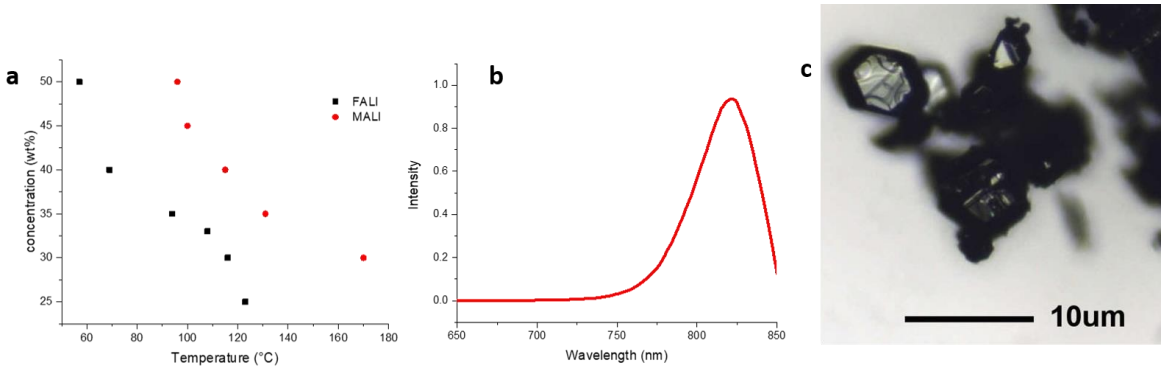

Figure 13 a) crystallization onset of FALI in GBL b)PL of selected FALI crystal c) photograph of freshly grown crystals

2.4 Mixed halide crystals

Mixed halide, mixed cation hybrid perovskite single crystals were successfully prepared using the method outlined above. Replacing iodide with bromide allows fabrication of materials spanning a wide range of bandgaps and resulting colours which is of particular interest for not only PV but also other optoelectronic devices [63].

While detailed implications and recent development in compositional optimization of hybrid halide perovskites shall not be discussed here, it is worthwhile noting that the availability of large single crystals as well as simple preparation of these in various compositions is important to those aiming to investigate the material in a context with minimal complexity.

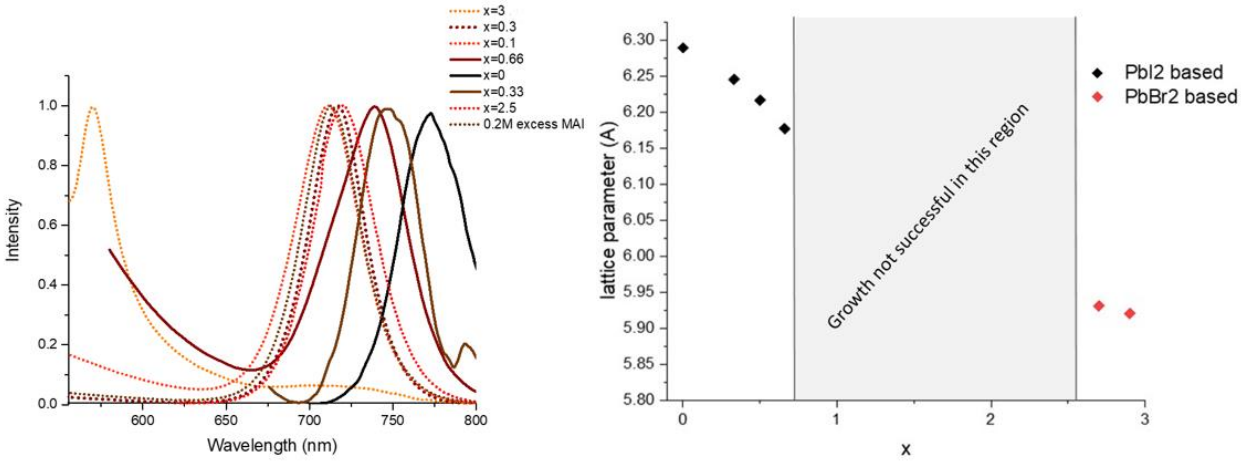

Figure 14 a) PL spectra of $CH_3NH_3PbI_{3-x}Br_x$ mixed halide single crystals, x indicates nominal values b) corresponding lattice parameters

To grow mixed halide samples, the ammonium salts were varied. The crystallization temperatures for mixed halide samples were found to follow the single-halide samples' trends, i.e. addition of MABr to a PbI_2-MAI-GBL precursor reduced the crystallization onset temperature observed with respect to a single halide composition of the same concentration while addition of MAI to a $PbBr_2$-MABr-DMF precursor produced an increase. Figure 15 shows the onset of crystallization for single-halide compositions and

mixed-halide compositions. It can be observed that the onset of crystallization is dependent on overall concentration as well as composition.

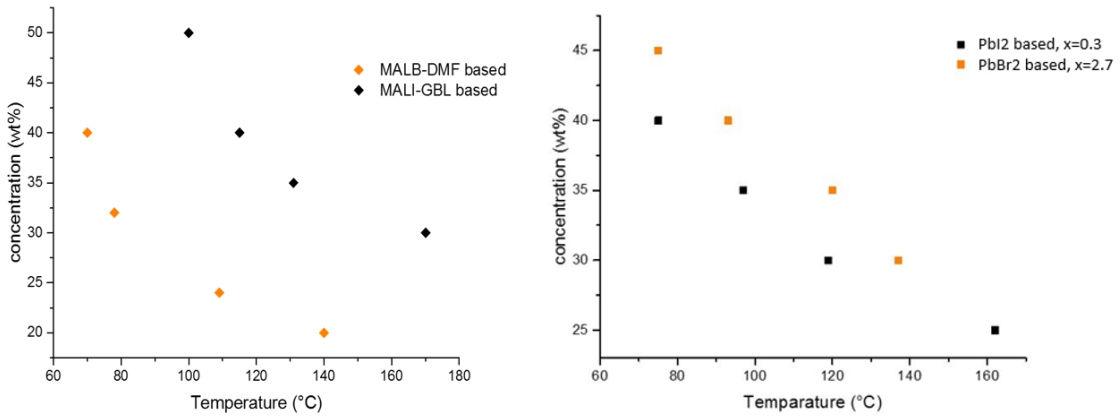

Figure 15 Onset of visible crystallization in single-halide compositions (left) and mixed-halide compositions (right)

Growing crystals by mixing two different lead halide salts was not successful. Consequently, the range of compositions that was successfully prepared does not span the entire theoretically possible compositional space. Results of photoluminescence measurements carried out on selected crystals from single batches are shown in Figure 14 a[4]. Dotted lines indicate compositions achieved by using $PbBr_2$ as lead halide and continuous lines denote those based on PbI_2. The plot shows that even relatively small nominal substitution of bromide with iodide leads to a Stark red-shift of the observed photoluminescence. The culmination of PL peaks secondly indicates the difference between theoretically possible maximum substitution based on precursor composition and actual substitution achieved.

Lattice parameters of several selected crystals of various compositions can be seen in panel b) of the same figure. Black diamonds indicate samples grown with PbI_2 as Plumbohalide and orange diamonds denote those grown from $PbBr_2$ based precursors. It was not possible to produce crystals with substitutions of $0.66 < x < 2.6$ with the present method.

[4] For single crystal XRD and X-ray fluorescence on the samples, please see corresponding section of the Annex

2.5 Comparison to high-yield vapor induced crystallization

Anti-solvent vapor induced crystallization has been proven to be very effective to grow single crystals of the MAX_3 family. Using an anti-solvent vapor of a volatile antisolvent with high vapor pressure such as dichloromethane or chloroform poses practical advantages over the temperature-dependent method outlined in this chapter. Anti-solvent vapor induced growth can be performed at room temperature with minimal equipment and requires less constant supervision than temperature-dependent methods. Further, in the case of $CH_3NH_3PbX_3$ (X= Br, I), high yields could be obtained within hours of growth.

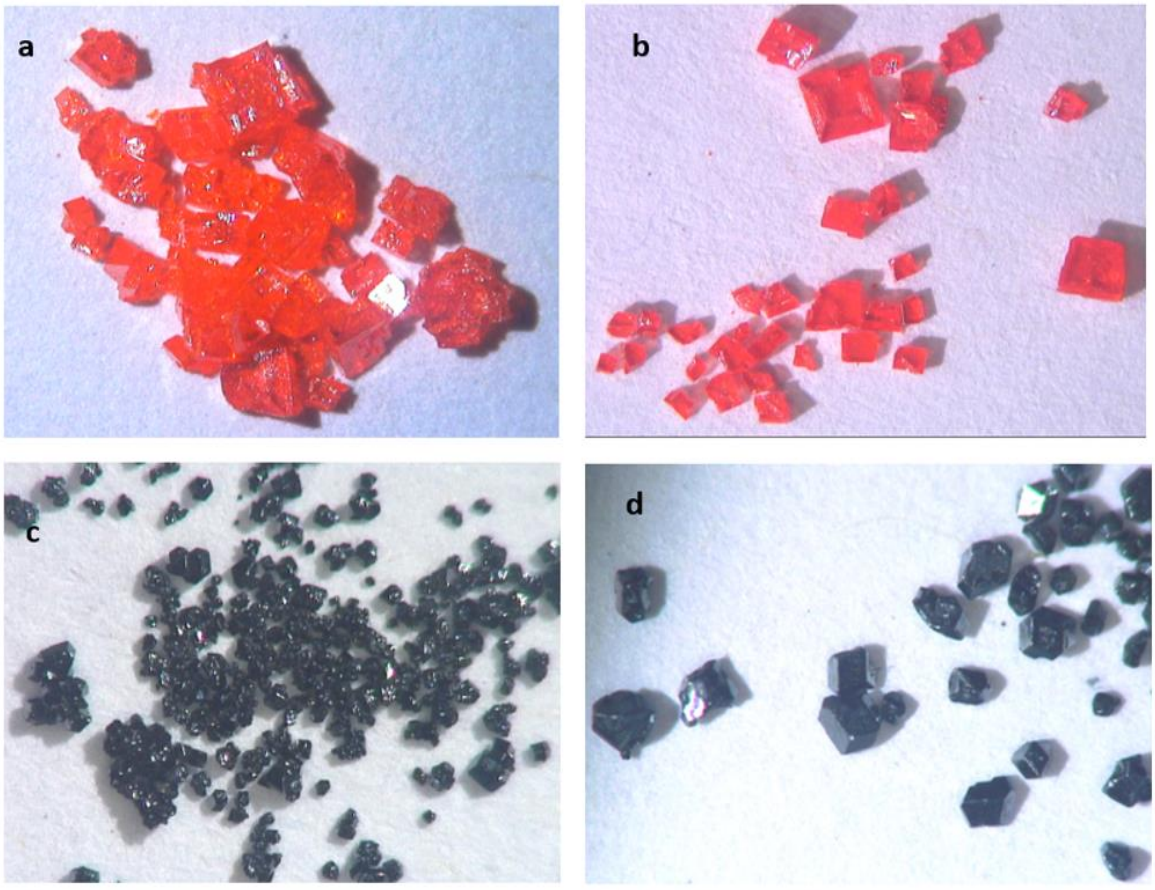

Figure 16 Photographs of freshly grown crystals a) MALB, vapor-induced crystallization, b) solution-heating approach, c) MALI, vapor induced growth, d) solution-heating crystallization

The drawback of this simple method compared to heat-induced solution-crystallization lies in the morphology of the obtained samples. Figure 16 shows photographs of freshly grown crystals of $CH_3NH_3PbBr_3$ (a+c) and $CH_3NH_3PbI_3$ (b+d) grown by vapor-induced crystallization (a+c) and by heating precursors (b+d). Crystals of both compositions grown by the anti-solvent method can be seen to stick together and form agglomerates while the solution-heating method yields truly freestanding single crystals.

2.6 Conclusion

$CH_3NH_3PbI_3$ was found to exhibit negative temperature dependence of solubility in a common organic solvent. Using this rare phenomenon, we have presented a facile method for the preparation of large, freestanding crystals of $CH_3NH_3PbI_3$ without relying on capping agents and other additives. Crystals can be grown without employing particular equipment in very short growth times. The nature of the nucleation process, the kinetic processes enabling crystal growth under the investigated conditions, and the reasons for the observed extraordinary phenomenon of inverse solubility of $CH_3NH_3PbI_3$ remain under investigation. Our finding may further aid in understanding the mechanism behind the crystallization of $CH_3NH_3PbI_3$ which is crucial for the optimization of deposition processes. Better understanding of the crystallization process as well as quantification of the solubility at high temperatures will facilitate the development of new deposition techniques of $CH_3NH_3PbI_3$ on flat or structured substrates for a range of applications.

2.6.6 Methods

Crystal growth

The growth solutions were prepared under nitrogen by dissolving PbI_2 or $PbBr_2$ (99%, Sigma Aldrich) and CH_3NH_3X (I, Br, synthesized in-house or purchased from Dyesol) in γ-Butyrolactone (98%, Sigma Aldrich) or dimethylformamide (Arcos). Commercially available chemicals were used as received without further purification. Solutions of 0.3M to 0.9M were prepared. The solvent was added to the salts at room temperature. Tightly closed vials were heated on a conventional hotplate at 100°C until no visible traces of undissolved salts remained. Solutions were then transferred out from the glovebox. Once the salts were completely dissolved, no visible turbidity or precipitation occurred for days for equimolar solutions and for solutions with excess of CH_3NH_3I. Solutions below 0.8M concentration were found to be stable for weeks and no turbidity or precipitation was observed.

To grow the crystals, screw-top scintillation vials of 15ml volume were used for solution volumes of 1.5ml. After stabilizing the temperature of the solutions for 10min at 100°C, temperature of the hotplate was increased until crystals formed between 110°C-190°C, dependent on composition and solvent. To avoid boilover, the solution temperature was monitored by directly inserting a thermometer into a vial of identical dimensions with the corresponding volume of the pure solvent.

Crystals were recovered from the hot solutions and immediately dried carefully prior to storage in anhydrous chloroform or dichloromethane.

Anti-solvent induced crystallization

Precursors were prepared in DMF and GBL, as outlined above. Open vials of 3ml volume containing 1ml of precursor were placed into larger vials of 12ml volume filled with approximately 3ml of dichloromethane (DCM, Sigma) or dry chloroform (Arcos). Both vials were covered by a small pyrex beaker placed upside-down. The anti-solvent was left to evaporate at room temperature until desired numbers/volumes of crystals were grown at the liquid precursor surface.

Material Characterization

Powder X-ray diffraction patterns were collected on a Bruker D8 Advance X-ray diffractometer using Cu Kα radiation. Small crystals were prepared by rapid heating in order to obtain a powder fine enough for powder diffraction.

Photoluminescence spectra were collected on a Horiba Jobin Yvon Fluorolog-3 spectrofluorometer with excitation at 480nm.

The CL-SEM measurements were performed at room temperature using an Attolight Rosa 4634 CL microscope, with a beam probe of 5 nm, an accelerating voltage of 2 kV and a beam current of 20nA. This CL microscope tightly integrates a high numerical aperture (NA 0.72) achromatic reflective lens within the objective lens of a field emission gun scanning electron microscope (FEG-SEM). The focal plane of the light lens matches the FEG-SEM optimum working distance. The CL collection efficiency is constant over a 300µm field of view so that CL emission can be compared quantitatively between two separate points. CL was spectrally resolved with a Czerny-Turner spectrometer (320 mm focal length, 150 grooves/mm grating) and measured with an UV-vis. CCD camera.

Optical absorption spectra were collected on a Varian Cary 5 spectrophotometer.

Thermogravimetric analysis (TGA) was carried out on a Perkin Elmer Pyris 6 TGA Thermogravimetric Analyzer at heating and cooling rates of 1K/min under constant Argon flow of 20ml/min.

3 Proof-of-Concept for Perovskite Solar Cell Recycling

This chapter is an adaptation of the article "Proof-of-Concept for Facile Perovskite Solar Cell Recycling", published as *Energy Environ. Sci., 2016, 9,3172*

DOI: 10.1039/C6EE02013E

Jeannette M. Kadro[15§], Norman Pellet[2,3,§], Fabrizio Giordano[2], Alexey Ulianov[4], Othmar Müntener[4], Joachim Maier[3], Michael Grätzel[2,3*] and Anders Hagfeldt[1*]

[5] 1-Laboratory for Photomolecular Science, EPFL, 1015 Lausanne, Switzerland

2-Laboratory for Photonics and Interfaces, EPFL,1015 Lausanne, Switzerland

3- Max Planck Institute for Solid State Research, Heisenbergstraße 1,70569 Stuttgart, Germany

4- Institut des Sciences de la Terre, Université de Lausanne 1015 Lausanne, Switzerland

§ these authors have contributed equally

Abstract

Perovskite solar cells based on $CH_3NH_3PbI_3$ and related materials have reached impressive efficiencies that, on a lab scale, can compete with established solar cell technologies, at least in short-term observations.

Despite frequently voiced concerns about the solubility of the lead salts that make up the absorber material, several life cycle analyses have come to overall positive conclusions regarding environmental impact of perovskite solar cells (PSC) production. Their particularly short energy payback time (EBPT) in comparison to other established PV technologies makes them truly competitive. Several studies have identified valuable components such as FTO, gold and high temperature processes as the most significant contributors to the environmental impact of PSCs. Considering these findings, we have developed a rapid dismantling process allowing recovery of all major components, saving both raw materials, energy and production time in the fabrication of recycled PSCs. We demonstrate that the performance of PSC fabricated from recycled substrates can compete with that of devices fabricated from virgin materials.

3.1 Introduction

Despite unprecedented increases of reported energy conversion efficiencies for any type of novel solar energy harvesting technology, perovskite photovoltaic still comes with significant challenges that require urgent addressing.[15] The tight regulation of hazardous substances in consumer products is one of them. The European Union is implementing policies phasing out hazardous substances - including lead - in consumer electronics, due to concerns of their long term exposure effects on humans and environment. Even so, stationary photovoltaic installations have been exempted from those regulations[27]. As a consequence, PSC solar farms or rooftop installation should be exempted from compliance with the RoHS. The challenges towards the realization of perovskite solar farms remain therefore mostly technical: long-term stability, encapsulation, fabrication of large-area modules and end-of-life processing.

The highest efficiencies for PSCs today are achieved with multi-layer devices comprised of a number of highly valuable components, such as gold, fluorine doped tin oxide (FTO) and mesoporous TiO_2.[64] Their production not only contributes to the deprivation of important elements, but also is responsible for severe environmental impacts at the exploitation sites. In addition, gold value is subjected to strong price fluctuations due to market speculation and not directly tied to production volumes or scarcity factors.

Recently published studies have come to varying conclusions regarding the environmental impact of the production and disposal of PSCs. [65–68] Some indicate that solvents (including chlorobenzene, diethyl ether, dimethyl sulfoxide and N,N-dimethylformamide), the synthesis of CH_3NH_3I and some of the other components used in the fabrication of the PSC - are among the main concerns.[68] Others argue that the overall impact is dominated by the gold and the transparent conductive oxide, used as the back and front contact, respectively.[67]

It is, however, of common consensus that the lead content in the perovskite layer is not the main issue in terms of environmental impact of PSC production.[6,7,3,8] Pb^{2+}, in the form of the perovskite $APbX_3$, content in the operational device can vary based on the device architecture but based on today's most efficient cells with perovskite layers of around 300-400nm thickness would amount to less than 1000mg/m^2 . Recently published estimates on the potential of environmental pollution from damaged PSC panels have shown that the direct impact of lead leaking from damaged panels would be modest compared to

potential damages from other anthropogenic lead sources, such as use of lead paint or lead smelting for car batteries.[70,71] Calculations based on lab scale device efficiencies have shown that potential lead pollution from leaking PSCs would still be low compared to the amounts of lead released from to other energy conversion methods. For example, lead emissions from a 1GW coal-power plants vary considerably based on lead content and quality of the coal burned but commonly range from 0.1t to 1t per year, and usually are not sequestered.[72] Hailegnaw et al. have estimated that a 1GW solar field of PSCs would contain up to 30t of Pb.[71] If lead contained in PSC solar panels is retrieved and recycled safely, PSC solar farms would allow a reduction of direct lead emissions. Certainly, measures to prevent large amounts of lead from damaged panels, for example as consequence of natural disasters such as earthquakes, floods or wildfires, should still be considered and installations of large numbers of PSC panels in areas prone to such natural disasters or within the vicinity of important groundwater reserves might require special regulations.

Aside from reliable encapsulation, development for safe recovery processes of the slightly water soluble lead salts (K_{sp} 10^{-8} for PbI_2 as opposed to 10^{-27} for CdTe[73]) from PSC modules together with successful implementation of take-back-systems, such as already in place for CdTe solar panels, will be key to successfully bringing perovskite PV to the market.[74]

Substitution of lead by tin in organic-inorganic hybrid perovskites has been realized[50,75,76] and solar cells with power conversion efficiencies exceeding 6% have been reported,[24] but several studies have come to the conclusion that tin substitution is not advisable for numerous reasons. Leaving aside lower attained conversion efficiencies and the inherent instability of its 2+ oxidation state in air, organic tin compounds have also been found to be more environmentally harmful than their lead analogues. [24,65] Tin based perovskite solar cells have been found to score higher in all environmental impact categories investigated as compared to their lead analogues in a recent study presenting an LCA including end-of-life scenarios of incineration or landfills, and thus will not be considered in this study. [65]

Tin is a strategically highly critical metal as it is indispensable in a very broad range of applications in technology today, particularly in solders, alloys and coatings and it is used in sizable quantities as fluorine-doped tin oxide in PSCs. A small number of countries including China, Indonesia and Peru control more than 4/5 of the global production with no significant exploitation sites in Western Europe and North America.[77]

Due to limited technological substitutability of tin, strongly geographically concentrated supply and risks associated to political instabilities in its main production countries and growing global tin demand the metal has been assigned with a high material security index in a recent report.[78] Tin has recently been added to the European Commission's report on critical materials.[79]

So far, published LCAs confirm lead-based PSCs as environmentally friendly alternative to other PV technologies, particularly emphasizing their short energy payback times (EPBT) calculated based on lab-scale device efficiencies.[67] Based on such considerations, we developed a rapid and highly selective process allowing full recycling and/or recovery of the most precious components of a standard PSC device. We demonstrate that PSC devices can be easily dismantled in reverse order of fabrication and that materials can be extracted with high purity for direct reuse or further recycling. The process we introduce eliminates energy intensive processing steps such as sintering of the TiO_2 in the fabrication of recycled devices, significantly reducing both fabrication time and energy input. Furthermore, sequestration of the lead salts contained in devices is achieved with a remarkable degree of segregation. Most importantly, we demonstrate that our high efficiency PSCs can be recycled at least twice without significant losses in performance.

Recovery and reuse of the FTO-coated glass substrates with mesoporous TiO_2 is desirable. Calculations based on devices of similar architecture as we use in this study the FTO substrate alone has been shown to contribute 40% to the overall carbon footprint of all materials embedded and its manufacturing consumes 36% of all primary energy of embedded materials.[67] In addition, the prolonged, high temperature associated to the TiO_2 layers have been shown to contribute significantly to both carbon footprint and primary energy consumption of PSC fabrication.[80] Using a simple process, we show that FTO glass can be reused with little losses in performance.

Gold being a scarce but technologically and economically highly valuable metal makes its recovery and recycling from used appliances particularly desirable. Its production and refining can have significant environmental impacts at exploitation and refining sites.

Among normalized cradle-to-gate contributions of production of important metals, gold ranges second behind rhodium in terms of release of greenhouse gas emissions and toxic substances[81,82] Aside from mitigating severe detrimental effects at the exploitation sites on eutrophication, acidification and land use, employing recycled gold can save up to 98% in energy required as opposed to use of newly mined material.[81,83]

Gong et al. have shown in their recently published LCA that extraction, refining and processing of the gold alone contributes up to 53% to the overall carbon footprint of all embedded materials.[67] During the review process of this publication, a paper describing a similar process to the one we are introducing here has been published using solar cells without mesoscopic layers.[84] We find it highly encouraging to see that sustainability and recycling of PSCs are receiving attention from many in the field.

The entire dismantling process was carried out at room temperature in ambient conditions, A schematic outline is presented in Figure 17.

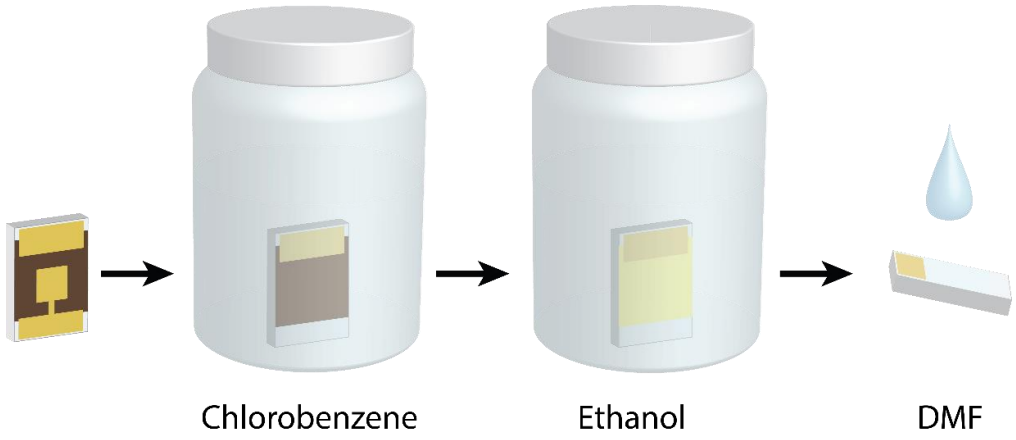

Figure 17 schematic process outline: fully assembled PSCs are immersed into chlorobenzene, after complete dissolution of the HTM and cathode removal, EtOH is used to dissolve MAI, small amounts of DMF are used to completely remove PbI_2

To remove the gold counter electrode, fully assembled (non-sealed) PSC devices were fully immersed into chlorobenzene in a round-bottom-flask with the gold cathode facing upwards. Due to the dissolution of the organic, doped hole transport layer a slight color change of the solvent can be observed while the counter electrode eventually peels off from the substrate completely. Gold removal was typically completed within 2-5min. Figure 18 shows a photograph of a fully assembled device undergoing gold and HTM removal in chlorobenzene. Gold flakes can be seen floating on the liquid surface. The collected gold was separated by decanting from the solvent and washed briefly with acetone, an aqueous solution of 20% HCl, and distilled water, successively.

After complete removal of the gold cathode and the organic HTM, the hybrid perovskite absorber layers were removed in two steps, inverting the process for sequential deposition of $CH_3NH_3PbI_3$ reported elsewhere[11].

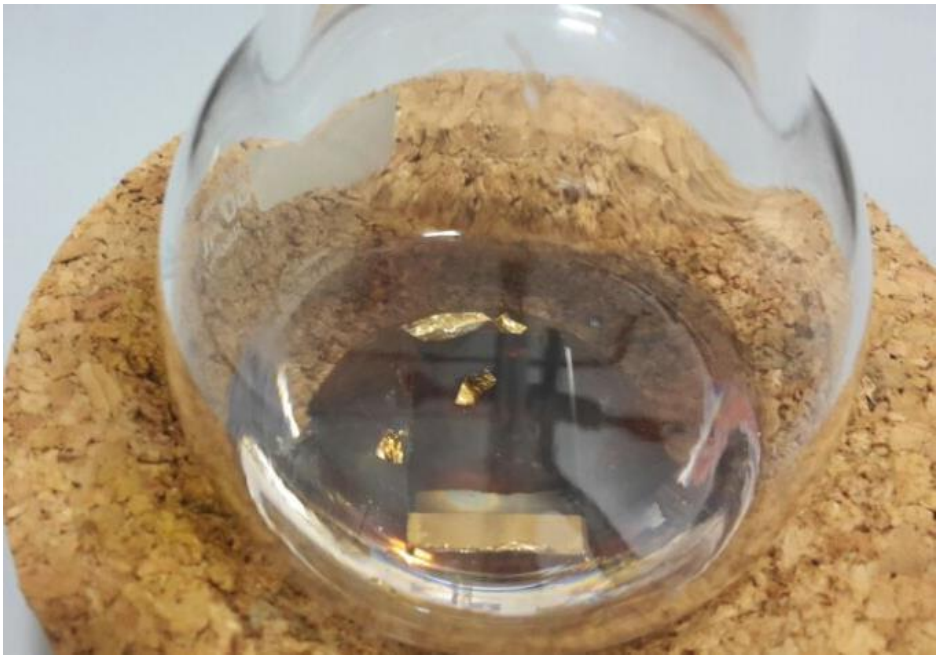

Figure 18 Device immersed in anisole, peeled gold counter electrode can be seen floating in liquid

Substrates were fully immersed into EtOH immediately following the chlorobenzene treatment. A vivid colour change from black to bright yellow can be observed as CH_3NH_3I dissolves into the solvent, leaving PbI_2 behind. Upon completion, PbI_2 was removed from the films by carefully dropping small amounts of DMF onto the surface of the substrate.

As-treated substrates were carefully washed with EtOH to remove any remaining solvent and left to dry naturally. The entire dismantling process could typically be completed in less than 10min. The TiO_2 coated FTO substrates were then treated for 10 minutes by UV/O_3 and reused without further heat treatment. The recycled substrates were processed again within 4-5 hours of the previous depositions. The same fabrication protocol described above and the same stock solutions were employed.

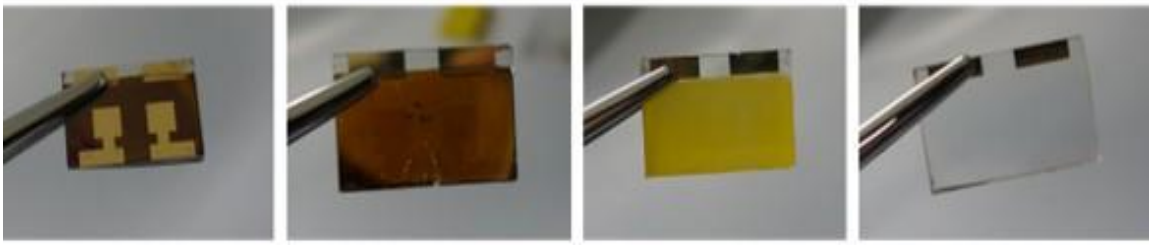

Figure 19 Photographs of device undergoing recycling process f.l.t.r: fully assembled device, after immersion in anisole/chlorobenzene, after immersion in IPA, after removal of PbI2 with DMF/DMSO

3.2 Results and discussion

The selectivity and completion of each of the three recycling steps was assessed by scanning electron microscopy, thin film X-ray diffraction, ICP-MS, mass spectrometry and X-ray fluorescence.

Photoanode

Figure 2 shows top-view and cross-sectional SEM micrographs of the full device and after each recycling step and confirms the selectivity of each steps. It can clearly be seen that the perovskite absorber layer remains intact after cathode and HTM removal in chlorobenzene. Upon MAI dissolution in EtOH (Figure 2c and g), hexagonal structures typical of PbI_2 are formed on the mesoporous TiO_2 layer and appear to be completely absent after DMF treatment as (Figure 2d+h). Figure 2d shows a top-view image of the mesoporous TiO_2 layer after removal of PbI_2 in DMF. No indications for detrimental effects of the dismantling process such as delamination or scratching of the photoanode were observed; the TiO_2 layer appears to remain completely intact.

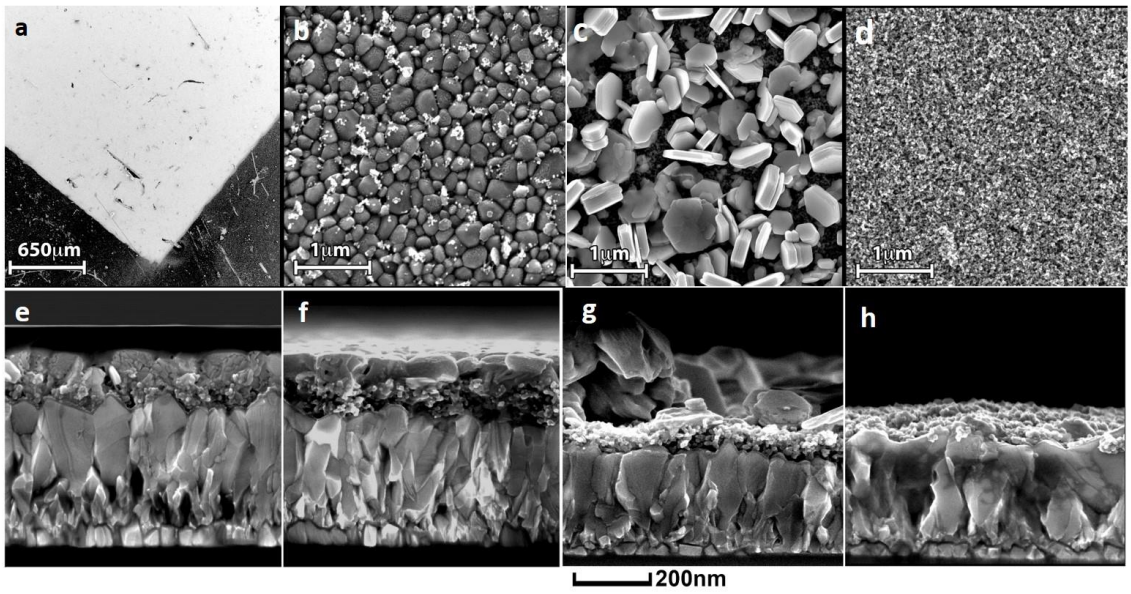

Figure 20top-view and cross sectional secondary electron micrographs of devices at all recycling stages a+e: before recycling treatment b+,f: after chlorobenzene treatment, c+g: after MAI dissolution d,h after PbI2 removal

Structural characterization by X-ray diffraction was carried out on twin samples analogous to those presented in Figure 2. The diffraction patterns presented in Figure 3 confirm the purity of each expected phase after the sequential solvent treatment steps.

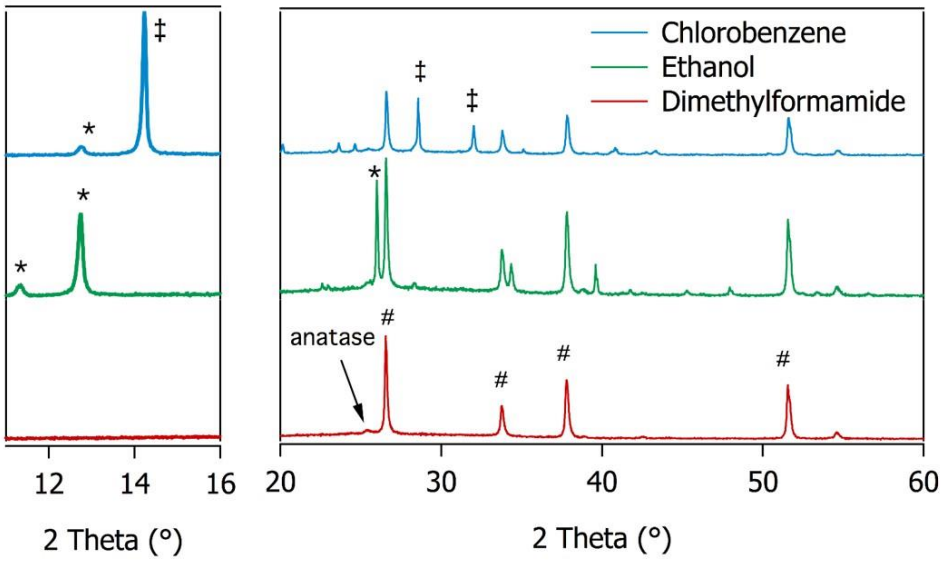

Figure 21XRD patterns of substrates after each processing step. In blue, the original device stripped from gold and the HTM layer. In green, the device stripped from gold, the HTM layer and CH3NH3I. In red, the FTO substrate covered with the compact and mesoporous TiO_2

Back contact

Purity of the recovered gold was confirmed by X-ray fluorescence (XRF). No traces of lead were found on the material recovered from the chlorobenzene bath (see SI). The possibility of slight organic contaminations on the surface stemming from dissolved organic HTM cannot be completely be excluded due to detection limitations of XRF although we deem such remaining organic contaminations improbable as the recovered material is washed in acetone and HCl. As no foreign metal traces were found, it can be assumed that the recovered gold can be reused without extensive energy-intensive refining.

Although all gold deposited on the HTM could be successfully recovered with high purity, the recovered material could not be used for fabrication of recycled devices due to purely practical reasons. Firstly, the amount of gold that is required to deposit a ca. 100nm thick layer, (see experimental procedures) exceeds the amount of gold actually deposited (ca.0.4mg) on each device by several orders of magnitude in our evaporator. This is due to an unfavourable geometry of the experimental setup used and could be optimized on a larger scale. Collecting sufficient material for one single evaporation would require processing of at least 900 devices.

Secondly, gold recovered in the recycling process remains in its original shape, that is, ca.100nm thick, freestanding films. Due to the low mass of these films, they would not withstand the suction produced in the evaporator during pumping and would be removed from the evaporation boat in the process of evacuating the machine.

Lead in solvents

Methanol, ethanol, 2-propanol, ethyl acetate and deionized water were used for the dissolution of the methylammonium iodide. The fastest observed conversion from $CH_3NH_3PbI_3$ to PbI_2 was achieved using MeOH, followed by deionized water, EtOH and isopropanol. Complete MAI dissolution in ethyl acetate could be achieved only after several hours, which was found too impractical for further consideration.

EtOH was chosen for device recycling over MeOH, despite the slower dissolution considering its lower toxicity to workers and environment and reduced processing times due to higher drying rates as compared to water.

The remaining lead content in each solvent was assessed by ICP-MS to evaluate the process selectivity with respect to lead sequestering. Lead quantities are shown in Table ***1*** 1 relative to the total lead content in the chlorobenzene, ethanol (water, isopropanol or methanol) and DMF. They underline the relative selectivity of each recycling step. Among the four solvents we have tested, water seems to perform with the highest selectivity. Only 0.14% of the total Pb amount could be detected, which is similar to the selectivity of chlorobenzene. After purification in Amberlite 120 IR, contents in the water dropped down to 0.03%, but in this case, lead sequestration by the resin may be limited by the slower uptake at extremely low concentrations (0.2ppm). To confirm this, we prepared a saturated solution of PbI_2 in water with a 30-fold molar excess of MAI. Following decanting and filtering, analysis by ICP-MS showed concentrations of 43.5 ppm ml^{-1}, which we believe is close to the upper dissolution limit of PbI_2, in particular since the large excess of I^- anions can help solubilize PbI_2 by producing the soluble $(PbI_4)^{2-}$ complex, soluble in water. After lead removal by the resin for 16h (1g / 30mL), concentrations of lead down to 0.44 ppm mL^{-1} were recorded, which corresponds to a sequestration of 99%.

2-propanol showed the second best selectivity after water, with only 0.35% lead content in the solution. The slow dissolution of the MAI in 2-propanol (about 20 minutes) makes this solvent less appropriate.

Then follows ethanol, with up to 3.4% Pb with respect to all extracted lead from the device. Finally, methanol showed the poorest performance, with up to 7% Pb in the solvent with respect to the total Pb quantity.

Ion exchange resins such as Amberlite IR 120 can be used for purification of a range of organic solvents as well, including MeOH and IPA.[85,86] An efficient, electrochemical process for lead recovery from PSC devices via electrodeposition of lead on lead using ethylene glycol with choline chloride as solvent has been demonstrated recently in a model experiment by Poll et al.[87]

Table 1: Segregation efficiency of the solvents used in the recycling process. Lead content is reported with respect to the total amount of extracted lead. Solvent volumes were 5mL for chlorobenzene, 5mL for ethanol, methanol, water and isopropanol, and 0.5mL for DMF.

Sample	Relative lead content
Chlorobenzene	0.09%
Ethanol **EtOH**	3.4%
DMF	96.5%
Methanol	
MeOH	7.1%
DMF	92.9%
2-propanol	
2-propanol	0.35%
DMF	99.6%
Water	
H_2O	0.14%
DMF	99.8%
H_2O (after purification)	0.03%

Fate of spiro-MeOTAD, dopants and additives

ESI-TOF mass spectrometry in positive and negative mode was carried out on samples of chlorobenzene, EtOH and DMF collected directly from each recycling step and resulting spectra are available in the Supplementary Information. Formic acid was used for protonation in the positive mode. Spiro-MeOTAD$^{+\cdot}$ could be found neither in the ethanol nor in DMF, confirming the high selectivity of the process towards spiro-MeOTAD extraction. $TFSI^-$ and what could possibly be $(LiTFSI)H^+$ was found in the chlorobenzene as well. Similar peaks were found in the EtOH and DMF, pointing at rather poor selectivity of the LiTFSI segregation. No iodide peak was found in the chlorobenzene, but appeared in the ethanol and DMF (negative mode). FK209 and TBP could not be found. It is possible that they appear as aggregates, such as the peak at m/z 217.1 observed in the ethanol and DMF, which is possibly $(TBP)_2H^+$.

Device performance

Figure 22 shows the device performances for the recycled FTO/TiO_2 substrates reused into new solar cells. Efficiencies of 15-16% were obtained for recycled devices with short-circuit currents ranging between 19.7 and 21.5 mA $cm^{-2,}$ values for recycled devices as well as reference cells are given in the histograms. Open circuit voltages did not vary significantly between all of the tested devices. No significant drop in performance after recycling the substrates twice was observed, upon comparison to respective references (using fresh substrates) but overall small but noticeable drops in Jsc can be observed for recycled cells, possibly due to the perovskite crystallization being affected by residual solvents. All PV characteristics fall within the expected statistical deviation occurring within a batch of devices.

Efficiencies obtained fall into the expected range for $CH_3NH_3PbI_3$ based cells with mesoporous TiO_2 scaffold, higher efficiencies are typically achieved with mixed-cation, mixed-halide perovskites.

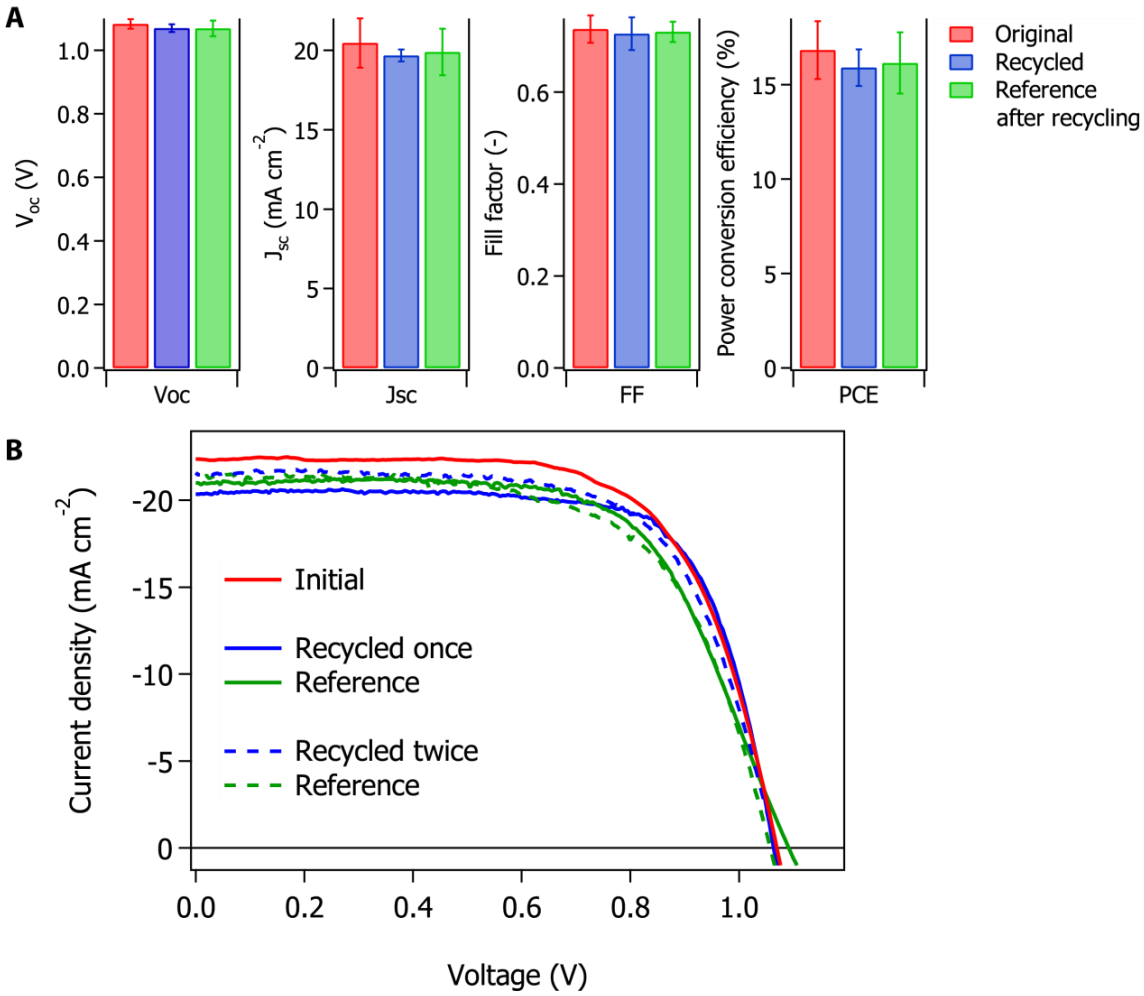

Figure 22(a) Open circuit voltages, short circuit currents, fill factors and power conversion efficiencies for a 30 samples batch of perovskite solar cells before (red) and after (blue) recycling. Green bars represent the mean values of the reference cells assembled at the same time

Figure 23 shows forward and backwards scan of an exemplary device before and after undergoing the recycling process. No significant increase in hysteresis of jV parameters can be observed.

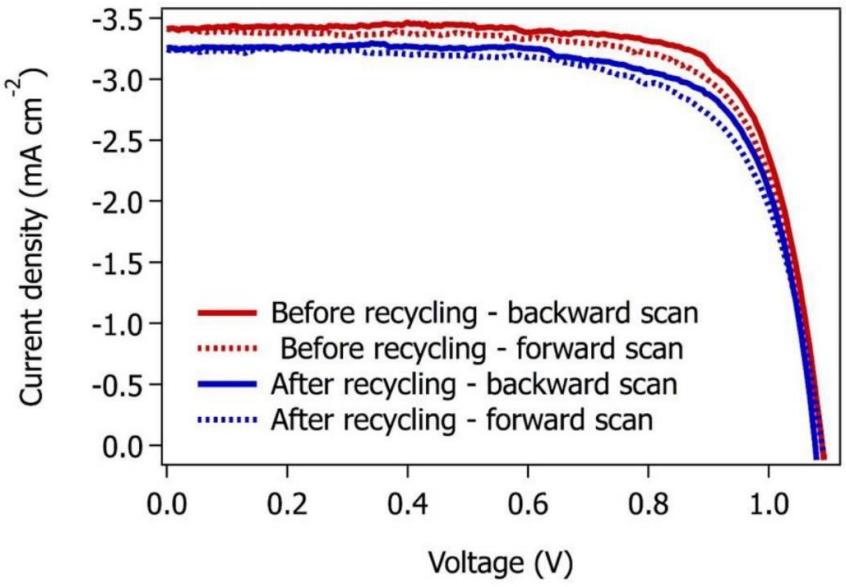

Figure 23 Hysteresis of jV characteristics of device before and after recycling

Encapsulation

With perovskite PV still in the R&D stage, it is difficult to predict how perovskite PV modules will be designed for large-area applications if they meet the market. The geometry of the wiring as well as the use and design of rigid frames will greatly determine design and success of dismantling processes.

To the best of our knowledge, there are no universally applied recycling processes for any type of PV modules today, but several processes have been developed on the lab scale and life-cycle analyses on silicon panel recycling including end-of-life stages have been undertaken.[88–92]

Common encapsulation used in silicon PV panels for example, relies on laminates of glass and ethylene vinyl acetale sheets (EVA) with aluminium frames for added stability.

Frame and wiring can be detached manually and sealed edges could be cut off mechanically. The possibility of direct deposition of the working electrode on sturdy glass substrates could prove an advantage in mechanical processing as the devices can themselves provide considerable structural integrity, other than, for example, brittle silicon wafers.

If scratches on the electrode surface are avoided in the dismantling process, it is unlikely for encapsulation to have a negative impact on the performance of recycled working electrodes as TiO_2 is both thermally and chemically highly stable, offering the possibility of both thermal as well as wet-chemical processing for removal of encapsulation residues.

Overall, it will be imperative to develop encapsulation techniques specifically for PSC devices that not only protect the active materials from moisture, air and dust but also meet strict requirements for mechanical stability, (e.g., those defined in ASTM E1830-15 Standard Test Methods for Determining Mechanical Integrity of Photovoltaic Modules) but at the same time offer ease of dismantling.

3.3 Limitations, Future Work and Possibilities

Although through the work presented in this chapter it could be demonstrated that PSCs in general, and TiO_2 substrates in particular offer potential for recycling at their end-of-life, the process developed here can only be seen as a proof-of-concept. It does carry a significant number of flaws that would inhibit its large-scale use in both research laboratories and industry alike. While some issues have already been solved in the meantime since publication in 2017 or by other research groups in the field, others are less likely to be easily solved.

Firstly, the process as it is described in this chapter is performed on relatively clean, un-encapsulated devices. While this may be suitable for a research environment where the main motivation for recycling is to save material, EoL PSCs are likely to be encapsulated and contaminated after years of exposure to pollen, rain, snow and other elements. The FTO sheet with the active materials on its surface would have to be mechanically separated from the encapsulate, all the while ensuring that the coated surface receives no scratches or other damage. To facilitate this is the most rational way, modules would have to ideally be designed for dismantling and specific recycling treatments. While some legislative incentives are emerging[93], it is questionable weather this would actually be taken into consideration by manufacturers, considering the volatility of the PV market.

Secondly, minimal contamination has to be ensured. If chemicals (particularly liquid solvents) used in a hypothetical recycling plant are to be fed back into the recycling process or are to be used in the manufacturing of new panels, contamination by foreign molecules, particles or other entities must be avoided to achieve reproducible results.

Contamination by glass sharps would greatly increase the risk of damaging the TiO_2 surface. As it is crucial for the feasibility of this particular approach which is based on re-using patterned substrates, any factor posing a risk for damaging the TiO_2 must be kept to a minimum.

Aside from these mechanical processing considerations, the most obvious and at the same time most important flaw of the process introduced here is its reliance on organic solvents, including chlorobenzene (CB), highly flammable isopropanol and DMF, which entails multiple issues. Chlorobenzene is toxic to both humans and the environment and its use should be limited to absolutely necessary processes. For HTM dissolution and metal cathode recovery, this solvent can be replaced by anisole which, in our pilot experiments led to fast dissolution of the HTM comparable to that of CB. Leaving aside workplace safety related issues such as legal exposure limits, the use of solvent baths also may not be economically viable. Large amounts of liquid are required to fully immerse a panel and it is not clear how often a bath could be re-used before becoming unacceptably contaminated yet. High cost of not only purchase but also disposal of large volumes of chlorinated and/or flammable solvents poses a further hurdle to the implementation of the presented approach. Figure 24 below, adapted from Capello et al. shows results of a life-cycle assessment on a range of commonly used solvents in industrial production including corresponding two different end-of-life treatment options[94]. The authors assessed both the environmental health and safety (EHS) as well as the emissions and resource use of the entire solvent life cycle.

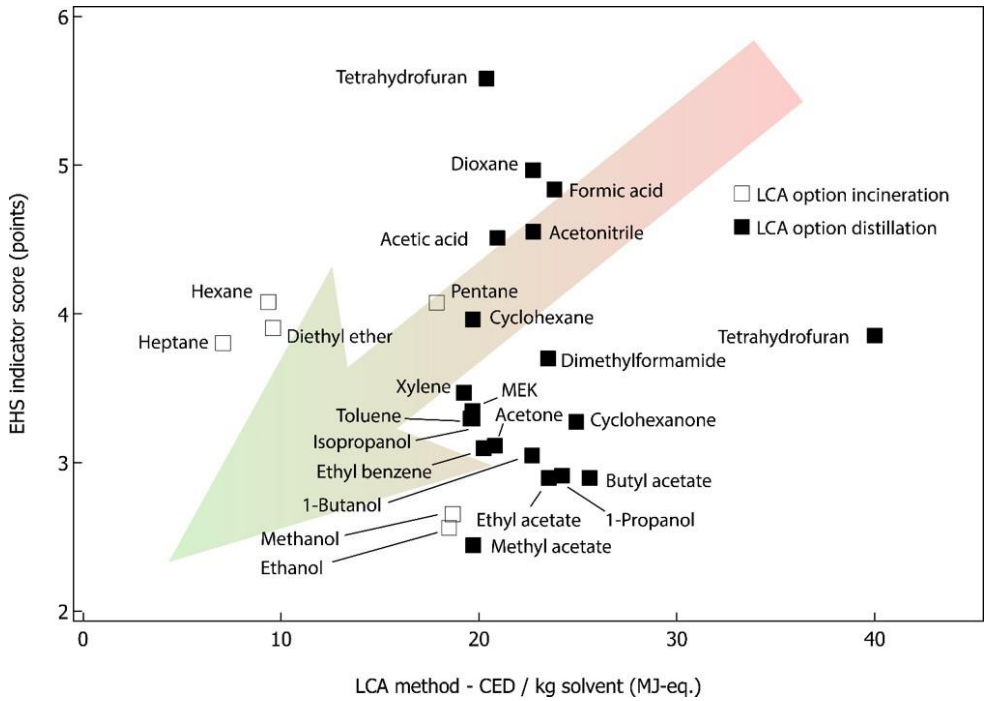

Figure 24 Life-cycle assessment of organic solvents, adapted from [94]

Overall, the results obtained show that alkanes and some alcohols have the best environmental performance. DMF, which to date is the most successfully used solvent in fabrication of perovskite layers, is shown to be not environmentally favourable. Table 2 shows results of solvent usability evaluation for industrial applications by three selected companies; Pfizer, Glaxo-Smith Kline (GSK) and Sanofi, applied to the main solvents used in PSC fabrication today. While the conclusions on individual solvents vary between companies, verdicts on most relevant solvents are similar. DMF is clearly undesired by all three companies and diethyl ether, which is used in MAX synthesis and purification, is even banned at Sanofi. Substitutions for these two solvents will likely have to be found before large-scale PSC fabrication can commence. Conclusions on acetonitrile differ greatly with GSK finding major issues in its use and Sanofi listing the same chemical as "recommended" and even DMSO, identified as environmentally friendly above, is not a preferred solvent.

Table 2 Conclusions compiled from solvent selection guides for main solvents used in PSC fabrication

Solvent	Pfizer	GSK	Sanofi	Purpose in PSC
Ethanol	Preferred	Some issues	Recommended	Spray pyrolysis
Toluene	Usable	Some issues	Substitution advisable	Solvent for HTM, Antisolvent treatment
DMSO	Usable	Some issues	Substitution advisable	PbX_2 solvent
DMF	Undesirable	Major issues	Substitution requested	PbX_2 solvent
Acetonitrile	Usable	Major issues	Recommended	Solvent for HTM, dopant, antisolvent
Diethyl ether	Undesirable	Major issues	banned	MAX synthesis

3.4 Recycling with eco-friendly solvents

Comparisons between various solvents for MAI dissolution presented in Table 1 show that water exhibits excellent segregation efficiency and can be used to replace isopropanol. Lead iodide is soluble in strong mineral acids such as HCl which could technically be used to replace DMF in the last dissolution step. While HCl as strong acid requires specialized handling procedures, particularly in a large-scale industrial process, it is not (eco)toxic per se. Another advantage of using this or a similar mineral acid is that extensive cleaning to remove residuals from the previous recycling step would not be necessary as long as the substrates are dried before immersion into the acid bath. As TiO_2 is chemically inert, exposure to acids is unlikely to chemically damage the surface. DMSO has been identified as another environmentally friendly solvent and can be used to feasibly remove the residual PbI_2 layer[95]. With its high boiling point of 189°C and low vapour pressure at standard conditions, additional measures to remove residues of the solvents are likely to have to be implemented.

Preliminary experiments carried out replacing CB with Anisole, IPA with water and DMF with 2M HCl rendered encouraging results. Full devices were dipped into Anisole to dissolve the HTM and remove the gold contact, followed by immersion into deionized water for about 120s, which led to clean PbI_2 surfaces, showing its characteristic hexagonal, thin platelets. The PbI_2 was finally removed from the mesoporous TiO_2 by immersion into a 2M solution of HCl in H_2O until transparent films were obtained. The entire process with replaced solvents was only slightly more time consuming than the original process reported. Electron images showing the PbI_2 and TiO_2 surfaces obtained in the process are shown in the following figure. Both surfaces are uniformly clean and show no signs of cracking, delamination or other damage through the solvent treatments.

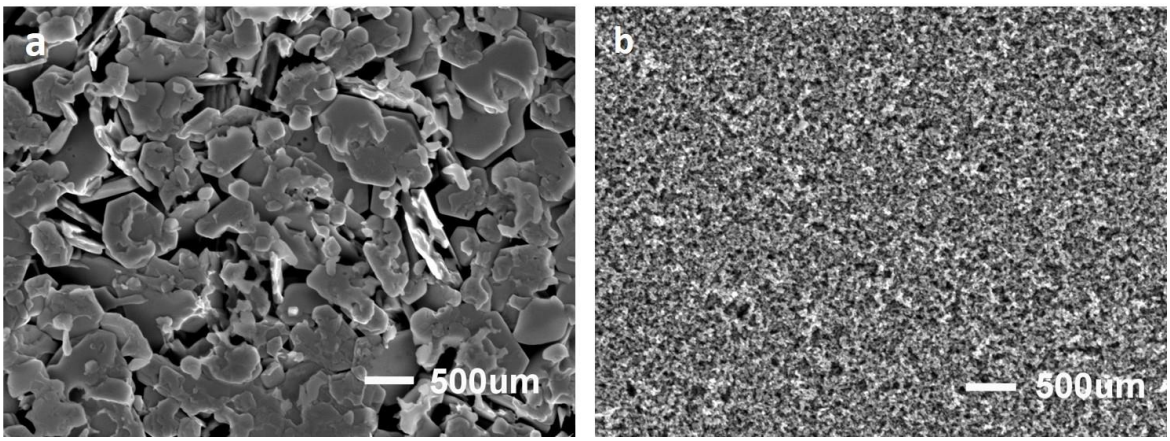

Figure 25 Scanning electron micrographs of a) PbI_2 surface formed after immersion in Anisole and water and b) clean mesoporous TiO_2 surface after immersion into HCl

Leaving all chemical aspects aside, this particular recycling process may require a high degree of manual labour. While pilot recycling processes such as those developed at First Solar (see chapter 3) can be automated to a large degree, preserving the integrity of the FTO/TiO_2 sheet is likely to be difficult or expensive to automate. In order not to face the fate of the recycling process developed by *Deutsche Solar,* which had to be abandoned in the development stage due to excessive labour cost in Germany, appropriate recycling sites would have to be identified. [96] Another factor that has to be considered when assessing the economic and ecological feasibility of large-scale recycling of PSC panels is transport to and from the recycling site. A detailed cradle-to-cradle LCA is crucial to be carried out in order to make qualified predictions about the recycling potential of PSC panels.

3.5 Conclusion

A rapid, highly selective model recycling process for PSC devices has been developed. Valuable components could be extracted and collected for recycling into new PSCs or valued in other applications. By repeating the sequential recycling process, it was demonstrated that efficiencies rivalling those obtained using fresh substrates can be easily attained from reused substrates. Fabricating solar cells from recycled materials can drastically reduce both fabrication cost, time and environmental impact. Use of recovered materials will have a positive impact on environmental assessment of PSC technology and may make this technology even more competitive. Several solvents used in lab-scale PSC fabrication today will likely have to be replaced by more industry-compatible alternatives before large-scale production can take off.

3.5.7 Methods and Materials

Device fabrication

All chemicals were used as received without further purification or treatment unless explicitly stated.

Fluorine-doped tin oxide (FTO) glass NSG10 (Nippon Sheet Glass 10 Ohm square) was cleaned in a sonication bath of water with the addition of 2% in weight of Helmanex for 30 minutes. The substrates were rinsed in water and ethanol.

30-nm TiO_2 compact layer was deposited on FTO via spray pyrolysis at 450 °C from a precursor solution of titanium diisopropoxide bis(acetylacetonate) in anhydrous ethanol. After the spray, the substrates were left to cool down to room temperature. A mesoporous TiO_2 layer was deposited by spin coating for 20 s at 4,000 r.p.m. with a ramp of 2,000 r.p.m. s^{-1}, using 30 nm particle paste (Dyesol 30 NR-D) diluted in ethanol to achieve 150- to 200-nm-thick layer. After the spin coating, the substrates sintered again at 450 °C for 30 min under dry air flow. After cooling down to 150 °C, the substrates were transferred in a dry box for the deposition of the perovskite films.

The perovskite films were deposited from 1.22 M precursor solution of $MAPbI_3$ in anhydrous dimethylsulphoxide. The perovskite solution was spin coated in a two-step program at 1,000 and 6000 r.p.m. for 10 and 30 s, respectively. During the second step, 100 µl of chlorobenzene was poured on the spinning substrate 10 s prior the end of the program. The substrates were then annealed at 100 °C for 1 h in Dry air-filled glove box.

After the perovskite annealing, the substrates were cooled down and a spirofluorene-linked methoxy triphenylamines (spiro-OMeTAD, from Merck) solution (70 mM in chlorobenzene) was spun at 4,000 r.p.m. for 20 s.

The spiroOMeTAD was doped with bis(trifluoromethylsulfonyl)imide lithium salt (Li-TFSI, from Aldrich), tris(2-(1H-pyrazol-1-yl)-4-*tert*-butylpyridine)- cobalt(III) tris(bis(trifluoromethylsulfonyl)imide) (FK209, from Dyenamo) and 4-*tert*-Butylpyridine (TBP, from Aldrich) The molar ratio of additives for spiroOMeTAD was: 0.5, 0.03 and 3.3 for Li-TFSI, FK209 and TBP, respectively. Finally, 70–80 nm of gold top electrode was thermally evaporated under vacuum using ca. 360mg of gold tears.

Water purification

A commercial ion-exchange resin was used to remove remaining lead contamination from H_2O used for MAI dissolution. Amberlite IR 120 hydrogen form (Sigma Aldrich) was washed repeatedly in deionized water and EtOH and dried in a vacuum oven at 60°C for 16h. 1g dried resin was added per 30 ml solvent in a round-bottom flask and stirred at room temperature for 16h. The water was filtered using hydrophilized 0.2µm PTFE syringe filters to remove Amberlite residues for analytical purposes.

ICP-MS

All lead assays were performed using an aqueous solution of tetrabutylammonium hydroxide (1% wt), Ethylenediaminetetraacetic acid disodium salt (NaEDTA, 1.25% wt) and bismuth nitrate (0.3ppm or 0.6ppm Bi) to provide an internal calibration. All lead contents were extracted from the integrated signal of 208Pb and 209Bi, calibrated using solutions of 0.05ppm, 0.15ppm and 0.3ppm Pb and 0.3ppm Bi. The lead source for the calibration standards was the same PbI2 as the one used for the devices, to avoid fluctuations in isotopic distributions. All measurements were done on an Agilent 7700x ICP-MS system and the same matrix was used for all the samples.

Devices (2.5x1.5cm) were immersed into 10mL of anhydrous chlorobenzene in a round bottom flask, until the gold was removed and the HTM layer was dissolved. 5mL of the resulting solution was pipetted out and dried by rotavapory evaporation. The remainder was dissolved into 0.5mL of N, N-dimethylformamide and 10mL of the aqueous solution described above. The same process was repeated for the dissolution of the organic component using ethanol, water, isopropanol or methanol. PbI2 was removed from the substrate by dropping 0.5mL of N, N-dimethylformamide onto the substrate followed by dilution into 10mL of the matrix. The resulting solution was further diluted 100 fold for ICP-MS measurements.

Structural characterization

Thin film X-ray diffraction patterns were collected on a PANaltytical MPD Pro diffractometer using Cu K_α radiation at 40mA and 45kV.

PV device testing

The solar cells were measured using a 450-W xenon light source (Oriel). The spectral mismatch between AM1.5G and the simulated illumination was reduced by the use of a Schott K113 Tempax filter (Präzisions Glas & Optik GmbH). The light intensity was calibrated with a Si photodiode equipped with an IR-cutoff filter (KG3, Schott) and it was recorded during each measurement. Current–voltage characteristics of the cells were obtained by applying an external voltage bias while measuring the current response with a digital source meter (Keithley 2400). The cells were masked with a black metal mask (0.1225 cm^2).

X-ray fluorescence

XRF spectra were collected on a Fischerscope x-ray XAN with tungsten nickel anticathode.

4 The End-of-Life of Perovskite PV

This chapter is an adaptation of the article “The End-of-Life of Perovskite PV” Jeannette Kadro and Anders Hagfeldt, published in Joule, 1, 1, September2017.

Authors: Jeannette Kadro and Anders Hagfeldt

Abstract

Awareness of the finite nature of fossil fuels and their impact on climate and environment as well as concerns about potential unstable supply have led to implementation of programs promoting renewable energy in many parts of the world. Rapid increase of the deployment of photovoltaic installations since the beginning of the century has led to the global capacity exceeding 220GW today. Projections foreseeing growing deployment rates in large markets such as the US and China show that PV installations will be an important asset in facilitating the development of a more environmentally sustainable world economy. Rapid increase of PV deployment rates today will lead to waste PV modules representing an important portion of the electronic waste of the future. With lifetimes of commercial PV panels typically exceeding 20 years, large numbers of decommissioned panels can be expected by the middle of this century and efficient end of life treatments will be needed to recover valuable components.

Perovskite solar cells were first reported only half a decade ago and improvements in efficiency of lab-scale devices have been achieved at unprecedented pace. Efficiencies exceeding 20%, ease of fabrication as well as flexibility in choice of materials have spurred widespread interest and high hopes in this technology. Like any other energy conversion technology, perovskite solar cells are not without drawbacks; material instability in combination with an absorber material relying on soluble lead halides have been frequently pointed out. While published LCAs have found the environmental impact related to the lead halides to be surprisingly small, limited panel lifetimes have been identified as key factors limiting their environmental competitiveness with other PV technologies. Considering the very early stage of PSC research, breakthroughs solving the device lifetime issues are far from impossible. This mini review discusses some important environmental, regulatory and practical aspects potentially arising at the end of life of decommissioned perovskite solar cells.

4.1 Introduction

In 2014, the global electronic and electric waste (e-waste) volume reached an unprecedented41.8 million metric tons. Solar panels today make up only a small fraction of all waste electric and electronic equipment (WEEE) as less than 1% of the total 222GW installed met their end of life.[34] As installed capacity is projected to grow 20-fold by the middle of this century, particularly due to stark growth in markets like China, India, the US, Japan and Germany, waste stemming from PV modules can equally be expected to increase with a 20-30-year lag. Based on today's installations, significant growth of waste from silicon panels meeting their end-of-life 30 years after installation is anticipated to occur in the early 2030s. By 2050, waste PV modules could make up for as much as 10% or 60 million tons of all e-waste produced globally, as illustrated in Figure 26.

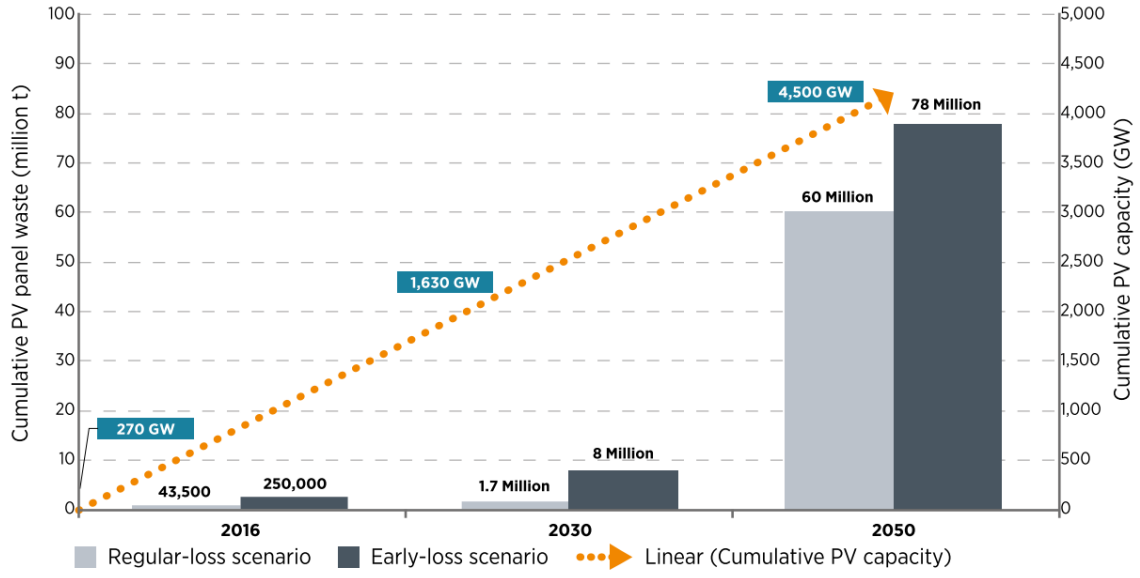

Figure 26 Estimated cumulative global waste volumes (Mt) of end-o-life PV panels, reproduced from the International Renewable Energy Agency

Possibilities for value generation from waste solar panels has been addressed by numerous studies. It has been estimated that, theoretically, raw materials extracted from the panel waste can result in cumulative value of 450 million USD by 2030, equivalent to the value of the materials needed to produce 60 million new panels, delivering 18GW with today's state of the art technology [34,97,98].
Today, recycling rates for PV panels are negligible, owing to both lack of economic incentive as well as the small waste volumes that make exhaustive recycling or re-use efforts less feasible [99].

Table 3 Market share of PV panels by technology groups (2014-2030) Technology, Based on Fraunhofer Institute for Solar Energy Systems (ISE) (2014), Lux Research (2013) and IRENA, adapted from ()shows current and projected market shares of PV panels grouped by technology The most commonly installed type of PV panel today is based on crystalline silicon (c-Si) wafers. It is used both in solar farms and residential rooftop applications. Crystalline silicon and thin film technologies (CIGS, CdTe and CIS) make up for about 90% and 10% of the market, respectively. Yet, other promising technologies are expected to nibble some market shares in the coming years.

Table 3 Market share of PV panels by technology groups (2014-2030) Technology, Based on Fraunhofer Institute for Solar Energy Systems (ISE) (2014), Lux Research (2013) and IRENA, adapted from ()

Technology		2014	2020	2030
Silicon based (c-Si)	Monocrystalline	92%	73.3%	44.8%
	Poly-or multicrystalline			
	a-Si (amorphous/microamorph)			
	Ribbon			
Thin-film based	Copper indium gallium (di)selenide (CIGS)	2%	5.2%	6.4%
	Cadmium Telluride (CdTe)	5%	5.2%	4.7%
Other	Concentrating PV (CPV)	1%	1.2%	0.6%
	Organic PV/dye-sensitized cells		5.8%	8.7%
	Advanced crystalline silicon		8.7%	25.6%
	CIGS alternatives, heavy metals (e.g. perovskites), advanced III-V		0.6%	9.3%

Lifetimes typically covered by manufacturer warranties for conventional silicon panels are 20-30 years but in practise, lifetimes may exceed this. The PV market being very dynamic and lifetimes of PV panels spanning decades, manufacturers may exit the market before their product meet their end of life. Markets

like the EU have passed regulations that guarantee that waste PV panels will be dealt with regardless, which will be discussed in section 4.3.

Aside from fulfilling existing or future regulations, there can be multiple incentives for investigations and investments into PV waste recycling. Solar panels contain an array of valuable components that may be recycled without PV specific processes. These include aluminium frames, stainless steel railings as well as junction boxes and other periphery. The case of CdTe panels shows that the scarcity of raw materials can also be a major driver for the development of material recovery processes and take-back systems.

There are many opportunities for potentially reducing the energy payback time (EPBT) of PV panels through improved recycling schemes. Efficient material recovery processes and re-integration of energy-intensive components of a waste panel into new units can reduce both process energies and environmental impacts at raw material production sites. Several review articles on recycling processes for Silicon PV have been published and numerous research groups and commercial entities have been addressing these questions [90,100].

Aluminium frames and stainless steel railings typically make up a significant percentage of the installation weight are ubiquitous to all types of PV panels and their recovery and recycling is not technology specific. All types of PV panels contain valuable and hazardous materials, some of which offer the potential for recovery and re-use. Aside from silicon wafers or valuable semiconductors such as in CIGS based cells, PV panels frequently contain valuable metallic components, such as metallic back-contacts and leaded solders. Some research efforts have been undertaken regarding recovery of silver from waste panels[101,102].

Fluoropolymer back sheets (used in older PV installations) are highly stable materials that are designed for maximum durability in harsh conditions[103]. Consequently, they do not degrade in landfills and the toxicity of their decomposition products is a major challenge during thermal recycling. Other polymer components contained in a panel can frequently be thermally recycled[104]. Repair and re-use of damaged panels may result in new business models in developing and transitioning countries where manual labour comes at low costs.

Reduced material use while maintaining performance is desirable in any technological application. In the case of perovskite solar cells (PSCs), the weight of the electrically active component is similar to the one of current thin film technologies, usually so low that the panel weight is dominated by the glass substrate or superstrate, encapsulation materials and other components necessary for structural integrity.

Components comprising the Balance of System (BoS), i.e. wiring, junction boxes, inverters and mounting structures are not different from other commercialized solutions.

This chapter is structured in four sections. The first section gives an introduction to perovskite solar cells, the materials embedded and discusses frequently voiced concerns. Section two addresses important regulations that can affect the EoL of perovskite solar cells. Section three introduces published recycling processes and discusses results of LCAs and their implications for recycling PSCs. Section four summarizes the most important points presented in this paper and gives a brief outlook.

4.2 Developments in PSC and materials contained

Since 2012, solar to electric power conversion efficiencies (PCE) of hybrid perovskite solar cells (PSCs) have increased at an unprecedented pace, with small lab-scale devices today reaching over 21% after less than a decade of development[7,9,105,106]. Hybrid perovskites used in high efficiency solar cells are based on a hybrid combination of lead halide salts and organic cations.

Figure 27 shows a schematic cross section of a typical perovskite solar cell. PSCs typically consist of a transparent conductive oxide (TCO)-coated glass superstrate or substrate, which makes up more than 99% of the mass of an unencapsulated device. The perovskite photoabsorber is sandwiched between the electron transport layer (ETL) and hole transport layer (HTL). The ETL can be of organic or inorganic nature and typically is around 100nm thick. The perovskite layer thickness generally does not exceed 500nm. Similarly, hole transport materials (HTM) can be either organic or inorganic with thicknesses similar to those of the perovskite and the ETL. The cells are completed with a counter electrode: the best performing PSCs rely on noble metals (deposited by thermal evaporation) but reports of carbon counter electrodes are not uncommon. The thickness of the entire cell excluding the glass support typically does not exceed 1µm.

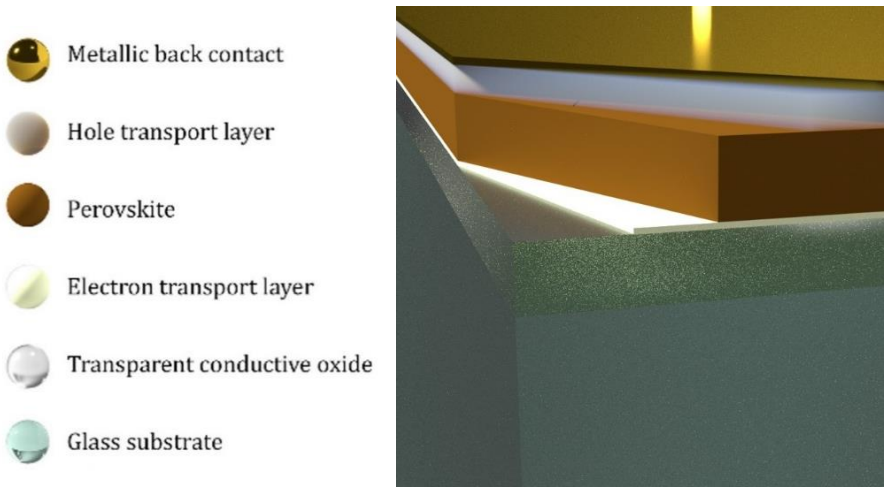

Figure 27 schematic cross-section of typical PSC device

Numerous reviews have been published discussing the properties of the hybrid perovskite material, the physics of PSCs and device architecture[14,15,107]. Long-term device and material stability in realistic conditions is currently one of the main limitations and concerns addressed by many research groups and reviews[108–112]. Improvements of stability of PSCs have been under intense research and advances have been achieved through a multitude of approaches, including ETL free [113] cells , use of dopant free HTM [114] as well as use of HTMs with fluorinated dopants [115], variations of the metal oxide [116], multi-cation approach[117] , design of planar, inverted structures [118] and even cells stable at 100°C have been reported[119]. As a consequence of the reported sensitivity to even low levels of moisture, efficient and stable encapsulation to increase the lifetime for PSCs is a very crucial aspect of cell design and various solutions have been presented and tested [120–123].

Another drawback of the technology to date is the use of lead halides in the active material, even if the active material is likely to comprise less than 0.5% of the entire cell mass if a glass substrate is used. Perovskites with reduced lead content achieved by tin substitution in all-inorganic and hybrid perovskites have been reported[124–126]. Regardless, the development of tin based hybrid perovskite photoabsorbers has been facing challenges and are problematic for various reasons. Aside from the instability of the Sn^{2+} oxidation state in air, devices based on tin perovskites have been suffering from comparatively low efficiencies[127]. In addition, strong concerns about the environmental impact and toxicity of organic tin compounds has been voiced [65,128]Published Life Cycle Assessments (LCA) identified tin-based PSCs to be more environmentally problematic than their lead-based analogues[128]. Other completely lead free perovskite photoabsorbers have been reported and are under intense investigation but to date have not achieved efficiencies rivalling those of the most commonly used lead halide based materials[24–26,129–131].
The chemical composition of the active material make-up can and is likely to undergo further development but comparison between early and state-of-the-art cell design shows that the device composition has not significantly varied since the early reports of perovskite solar cells. [9,63,117,132–137].

A potential market entrance point for large-scale energy applications is to integrate PSCs as a top-cell in tandem devices with crystalline silicon cells[138–140].
Aside from numerous academic research groups, the company Oxford PV is pursuing the development of this technology[23].

The composition of a marketable PSC is unknown to date, but the unique properties of the perovskite material make several layouts possible, including the use of organic ETL and inorganic HTM, HTM or ETL-free panels as well as the use of flexible polymer substrates.

4.2.1 Potential Applications for PSCs

From a technological standpoint, there is a potentially broad field of applications for perovskite solar cells. Fabrication of flexible cells [141–144] offers possibilities for unconventional applications such as flexible and rollable solar cells for travel, temporary or emergency use, solar windows, lightweight or portable chargers for small electronic devices. The use of ultra-lightweight cells with high power-to-weight ratios is interesting for applications where weight is a primary concern such as drones or solar powered small airplanes. Impressively high power-to-weight ratio has been achieved for flexible lab-scale PSCs using a lead halide based absorber[123].

On the other hand of technical considerations, there exists the possibility that the lead content in PSCs might reduce consumer acceptance, even if it remains below the legally acceptable threshold. For consumer electronics in the EU, lead content must not exceed 0.1% in a homogenous material[27], the relevant directive will be discussed in Section 3. Depending on the interpretation of the concept of homogeneity, lead contents in current PSC design can be above or below this threshold. Even so, consumer acceptance may represent a lesser issue when PSCs are deployed in large-scale solar parks.

Materials embedded

Glass

Aside from organic flexible thin film cells, all PV panels today contain large amounts of float glass to provide both structural integrity and protection from the environment. Depending on the technology considered, glass can make up for more than 97% of the total panel mass[34]. While in thin film CdTe modules glass is used as superstrate as well as back plate, silicon panels typically comprise of only one sheet of glass and a different back support. Glass recycling is common and technologically well established.

Burrows and Fthenakis showed that the PV industry may consume as much as a tenfold of today's float glass capacity by 2030 (as opposed to ~2% today) if growth trends of PV deployment continue to grow as expected [145].

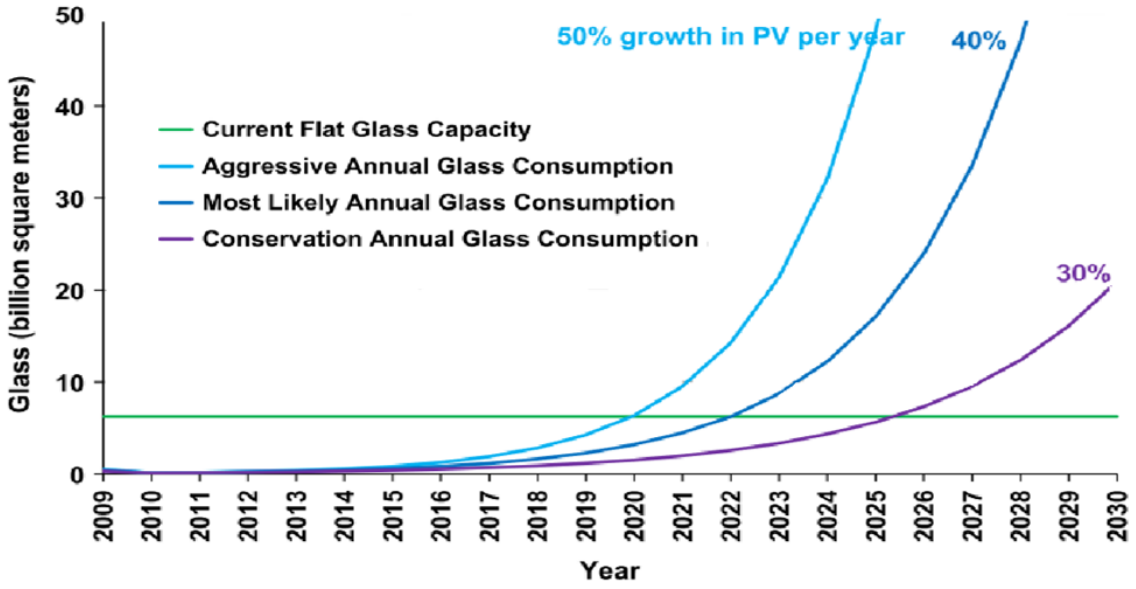

Figure 28Global flat glass use for PV and capacity in 2009. Adapted from Fthenakis and Burrows

For photovoltaic applications, low-iron glass is preferred for higher optical transmission. In case the iron content of recycled glass is too high for applications in PV panels, contaminated cullet recovered from processed end of life PV panels can be downcycled to fiberglass. In case of direct re-use of the substrate, process energy can potentially be saved and fabrication would not be affected by possible shortages or price increases projected if PV expands as predicted.

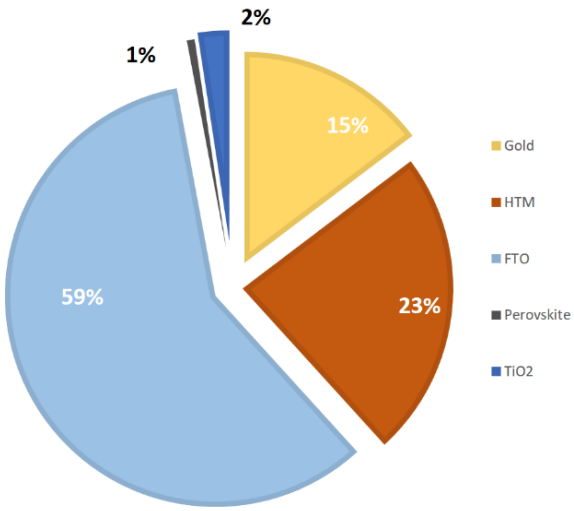

Figure 29 Estimated cost per sqm PSC module without encapsulation and BoS, adapted with numbers from ()

Aluminium

While aluminium frames and railings are not specific to PSCs, they are major contributors to the EPB, environmental impact and cost of a system. While they are not technology specific, lower efficiency modules would require larger installed capacity (when normalized to power output) and, consequently, larger amounts of aluminium. Recycling networks for aluminium are well established and significant process energy savings can be expected from the use of recycled aluminium versus virgin materials.

Lead

Aside from its sensitivity to moisture and the resulting short lifetimes, the lead content of the somewhat soluble perovskite material used in PSCs today has probably been the most commonly voiced concern regarding this technology. Absorber materials such as $CH_3NH_3PbI_3$ in lead halide based PSCs typically contain about 33% lead by weight. Considering that the absorber thickness does not exceed 500nm, the overall lead content of devices of state-of-the-art architecture is relatively small (<1g/m^2). PSCs are not the only PV technology containing lead; as has frequently been pointed out, c-silicon panels for example, typically employ leaded solder.

The major concern with regards to lead in PSCs stems from the fact that the lead halides contained are slightly water soluble and may leach into the environment and groundwater from damaged panels[73].

Assessing catastrophic failure of a potential solar farm, Hailegnaw et. Al showed in a "worst-case scenario" with exposure to simulated rain of various pH that the perovskite material will completely dissolve, leaving behind moderately soluble PbI_2[71]. The solubility constant of PbI_2 in water is $k_{sp}=9.8x10^{-9}$, which is low but still considerably higher than that of CdTe at 10^{-27}.[73] Hailegnaw et al. estimated the increase of Pb concentrations from leachate of a broken PSC panel in the model soil to be approx. 70ppm, which is moderate compared to background values in urban areas where up to 400ppm are considered "low levels of contamination"[146]. They concluded that levels of lead released into the environment would be undesirable but far from catastrophic. This estimation is based on the leaked lead spreading over the area of a potential solar farm. Estimates comparing potential lead release from PSC panels with lead emissions from coal came to similarly favourable conclusions[70].

The World Health Organization and other organizations regard lead exposure, including through drinking water as major public health concern [147,148]. There is no universally accepted safe threshold for lead exposure[149] and countries all around the globe have gone through programs promoting the elimination of leaded paint, petrol and drinking water distribution networks[148].

Children have been found to be particularly at risk of developing lead-induced, irreversible health damage, and are more susceptible to absorbing lead (higher breathing –to-body-mass-rates, hand-to-mouth contact, overall higher lead absorption rates, lower amounts of Pb expelled by the body)[150151]. In the US, main source of lead exposure of children stems from leaded paint[152].

A reduction of maximum acceptable BLLs (blood lead levels) from today 10µg/dL to 5µg/dL has been suggested for children as even low concentrations have been found to lead to severe consequences, including intellectual impairment [153–155]. Aside from this, relationships between lead exposure and delinquency have been indicated[156,157].

Consumers are rarely exposed to leaded products anymore, but the workplace hygiene - for example for mechanics handling lead acid batteries - must be guaranteed. Elevated BLL over the recommended limit of 10µg/dL are frequently found in battery recycling facilities in developing or transitioning countries where strict workplace hygiene standards are not always enforced [151,158–160] as well as US territory [161].

Significant deposits of lead ores are located in Australia, Canada, China, Mexico, Peru, Kazakhstan, Russia, and the United States [162] Lead ores can be found in politically relatively stable regions. Nearly 90 percent of primary lead ores come as a by-product of zinc and silver mining[163]

The main consumer of lead today is the lead acid battery (LAB) industry with 2.9mio tons of LABs were generated in the US in 2013, representing 1.1% of the total municipal solid waste in the US where LABs achieve remarkably high collection rates as well[164]. More than half of the total lead refinery demand is met by the recycling of spent lead, mostly from car batteries [162,165]. The main anthropogenic lead emissions stem from fuel combustion including coal[166].

Iodine

Iodine is a trace element essential to human health with a recommended daily intake of 150-250µg [167,168]. Iodine deficiency leads to severe health issues including goitre and, more severely, damages to reproduction. [168–170].

It has been estimated that about half of the world's iodine production finds its applications directly related to human health, e.g. in X-ray contrast media, sanitization products and artificial thyroid hormones [171–173]. In many of these important health-related applications, iodine is non-substitutable.

Iodine is placed 61th of 96 elements comprising the lithosphere, making it one of the scarcest non-metallic elements on earth. It is also the least abundant halogen. [174] It is contained in a small array of substances, including seaweeds, corals, sponges and waters from oil/gas well boring[175,176]. Seawater is the planet's largest iodine reserve but extraction has no economic viability[171].

The most important sources of iodine are sodium nitrate deposits, "caliche", found in Chile's Atacama Desert. Still, even in caliche ore, iodine content does not exceed 0.2%.[174]

Chile and Japan are the most important producers of iodine, accounting for ca. 91% of the market. Such strong geographical concentration of production makes the production very vulnerable to external, possibly unforeseeable factors such as water shortages (which are of concern in the Atacama Desert), floods or earthquakes (which are a concern in Japan). The production of iodine is expected to be stable but it has been argued that large increases in production volume are restricted due to particular situations at the main exploitation sites; namely restrictions on underground water use in the Atacama Desert and land subsidence in Japan[177,178]. As a result, iodine prices are volatile, e.g. in 2013, 1kg of iodine was priced at 30USD/kg after dropping from 93USD/kg[179]. In comparison, lead is traded at around 2.2USD/kg[171].

Multiple processes for recovery and recycling of iodine from waste of important applications have been developed, for example for recovery from X-ray contrast media: [180] , polarizing film production [181] and other industrial waste sources [182].

Recycled iodine makes up for about 18% (approx. 6kt) of the global market[178].

Iodine in PSCs-practicalities

At 15% PCE, a single 1GW solar farm estimated to contain 30t of Pb [71]would contain 54t of iodine. The global production in 2012 was 28 700t and the yearly demand for iodine is projected to rise to 38kt in 2020[178]. Large-scale production of PSCs could potentially affect the iodine market price and availability. Theoretically, PbI_2 can be precipitated out form leaching solution, cleaned and re-used directly to reduce use of primary iodine.
Overall, Iodine has a relatively low economic value but if large amounts of PSCs were to meet the market, manufacturers might have interest in recovering iodine from waste modules if feasible processes are available.

Tin

Tin production is highly concentrated in a small number of countries including Peru, Indonesia and China, some of which may suffer from political instability. Tin is a strategic metal with low substitution potential, while finding broad and essential applications. Security of tin supply has been of concern and the material was added to the EU report on strategic metals [77,78].
While the use of tin is not as heavily regulated as that of lead, tin is several times more expensive than lead and ecotoxicity and global warming potential (GWP) arising from tin extraction and processing have been reported to exceed that of lead by one order of magnitude[65,81]. Table 4 shows a comparison of primary energy needed for the production of six selected metals relevant in PSC production.

PSCs today contain tin in the form of F: SnO_2 in amounts similar to that of lead contained in the perovskite absorber but tin may also be required for solder in connections, depending on the design of a PSC module.

Table 4 Primary energy needed for production of selected metals

Metal	Primary energy needed for production of virgin material cradle-to-gate MJ/kg
Silver	1500
Lead	25-50
Tin	250-320
Platinum	190 000
Titanium	360-750
Stainless steel 304	57-68

Gold

Exploitation of gold is not geographically as concentrated as that of iodine or tin but price fluctuations are frequent and often unrelated to production volumes [183].

The total amount contained in a single PSC panel today is low (at 100nm thickness approx. 1.9g/m^2) but recycling of Au contained in a solar farm undergoing recycling may be feasible and should be relatively simple[184].

By weight, gold is the costliest component of PSCs and reportedly one of the major contributors to the process energy required in device production. In addition, it accounts for a significant portion of the total environmental impact of the solar cell[65,67]. In addition, gold is not the most optically suitable metal owing to its relatively low reflectivity in comparison to other metals [185].

Considering the above, alternatives to gold counter electrodes for PSCs have been explored. Carbon based counter electrodes have been used successfully in a number of cell architectures using various deposition techniques[110,186,187]. Silver is cheaper and possesses better reflective properties but can oxidize and form silver iodide when in direct contact with the perovskite material, although in cell architectures that involve hole transporting layers, there should be no physical contact between the perovskite and the back contact. Silver has been reportedly used successfully in solid state DSCs which have similar device architectures as PSCs. [188] Chromium-oxide/chromium counter electrodes have been successfully implemented in flexible, ultra-thin PSCs and has shown superior environmental stability in comparison with other metal counter electrodes [123].

One of the main strengths of PSCs technology are the small quantities of materials required in the fabrication of the active layer. Similarly, to thin film solar cells, the cell weight will be dominated by the substrate. With active layer weight estimated to be approximately 1g/m^2, PSCs are not foreseen to contain large amounts of scarce elements. Although concerns about the use of lead in PV have been voiced frequently, the amount of material required to fabricate the active layer of the cell is small compared to e.g. the amount of lead contained in common car batteries. Although elements with low substitution potential in their main applications such as tin in solder or iodine in health related application would be used in PSCs, quantities required for fabrication of PSCs are small compared to other tin and iodine containing products. Unless PSC production undergoes very rapid expansion, it is unlikely to cause supply shortages.

4.3 PV panels in the EU RoHS and WEEE Directives

The deployment on the market and the end of life of PSC panels will fall under a multitude of regulations, we limit ourselves to the two most important ones.

4.3.1 EU RoHS directive

The European Union has implemented measures to promote the gradual phase-out of hazardous materials, which are regulated under Directive 2011/65/EU on the restriction of the use of certain hazardous substances in electrical and electronic equipment ("RoHS Directive") [27].

Under the RoHS directive, lead content in consumer products is limited to 0.1% in homogenous materials, (defined as a layer of "uniform composition through- out" or one "that cannot be […] separated into different materials by mechanical actions such as unscrewing, cutting, crushing, grinding and abrasive processes"). The composition of typical perovskite absorbers as used in lab scale devices today is above that limit if the active material in the cell is considered homogenous. PSCs in their current compositions may not find their way into consumer electronics easily under this directive; the definition of what comprises the definition of "homogenous material" will be crucial for incorporation into consumer electronics sold in the EU.

On the other hand, « […] Photovoltaic panels intended to be used in a system that is designed, assembled and installed by professionals for permanent use at a defined location to produce energy from solar light for public, commercial, industrial and residential applications." are currently exempt from RoHS directive but this does specifically not extend to solar cells embedded in consumer electronics or portable systems. The Directive aims specifically not to hinder development of energy conversion systems that are not harmful: "[…] *this directive should not prevent the development of renewable energy technologies that have no negative impact on health and the environment and that are sustainable and economically viable. Exemptions from the substitution requirement should be permitted if substitution is not possible from the scientific and technical point of view, taking specific account of the situation of SMEs or if the negative environmental, health and consumer safety impacts caused by substitution are likely to outweigh the environmental, health and consumer safety benefits of the substitution or the reliability of substitutes is*

not ensured […]". While this directive does not specifically target the end of life of PSCs, it will have implementations on design and material composition for marketable PSCs in non-traditional applications. Even if an appliance is RoHS compliant, the solubility of the lead compound contained can lead to its waste being classified as hazardous, which comes with numerous implications for disposal and exportation. To classify waste as hazardous, leaching tests are typically used. For example, the threshold for lead leached from waste to be classified "non-hazardous" in the US is 5mg/L with 20:1 solid: liquid (mass) in the leachate after employing the *Toxicity Characteristic Leaching Procedure 1311* [189]. Japan enforces stricter lead limits of 0.3mg/L 1 solid: liquid (mass) [190].

While the US do not have PV specific waste management regulation, lead as a pollutant is regulated by a multitude of laws administered by the Environmental Protection Agency (EPA), including, but not limited to: *Toxic Substances Control Act (TSCA), Residential Lead-Based Paint Hazard Reduction Act of 1992 (Title X), Clean Air Act (CAA), Clean Water Act (CWA), Safe Drinking Water Act (SDWA), Resource Conservation and Recovery Act (RCRA), and Comprehensive Environmental Response, Compensation, and Liability Act (CERCLA)*

4.3.2 The WEEE Directive

The European Union is the only market with PV specific waste regulations already in place in 2017. The new Directive 2012/19/EU ("WEEE Directive") covers specifically collection, recovery and recycling targets of wastes stemming from electrical and electronic appliances[191]. The extended producer responsibility principle can affect producers shipping to the EU, irrespective of where they are based with regards to financing of recycling panels deployed in the EU. Producers are required to offer guarantees upon placing their product on the market that the costs of recycling are covered, through recycling insurances, blocked accounts or through a "*participation by the producer in appropriate schemes for the financing of the management of WEEE*". Producers are allowed to pay the recycling costs upfront (Pay As You Put, or PAYP) or to join collective compliance schemes. Under this directive, WEEE from private households is treated differently from WEEE from other users, but interpretations differ between Member States. The WEEE regulates economic aspects of recycling and ensures that PV modules will be collected but nature of recycling or other end-of-life options is not part of this directive. Criteria for acceptance at landfill sites may require pre-treatment of PV panels[192]. Finally, China has passed regulations similar to the EU's WEEE[193]- and RoHS directives (111).

4.4 PV End of Life

4.4.1 Incentives

Incentives for recycling can be multiple, including resource preservation, reduction of environmental impact, reduction of EPBT or others of purely economic nature. Avoidance of depletion of abiotic resources to ensure availability as well as to secure price stability is of particular importance in technologies that rely on scarce materials (Tellurium in CdTe and all components of CIGS absorbers) or costly (aluminium frames, other critical metals[195]). Exhaustive material recycling helps to ensure material availability and helps to shield from price fluctuations. It also reduces environmental impacts at the production site and the ones induced by raw material transport from mines to refining and processing sites. In attempts to reduce EPBT, an increase in recycling rate may be easier and more feasibly achieved than significant improvements in panel efficiency [196]. The effect of recycling on EPBT is particularly pronounced for low-efficiency modules[99].

Policy and legislation can be strong drivers to the development of take-back and recycling systems, especially in situations where economic incentives are not strongly given. The EU has adopted a Circular Economy Package defining recycling targets as well as promoting the adaptation of closed-loop recycling systems [197,198].

4.4.2 Commercial Panel Recycling Solutions today

When treated separately, c-Si panels are typically processed through physical means which result in crushed Si wafers and glass cullet. [89,100,199]. Chemical and thermal means can be employed to process the organic components. [200] *Deutsche Solar* pursued development of a recycling process recovering wafers and re-incorporating them into new modules but to the best of our knowledge, the process has not been implemented in large scale as it was found not to be cost-effective[96,201].

PVCYCLE is a voluntary recycling and collection scheme established in Europe and expanding to other parts of the world, including Japan. It offers take-back and recycling of any kind of PV module, including thin film technologies. PV CYCLE claims breakthroughs in PV module recycling with a 96% recycling rate[202].

CdTe panels are notably recycled by the main manufacturer*, First Solar,* which owns a production size plant and is planning to add recycling plants to each of their production sites [203]. The take-back and recycling is organized through a pre-funded scheme that includes provision of transport and packaging material. The recycling comprises a multi-step process where the modules are reduced in size, glass and laminate are mechanically separated and the semiconductor is removed by dissolving in acid and peroxide. The metal rich solutions resulting are precipitated out and ultimately processed and refined. The glass cullet obtained in the process is recovered, cleaned and re-sold. [203] The company claims to achieve 90% recycling of glass and 95% of the semiconductors[204]. In the case of CdTe, the scarcity of tellurium is a major driver in the development of recycling processes as PV applications have been estimated to account for 40% of the global tellurium use[183]. The producers have an inherent interest in reducing tellurium cost and securing availability[7434]. Published estimates foresee an EPBT reduction of 0.5 years for exhaustive material recycling for CdTe panels [196].

3rd generation PV including OPV has a negligible market share today and waste volumes are consequently small. To the best of our knowledge, there are no established recycling or take-back systems in place specifically for OPV. Nevertheless, some efforts for the development of recyclable OPV devices have been undertaken, for example by employing cellulose based substrates [205]. Generally speaking, life cycle analyses make a strong case for PV recycling in general, particularly for low-efficiency modules where recycling can have pronounced effects on EPBT reduction. Even for c-Si panels, up to 1.1 years of EPBT reduction were foreseen for exhaustive recycling [196].

4.4.3 Life Cycle Assessments (LCA) of PSCs

LCAs analysing various architectures and fabrication processes of PSCs show overall relatively positive outcomes but all studies published point out short panel lifetimes as a limiting key parameter. None of the published cradle-to-gate studies found significant contributions to any impact category stemming from the lead halides in particular. The results from published LCAs come to greatly varying conclusions regarding the expected EPBT as well as GWP of PSCs. Figure 3 shows EPBTs and GWP found in selected

LCAs on solid-state PSCs. The study by *Zhang et al* is not included as the cells they modelled rely on a liquid electrolyte and this device architecture has not undergone promising development so far[68]. All LCAs on PSC-only panels find the EPBT expected to be relatively low in comparison with established technologies. Mean EPBTs of commercial PV technology are highest for monocrystalline Silicon with 4.1 years and comparatively low for CdTe at 1.0 year [206].

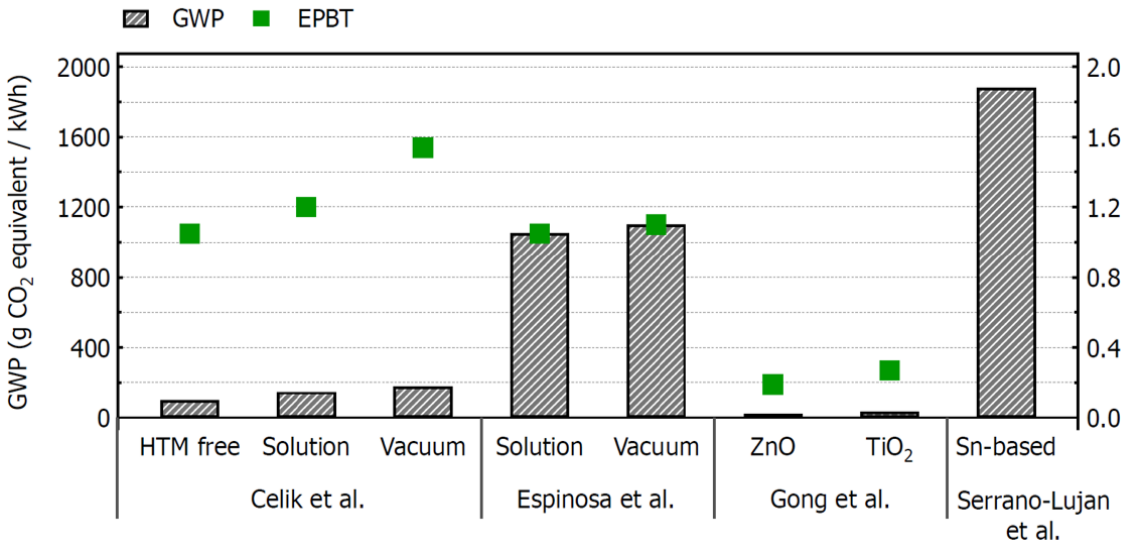

Figure 30 comparison of EPBT and GWP obtained in selected published LCAs, adapted from Celik et al [207]

The variations in estimates for GWP and EPBT reflect the different parameters modelled such as electricity mix, module size, panel efficiency, cell architecture and fabrication process, which varied considerably between the studies.

Espinosa et al. compared vapour and solution based deposition routes for the fabrication of two different types of perovskite cells [66]. The solution-processed device comprised of glass/FTO, TiO_2 ETL, solution deposited perovskite, spiro-MeOTAD as HTM and a silver counter electrode. The second architecture modelled used glass/ITO substrates, PEDOT: PSS as organic ETL, vapour deposited perovskite, PCBM as HTM and an aluminium counter electrode. In both cases, the main environmental impacts stem from the perovskite layer (materials and deposition). Interestingly, the contribution to human toxicity effects is dominated by CH_3NH_3I and its synthesis, not by the soluble lead halides. This study found environmental impacts dominated by electricity required in both solution-and vacuum perovskite depositions.

Gong *et.al*[67] considered two different solution processed lead halide based device architectures with basic PET encapsulation. They considered currently employed solution based processes such as spin-coating. Their overall assessment showed the dominant contributions of silver and gold back-contacts to the carbon footprint and primary energy consumption. In terms of processing, the TCO deposition, thermal evaporation of the back-contact and the sintering of the electron transport layer were identified as the main contributors to carbon footprint and primary energy consumption. As gold is likely to be replaced by a more economical as well as ecological alternative in large-scale production, these contributions may not be that critical once the technology reaches a more mature stage. It is encouraging to note that the study found minor direct effects from the perovskite material on all their fourteen analysed impact categories, including human toxicity. This study also comes to a very positive outlook on EPBTs for their modelled perovskite modules, reaching EPBTs as short as 0.22 years.

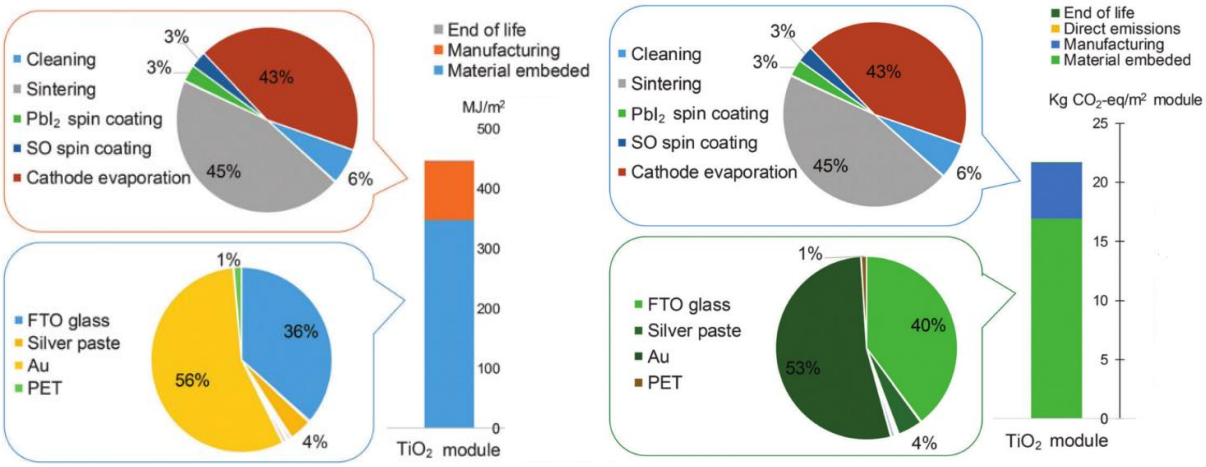

Figure 31 Distributions of the primary energy consumption (left) and carbon footprint (right) for manufacturing of TiO2 based perovskite module. Contributions less than 1% are not shown in the pie chart. Reproduced from Ref. 67 with permission

Most recently, Celik *et.al* published an LCA modelling only scalable processes ,such as inkjet printing and vacuum deposition, for the fabrication of PSCs with moderate efficiencies [207]. The study employed an inorganic HTM to replace the commonly used spiro-MeOTAD and a printed or vacuum deposited perovskite layer. Noble metals were replaced by carbon paste or MoOx/Al layers. The environmental impacts of production were found lower as compared to monocrystalline silicon but due to the expectedly shorter lifetimes of the PSCs, energy requirements were not found to be lower than expected for other commercialized solutions. The impact expected from unit electricity supplied was estimated to be higher than that of all commercial PV technologies. A detailed comparison of the modelled PSCs and commercially available PV technologies is shown in Figure 32, reproduced from Celik et al.. Overall, all modelled perovskite solar cells yielded 10-30% lower manufacturing impact as opposed to mono-Si but due to the acute differences of device lifetimes, the overall impact of PSCs remains significantly higher. They estimated that, depending on cell architecture and production processes, a PSC module would require lifetimes of 26-40 years at 15% efficiency to be environmentally competitive with traditional PV technologies.

The authors point out that the use of solvents was found to result in high marine eutrophication impact while the impact of lead was found negligible in that aspect. Tin use and waste stream were identified as main contributors to impacts associated to materials. This study found EPBT to be 1.0-1.5 years based on fabrication process and architectures modelled.

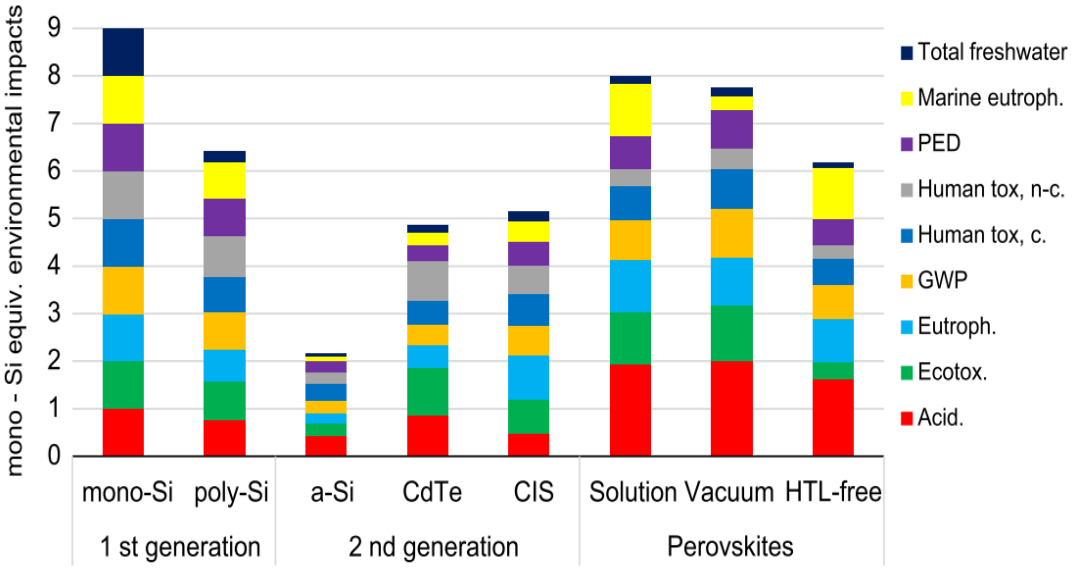

Figure 32 reproduced from (207) shows a comparison of perovskite devices with commercial PV technologies when normalized to mono-Si for selected impact categories. Note that GWP and PED stand for global warming potential and primary energy demand. Within each impact category, the impact (per 1m2/module) was divided by the impact of mono-Si. For mono-Si, the bar height is unity for each category. For nine impact categories, the total impact for mono-Si is given as nine units.

Serrano-Lujan et al. extended the system boundaries of their LCA to account for the end of life of their modelled solution processed lead halide based PSCs with PET substrates [65]. Two different scenarios were investigated; cells were either landfilled or incinerated with subsequent lead recovery from the ashes. In the landfill scenario, 70% of the lead contained was expected to leach out while after incineration, 98% of the lead was assumed to be recovered from ash. Landfill resulted in higher scores in all environmental impact categories considered as compared to incineration. While the lead content in the cells did not represent strong impact on human health effects (cancer and non-cancer effects) in the cradle-to-gate analysis, contributions from lead did pose significant risk in the cradle-to-grave scenario when landfill was chosen as end-of-life scenario. Figure 33 below shows details of the normalized impact scores for the two disposal scenarios.

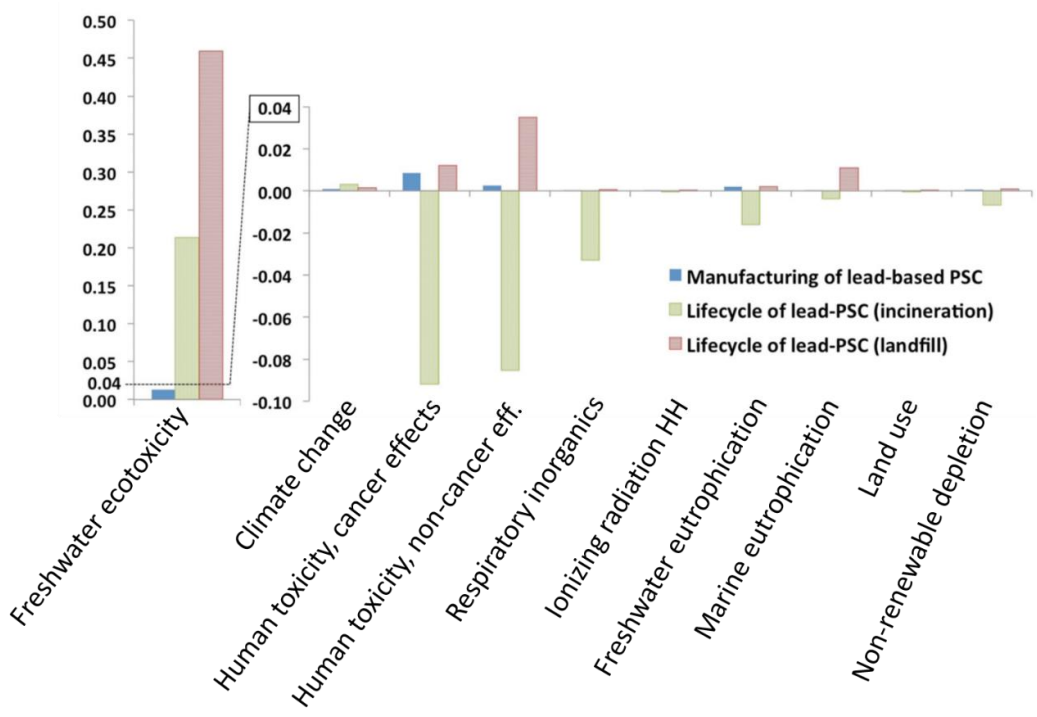

Figure 33) Normalized impact scores for the comparison between the manufacture of the cell and two disposal scenarios: when the cell is landfilled and when the cell is incinerated and lead is recovered. ILCD methodology has been applied. The system functional unit is 1kWh, adapted from Serrano-Lujan et al.

Si-Perovskite tandem cells

A frequently discussed potential application for hybrid perovskites in photovoltaics is incorporation into a tandem device architecture with a silicon cell and this approach is pursued by numerous academic research groups as well as emerging companies. A recently published LCAs investigating perovskite-silicon tandems concluded that the addition of a perovskite layer can potentially help reducing the EPBT of silicon modules by increasing their efficiency.[208] At the same time, aside from elimination of noble metals, the authors emphasize that use of solvents, e.g. in the deposition of the HTM should be avoided as solvents including chlorobenzene had most significant impact on most of the impact categories modelled. They conclude that the successful implementation of perovskite-silicon tandem devices will strongly depend on the stability of the perovskite layer after deployment as well as on the optical and electronic properties of its decomposition product if the lifetimes of the two cells do not match. Transparency, sufficient conductivity and suitable band alignment for charge transfer are prerequisites for the underlying silicon cell to still be able to operate efficiently after degradation of the perovskite layer. If these criteria are not met, the perovskite cell is likely to be the one limiting the lifetime of the tandem. Overall, the LCA found tandem devices to result in larger environmental impact in most modelled categories compared to Si-only cells. On the other hand, they expect that incorporation of perovskite can lower the impact on human toxicity as compared to a Si HIT if the lifetime of the tandem were to approach 20 years. This study found exhaustive panel recycling to be preferable over other end-of-life options considered.

The addition of a perovskite layer to a silicon cell may still have practical implications not only to its operation but also to its end-of-life treatment and special considerations may have to be taken in the adaptation of the recycling process.

4.4.4 Published lab-scale material recovery and recycling processes for PSCs

Several attempts on PSC recycling have been undertaken in lab scale, focussing on either recovery of lead or re-use of entire components of the cell.

An interesting proof-of-concept for electrochemical recovery of Pb from PSCs has been reported by Poll et al. [87] The process involves the dissolution and selective electrodeposition of Pb^{2+} deposited onto a Pb electrode. Recovery efficiency for Pb was up to 99.8%. The process requires little energy and yields a

recyclable product, which is an attractive alternative to traditional smelting. The concept might find applications in recycling other lead-containing systems with similar properties. Prerequisite is a soluble Pb compound matched with suitable solvent. In this case, the solubility of the absorber material poses an advantage for the successful and efficient recovery of its components.

Variations of selective dissolution of the individual soluble components of the PSC (HTM, perovskite) resulting in re-usable electrodes have been demonstrated in a number of publications [84,184,209]. Figure 34 illustrates the process reported by *Kim et al* as well as a commonly employed fabrication process flow. Briefly, the metal counter electrode is either removed mechanically or in a solvent bath together with the hole transport material. Owing to its extreme ductility, chemical inertness and high density, the recovery of gold from such a bath is simple. Following this, the perovskite absorber layer is removed either in a single step by treatment with dimethylformamide, dimethylsulfoxide, or a similar solvent or by using a two-step dissolution process. Using a two-step process increases solvent volumes necessary, but offers the possibility to separate PbI_2 from the organic component of perovskite absorber, which, theoretically, could be substituting virgin material in a new deposition process.

Despite several apparent advantages when applied in the lab scale, such solvent-based approaches do have significant drawbacks. Solvents used in the presented recycling processes such as chlorobenzene, isopropanol and dimethylformamide are toxic and flammable. The resulting financial investments into workplace safety translate into increased waste disposal costs. The high marine eutrophication potential of DMF, for example, has been specifically pointed at in the LCA by Celik et al. [207].

Application of these published processes results in clean TiO_2 covered electrodes, which could be directly re-used in the fabrication of new solar cell devices. The direct re-use of the substrates allows for reduction of the processing time and energy (the deposition of the electron transport layers and its sintering are avoided) and materials usage (TiO_2 precursors, nanoparticles as well as solvents used in preparation of the FTO substrates). Solution based methods have proven to be effective for a variety of cell architectures, including electron-transport layer free cells as well as TiO_2 based cells with and without mesoporous scaffolds. Encouragingly, devices fabricated from re-used TCO/TiO_2 electrodes obtained efficiencies matching those of cells fabricated from virgin materials

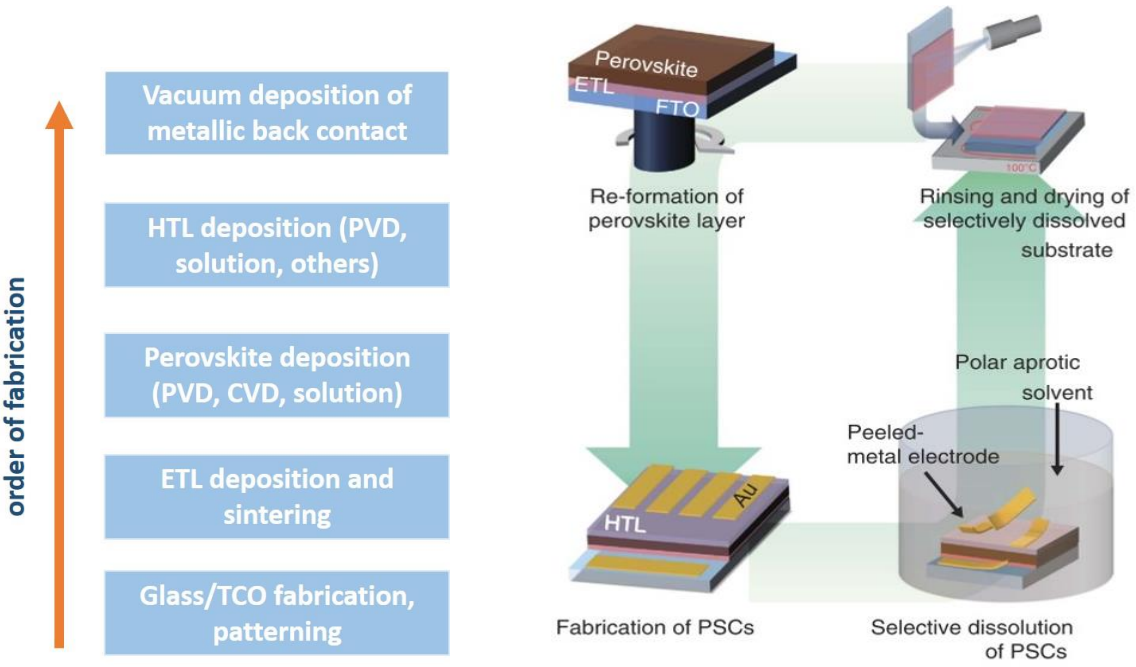

Figure 34 process flow for PSC device fabrication (left) and schematic of recycling process suggested by Kim et al.

4.4.5 PSC recycling: Practicalities

The design of the PV module affects possibilities for its recycling and material recovery once it meets its end of life. Generally speaking, a material recovery or recycling process for PSCs is likely to comprise of three main steps. After removal of components comprising the BoS, the panels would have to be de-laminated to recover the cover glass and access the active layer. Nowadays, PV panels are reduced in size to facilitate delamination, however, if the TCO substrate is to be re-used, specific processes for delamination have to be developed. A large variety of processes for delamination or separation of organic

and inorganic portions are under investigation, including cryogenic processes using liquid nitrogen, micro-emulsions or thermal decomposition[100,104,210].

While the encapsulant material requires environmental stability to protect the cell from years of environmental influence, it should ideally be easily removable or thermally decomposable without formation of toxic products. If solvents are required to remove the encapsulant, the solubility of the lead halide absorber, ETL and HTM and the resulting solvent contamination has to be considered. In the EU, regulatory attempts to enforce product design for simplified disassembly to improve practical recyclability and recovery of materials are being undertaken[93].

As discussed above, substrates with TiO_2 can potentially be re-used in the fabrication of new PSCs without losses in efficiency, which would save raw materials and process energy, depending on the material efficiency of the recycling process. This has been demonstrated for glass/FTO/TiO_2 substrates and might be particularly advantageous for patterned substrates, if damaged or degraded material can be removed feasibly. The use of lead halide absorbers in tandem devices with silicon cells may have detrimental effects on recycling processes that involve re-use of silicon wafers. As the perovskite top cell is likely to be the cause of failure, ease of removal would have to be ensured.

Considering the large contributions to a variety of environmental impact categories found by LCAs, the solvents employed in published lab-scale processes should be replaced or eliminated altogether.

The presence of a water soluble lead compound in the panels in addition to lead containing solders could have implications for workplace safety and measures to avoid inhalation of airborne dust particles or dermal uptake will have to be implemented. A perovskite-silicon tandem panel is expected to comprise of an overall similar material composition as silicon-only panels, with glass and aluminium dominating by weight. The sensitivity of the perovskite layer might require special and additional encapsulation.

Unlike CIGS or CdTe, PSC absorbers in their present configurations do not contain scarce material. Supply, for example of iodine, could become problematic if PSCs are deployed in large scale. Exhaustive material recovery and specialized recycling in closed-loop system might consequently not be economically viable, unless a steady, sufficiently large supply of waste modules is guaranteed. Nanoparticle layers used in some device architectures may be subject to special regulation if there is a risk of them leaching into the environment. Similarly, the solubility of residual lead halide perovskite on scraps can have important implications for disposal at landfill sites or storage as leaching tests might result in elevated Pb levels.

4.5 Summary and Outlook

Perovskite solar cells can be fabricated based on inexpensive and abundant elements. Their composition based on lead halides may require special considerations during fabrication, deployment and at the end of life. Solution processability of the lead halide based material can be an asset during production but equally represent particular challenges upon the end of life of the module. Low-temperature deposition processes such as inkjet printing are possible due to the solubility of the absorber and may offer the possibility to fabricate a wide variety of device architectures. However, the facile and rapid dissolution of the perovskite material can be an issue where large amounts of un-encapsulated panels are stored and processed, such as at recycling facilities or waste management sites as lead is at risk of being accidentally released into the environment. At the same time, facile dissolution of the absorber material may enable direct re-use of important components of a PSC module in closed-loop recycling. End of life treatment options may vary in different countries based on definitions of what constitutes hazardous waste and legally acceptable thresholds for lead in leachate. Important markets such as the EU and China have implemented legislation promoting the phase-out of lead and other hazardous substances from consumer products, limiting the possibility of incorporation of PSCs into portable devices. LCAs to date come to varying conclusions on the environmental competitiveness of the technology as compared to established photovoltaics. A primary point of concern today is their short lifetimes, but at this very early stage of development, significant improvements in device stability are still possible. Development of highly efficient and simple recycling and re-use processes may help the technology to become more environmentally and economically competitive.

5 High-throughput Combinatorial Research for PSCs

5.1 Introduction

Combinatorial, high-throughput research (cHTR) methods originate from the expensive, highly sensitive research performed in the pharmaceutical industry but is a relatively new approach [38,211–214].

Multiple critical reviews discussing practical as well as theoretical challenges of cHTR are available to the interested reader[215–218].

In materials science, cHTR commonly relies on the fabrication of so-called library samples. A library sample is used to screen variations of a target parameter, such as composition or thickness, which are varied systematically across the entire sample surface. A single library sample can encompass hundreds of material combinations or compositional variations. Ideally, such a sample array is characterized by automated means. Characterizing samples on a library minimizes the effect of systematic errors and ensures that all samples are processed in identical environmental conditions. This feature of combinatorial HTR is of particular importance when sensitive materials are being investigated. Fields that have particularly benefited from cHTR include the discovery of catalysts, fuel cells, and soft, polymeric materials[39,213,219]. Multiple branches of energy-related materials research have adopted cHTR successfully on both smaller and larger scales, including development of lithium ion batteries[220], thermoelectrics[221,222], oxide solar cells[36,223] and solar energy water splitting[224]. Preparative methods include PVD, CVD and printing[225].

Aside from materials research focusing on specific output parameters, cHTR has proven to be a particularly powerful tool for the important task of mapping phase diagrams of multinary ceramics as well as alloys [226,227]. When combined with (semi)automated scanning-type characterization techniques, this task can be performed significantly faster and more reliably than using traditional manual approaches. With countless ceramic and alloy compositions still not investigated, interesting material properties unique to some unknown compositions can still be expected to be found.

Despite many rational advantages of cHTR, the industry has not widely adopted HTR in materials development and the method still faces a multitude of challenges. Firstly, while cHTR is frequently considered to be the most cost-effective research method in certain areas, it requires large initial investments, highly skilled experimental planners, and a research environment that is adapted to the unique requirements of cHTR.

Another less easily addressed challenge in cHTR is the potential incompatibility between large-scale industrial preparation processes and the methods at disposal for the fabrication of compositional libraries. As thin films specifically can be highly sensitive to deposition methods, the characteristics obtained from two varying preparation processes may overshadow the effects of the target parameter to be investigated. Microstructural changes and the resulting build-up of stresses in the sample resulting from compositional variations are additional concerns that limit the practical applicability of combinatorial HTR. The sensitivity of microstructural development in PVD processes has been a topic of intense discussion dating back to investigations undertaken decades ago and are illustrated in, e.g., Thornton's structure zone model shown in Figure 35.

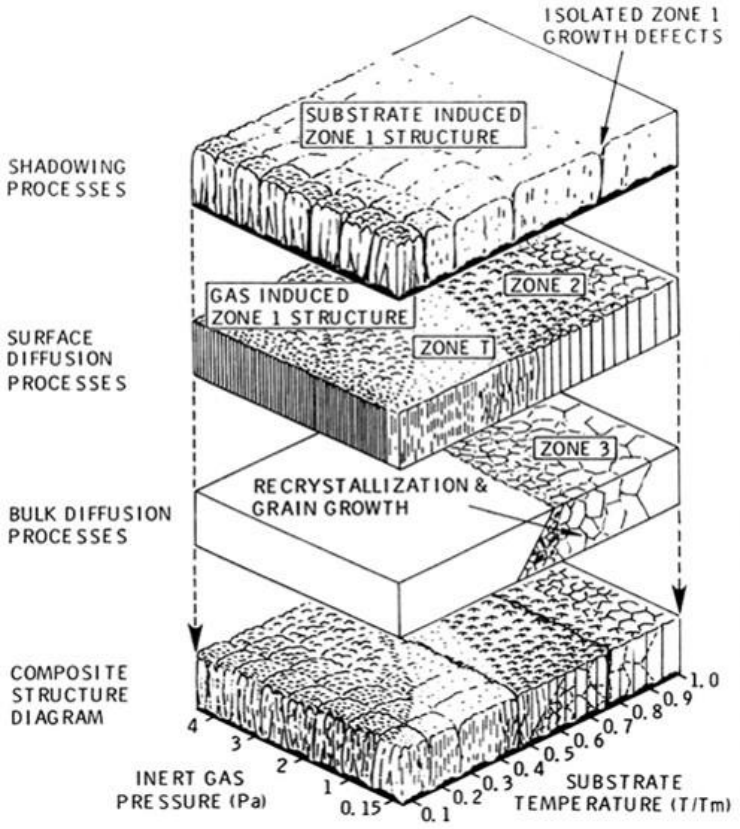

Figure 35 Thornton's structure zone model

It is realistically speaking extremely challenging and unlikely that one single parameter can be systematically varied across a combinatorial library while keeping all other properties constant. De-coupling effects of the target parameter from various characteristics of the material can be challenging at best and potentially impossible. De-coupling cause and effect might require a very large array of characterization tools and computational power.

Other complications typical for thin film analysis are that certain film properties maybe overshadowed be substrate effects, which is particularly challenging in the investigation of thermoelectric materials.

Leaving all material related challenges aside, the characterization of combinatorial libraries is not trivial and methods have frequently not kept up with developments in fabrication[37]. An example of the characterization of a library of oxide solar cells is shown in the following figure. The example adapted from *Anderson et al.* shows a solar simulator high throughput –jV scanner. The measurement in this case is almost entirely automated and the interaction of the operator and the same is minimized.

Combinatorial HTR inevitably leads to the generation of very large data sets which typically cannot feasibly be processed and analyzed “by hand”, i.e. by a single researcher using traditional methods to sort, plot, and analyze the data. Advanced data managing tools will be necessary to draw valuable conclusions from such large data sets and may ultimately lead to advances in machine learning as well as material science.

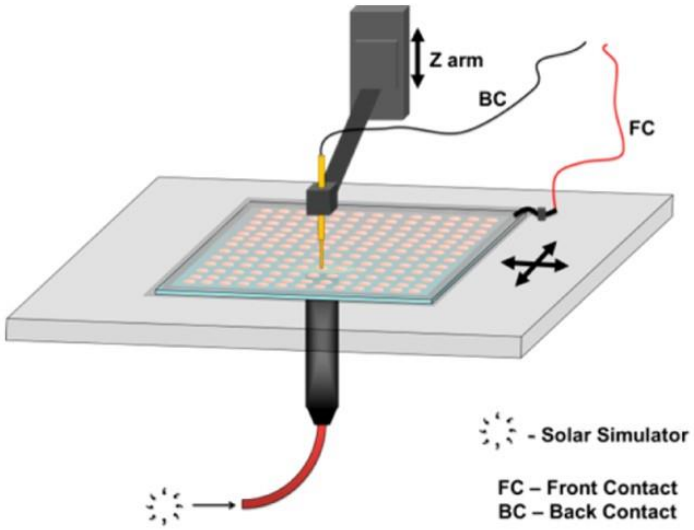

Figure 36 Adapted from Anderson et al.[228]Schematic drawings of the solar simulator current−voltage high throughput scanner. The equivalent illumination of 1 sun, AM1.5G, is incident on the transparent front electrode. A current− voltage curve is measured for each combinatorial cell. Reproduced with permission from the American Chemical Society

5.2 Motivation

The library-based, combinatorial HTR approach is particularly interesting for PSC research for a multitude of reasons. Among PV materials, hybrid perovskites can be considered exceptionally well suited for the implementation of such research approaches. Firstly, hybrid perovskite layers can be fabricated using a large variety of processes including, but not limited to, PVD, CVD, spin-coating from precursor solutions, dip-coating, spray-coating, and combinations and adaptations of such. Several of these methods allow for the preparation of combinatorial libraries with relatively little adaptation, including inkjet printing, PVD, CVD and spray-coating. The possibility to reliably fabricate combinatorial libraries with reproducible variations of parameters of interest is a prerequisite for the successful implementation of combinatorial HTR. Ideally, libraries should be fabricated by automated or semi-automated means and de-couple the operator or sample maker from the outcome of the preparative process, i.e. the human factor must be reduced as much as possible.

Aside from the above-mentioned fabrication-related restrictions, material specific factors also have to be taken into consideration when evaluating the possibility for implementation of HTR. Ideally, multiple sample compositions should be obtained on a single substrate, which requires compositional variations to be processible using the same deposition method. Further, these variations should be easy to monitor, i.e. they should manifest in material properties that can be assessed by scanning methods.

Research in hybrid perovskites has focused extensively on composition engineering. From single-cation, single-halide compositions that were used in the early reports of successful PSC devices, the material has undergone a rapid evolution to ever-more complex compositions with as many as five organic and inorganic cation variants and three halides involved. While the developments in PSCs since their first reports are undoubtedly impressive and rapid, the compositional optimization has, to the best of my knowledge, been achieved with hand-made devices and relatively small batch sizes. This traditional approach has yielded the desired results in many cases but comes at a relatively high cost for material, including TCO, precursors, cleaning solvents, precious metals as well as electricity but also requires large amounts of man hours.

Reducing the human factor in sample preparation can be expected to increase reproducibility as well as batch sizes. Ideally, a highly automated HTR process should be completely independent of the manual skills of the researcher performing the experiment.

In hybrid perovskites such as $CH_3NH_3PbX_3$, small variations in combinations of cations, halides etc. lead to large differences in their photophysical properties. Characteristic properties governed by their composition such as absorption, photoluminescence (PL), and lifetimes of excited carriers can indicate whether a certain compositional trend is promising for further, detailed experiments. Techniques such as PL and absorption measurements are suitable for being performed in a scanning fashion and several laboratories have developed their own home-built optical scanners.[35]

Jacobsson et al. systematically investigated the compositional space for mixed halide lead perovskites for solar applications using a matrix-based approach[40]. Through the course of their study, the authors investigated effects of variations of mixtures of formamidinium and methylammonium cations and variations of ratios between bromide and iodide. Their experimental planning led to a 7x7 matrix with 49 unique compositions. Details of the compositional matrix as well as photographs and absorption data reproduced from their original work are presented in Figure 37. While the publication does not explicitly state batch sizes and standard deviations of device performance date, it can be reasonably assumed that a relatively large number of samples as well as man hours were required to successfully prepare the devices corresponding to the 7x7 matrix. Precursor preparation for 49 solutions alone can be expected to have taken several hours of glovebox work, without accounting for preparations that had to be repeated during the optimization stage. Furthermore, the exceptionally detailed report of the study includes PL and absorption data as well as jV characteristics and XRD patterns for each composition. While XRD was probably carried out using a sample changer magazine with 12 samples, the PL and absorption measurements require manual manipulation of the setups the researchers had at their disposal. [6]

With more and more journals requiring detailed device performance statistics for solar cell manuscripts, larger batch sized are likely to become important not only for the parameter verification by researchers themselves but also for successful publishing[229]. The work by Jacobsson et al. is exemplary for the type of screening study that could massively benefit from the implementation of combinatorial HTR with a certain

[6] Jacobsson and several co-authors worked at the LSPM during the time of preparation of this study, instruments and manipulation are known to me

degree of automation. The following sections will outline possibilities for the implementation of such techniques specific to hybrid perovskite materials for PV applications.

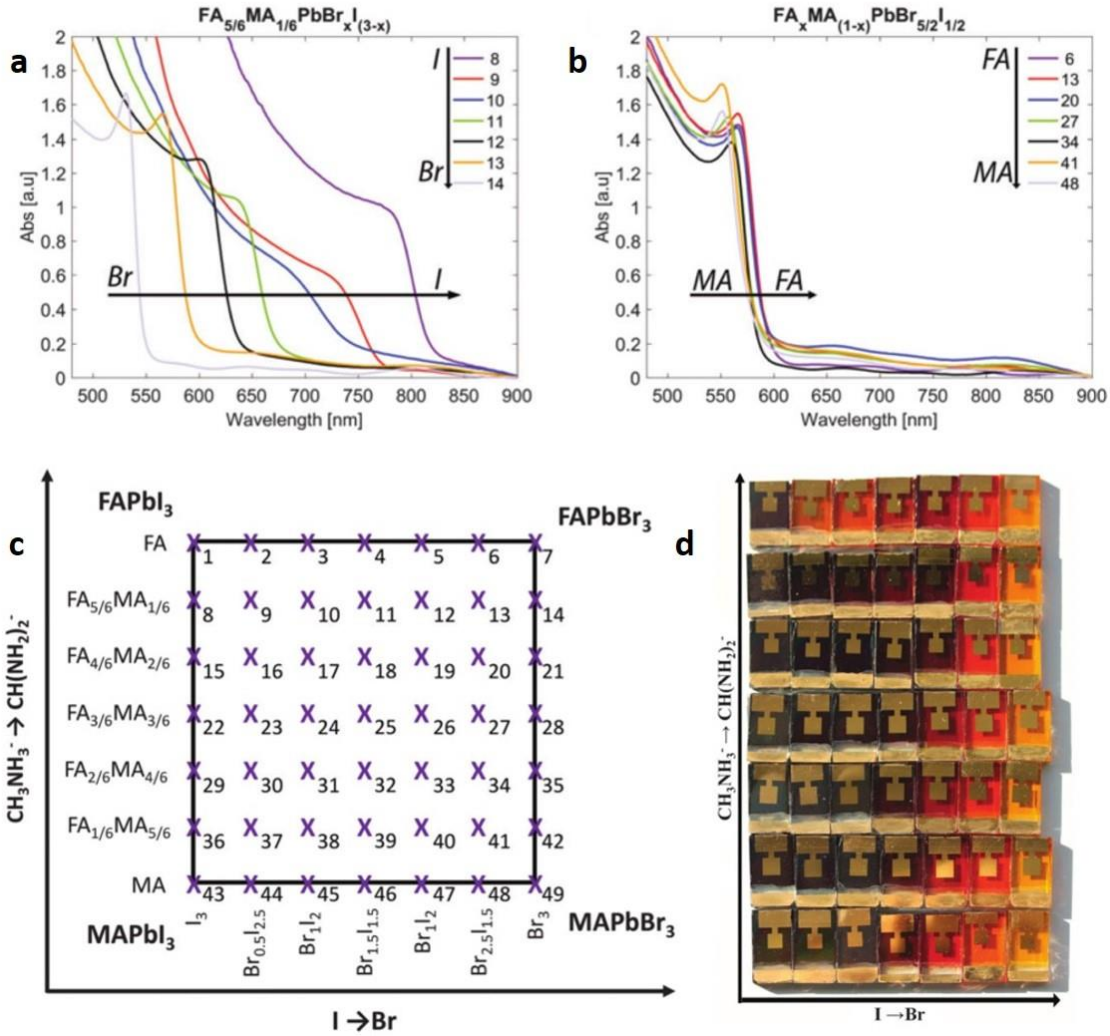

Figure 37(a) Optical absorption as a function of wavelength for a subset of the samples, corresponding to samples 8–14, FA5/6MA1/6PbBrxI3?x where the I/Br-ratio is changed. The background due to scattering is removed. (b). Absorption for the subset of samples corresponding to FAxMA1xPbBr5/2I1/2 where the MA/FA-ratio was changed, c) A graphical illustration of the compositional matrix with markings for all the compositions explored. The numbers next to the crosses represent the key between the intended perovskite compositions and sample numbers, d) photograph of the fabricated cells, with the Spiro-MeOTAD hole conductor and the gold contacts, showing the appearance in reflected light. The samples are arranged in the same way as in the sample matrix in c). Adapted from Jacobsson et al. Energy Environ. Sci., 2016, 9, 1706--1724

5.3 Processes Chosen

Thermal evaporation was the first process chosen for the tentative fabrication of combinatorial libraries. This process is typically used in PSC preparation for the deposition of metallic counter electrodes, but thermal vacuum deposition is also reported for preparation of the perovskite material itself in the literature. [230] The process allows depositions on cold substrates and, once optimized, the deposit quality and resulting device performance should be independent of the machine operator. Thermal evaporation is commonly used in OPV, indicating that most layers constituting a PSC device could be prepared by this method.

Inkjet printing is a highly automated, adaptable deposition process with minimal interaction of the operator and the sample.

Using a multiple channel approach similar to commercial multi-color printing, various perovskite compositions can be created. The composition can be varied gradually or abruptly, depending on which dimensions are to be examined. Printing offers the possibility to produce entire batches of cells in relatively short time without interference from an operator. Multi-layer printing is possible where solvent compatibilities are given. The multi-layer architecture of PSCs lends itself to inkjet printing as all functional layers can in principle be solution processed. Advanced research printers allow for even more parameters to be controlled such as the waveform applied to the piezo-driven printhead, drop volume, shape, velocity, and spacing between deposited drops. Details of the technology and its applications to perovskite solar cell preparation will be presented in chapter 5.

5.4 Perovskite Libraries by Thermal Flash Vacuum Deposition

Project Goals

- Reduction of human factor in sample preparation through automation
- Design of scalable process for absorber deposition
- Reduction of solvent use
- Design of reproducible deposition process to reliably achieve reproducible results
- Fabrication of compositional libraries on large area substrates
- Reduction of man hours spent on repetitive tasks by highly trained personnel
- Enabling of rational experimental design

5.5 Choice and Design of Deposition Process

The fabrication of perovskite libraries required the development of a new material deposition process as none of the fabrication processes at our disposal could be used to deposit multiple compositions, thicknesses, or morphologies of hybrid perovskite absorbers onto the same, comparatively large substrate:

Dip-coating could be used to deposit the liquid onto large substrates and possibly produce thickness gradients through variation of the withdraw speed[231], but could only be employed to fabricate films of a single composition.

Spin-coating has, to the best of my knowledge, so far been used to fabricate most record-efficiency cells but is unsuitable for large-area depositions. The motivation for employing spin-coating in thin film fabrication is typically the need for uniform, thin coatings with minimal thickness gradient and overall uniform characteristics. The process is consequently not suitable for the creation of libraries for HTR which require systematic, reproducible variations of multiple parameters.

Spray-coating has reportedly been used successfully for the preparation of the absorber layer in PSCs[232,233] ,and when automated can achieve a high degree of reproducibility. For materials that rapidly form insoluble stable phases upon contact with the substrate, such as TiO_2 when deposited using alcohol-based

titanium-tetraisopropoxide solutions onto a hot surface, spray deposition can also be used to systematically vary the deposit thickness across a surface.

Dual-source vacuum deposition is achieved through the controlled sublimation of the ammonium salt and the lead halide from two separate, heated crucibles under high vacuum.[230] The method has reportedly been used to fabricate perovskite solar cells and is also apparently employed by Oxford PV in their commercialization attempts at their pilot fabrication site.[12,23] The fabrication of films with reproducible composition relies on precise control over the sublimation and deposition rates of both precursor salts. While it appears to be possible to achieve stoichiometric compositions as reported, the optimization of such a process is not trivial, particularly in the case of hybrid organic-inorganic materials. The main challenge in fine-tuning the stoichiometry of the deposit lies in the difference in sublimation temperatures and behavior of the two salts commonly used. CH_3NH_3X are volatile solids with high vapor pressure and decompose quickly at moderately elevated temperatures under vacuum. Controlling the sublimation rate of this component requires particular attention for the PID parameters of the current source driver as even a small thermal overshoot can lead to very rapid decomposition and sublimation of the methylammonium salt. The formamidinium analogues behave similarly. The deposition of PbX_2 is less complicated as they decompose at higher temperatures and slight thermal overshoots are less likely to lead to extreme, sudden increases in sublimation rates.

As the dual-source vacuum deposition approach can only achieve stoichiometric compositions if the substrate is rotated, only one perovskite phase can be formed per substrate. This approach is thus not only challenging during the optimization stage but also is not suitable for the preparation of combinatorial libraries as desired for this project.

Process of Choice: Single-Source Thermal Flash Vacuum Deposition

In order to avoid the challenges associated to dual-source vacuum deposition as outlined above, the process was radically revised. Instead of subliming PbX_2 and CH_3NH_3X separately to form the perovskite phase upon condensation on the substrate, $CH_3NH_3PbX_x$ was deposited by rapidly heating ("thermal flash") single crystals of the target composition in one crucible. The material formed on the substrate had the same composition as the source material. A photograph of single crystals of $CH_3NH_3Br_3$ and the thermal decomposition profile of single crystals of CH_3NH_3Br/I_3 is shown in Figure 38. The crystals were prepared by a simple solvent-based growth process described and discussed in detail in chapter 1. Freshly

grown they were found to exhibit a wide size distribution from 0.1-3mm. To minimize inhomogeneity in decomposition behavior due to variations in surface-volume-ratios, the dried material was ground by hand in an agate mortar.

A minimum of 600mg dry material was used per deposition. A detailed description of the process can be found in the METHODS section at the end of this chapter.

Thermogravimetric analysis (TGA) clearly shows two main decomposition events with about 25% of the sample weight leaving at around 280°C and complete decomposition of the remaining material at 600°C. It should be noted that the TGA was carried out under atmospheric pressure and nitrogen flow. Decomposition temperatures observed in the actual vacuum deposition process are both shifted to lower temperatures, as expected.

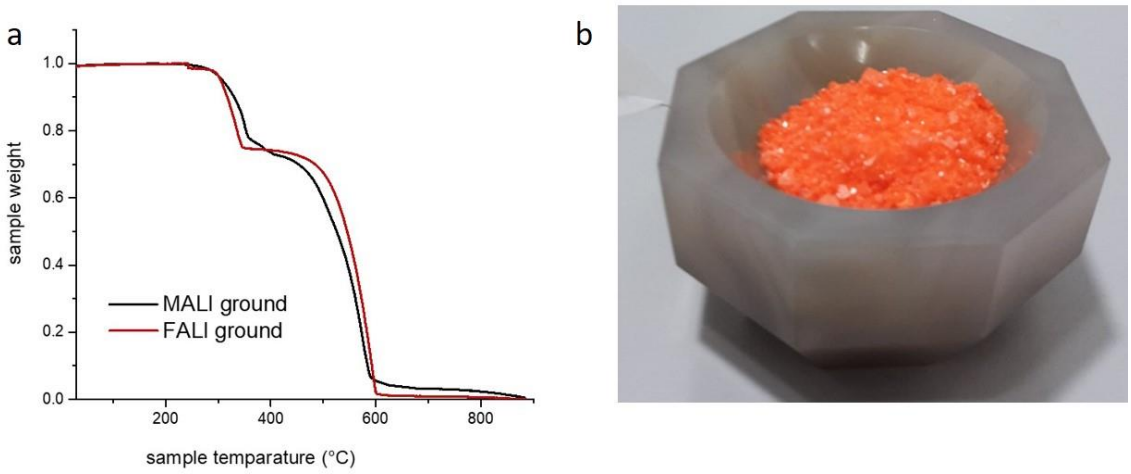

Figure 38 a)Normalized Thermogravimetric analysis of ground MALI and MABL single crystals, heating 10°/min in nitrogen b) single crystals for one deposition cycle before grinding

In order to achieve the correct stoichiometry on the substrate, it was important to heat the crucible containing the material as quickly as possible and to reduce the time between the two main sublimation events to a minimum, i.e. the lead halide has to decompose while uncondensed MAX is still present in the chamber. The actual deposition process could be completed within less than 180s.

5.6 Results

5.6.1 Appearance and Structure

Transparent, highly colored films could be fabricated using this rapid deposition process. Up to 1.6g of material could be sublimed within minutes. The deposited films reached thicknesses of 30-500nmwith 600mg of material required for a 30nm deposition. The thickness evolution did not appear to follow a linear trend and the material deposition efficiency (sublimed material weight/material on useable surface) can be assumed to be low owing to the relatively small deposition chamber.

The film adhesion varied with film thickness with thinnest films showing the best adhesion. Thick (>500nm) films tended to be sensitive to handling and easily scratched. Adhesion on glass was generally found to be better than adhesion on FTO or TiO_2.

The stoichiometry of the uniformly colored films was confirmed by XRD. Figure 39 shows diffraction patterns for thin films of $CH_3NH_3PbI_3$ (MALI, black curve) and $CH_3NH_3PbBr_3$ (MALB, orange curve) deposited on microscope glass slides. The linear intensity plot in b) indicates formation of preferential orientation, but the characteristic peaks can be easily identified in the log-scale plot in a).

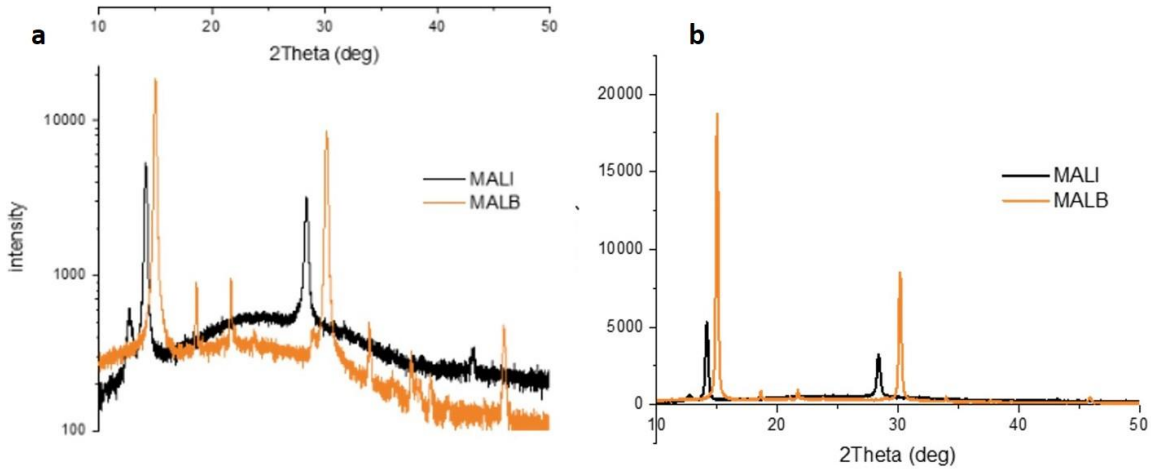

Figure 39 XRD patterns of evaporated single crystals on glass a) log scale for better intensity resolution and b) linear intensity plot of the same data

5.6.2 Morphology

The morphology of the sublimed films was examined by FE-SEM. Cross-sectional images were used to assess the film thickness and uniformity. Figure 40 shows cross-sections of three different vacuum deposited films (b-d) and a complete device with spin-coated perovskite absorber layer.

The thickness of the optimized spin-coated layer shown in a) is approximately 300nm with uniform thickness throughout the device. The contact between perovskite layer and TiO_2 surface is continuous without signs of delamination. Grains are clearly defined and range in size between 100-500nm.

Figure 40b shows the same material deposited by thermal flash vacuum deposition on FTO. The contact between the two layers is clearly not as intimate as seen in a); de-lamination of the film is apparent and explains the observed comparatively poorer adhesion. Two grain size regimes can clearly be distinguished in the perovskite layer.

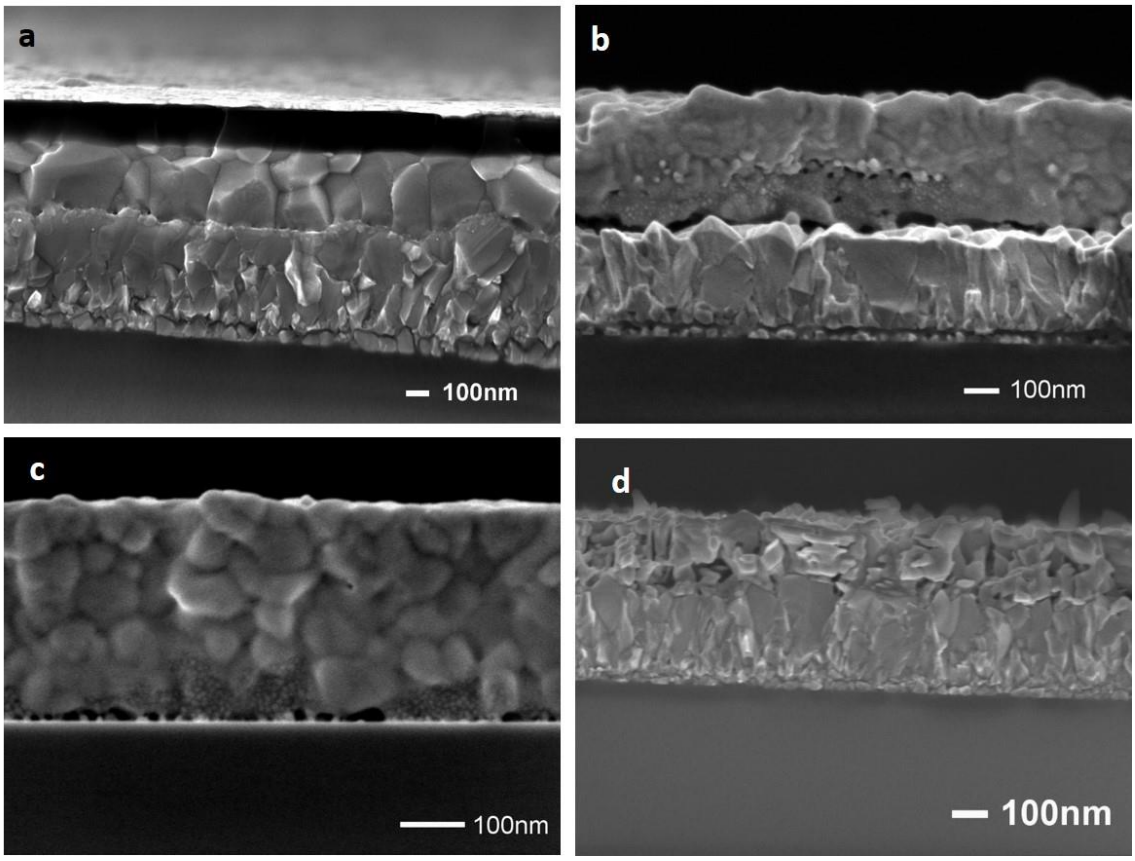

Figure 40 Cross-sectional electron images of a) a full PSC device prepared by spin-coating for reference b)MALI evaporated on FTO c) MALI evaporated on Si wafer d) PbI_2 evaporated on FTO

The same variation in grain size can be observed in c) which shows the same material vacuum deposited on a silicon wafer. The contact between coating and substrate is similarly poor as in b), indicating that this is possibly a consequence primarily of deposition method and not material combination.
The last panel in d) shows a cross-section of PbI_2 deposited by thermal flash vacuum deposition on FTO. The material forms characteristic hexagonal platelets and does not form a dense film.

5.6.3 Morphology and Substrate Temperature

While the coatings were found to be uniform regardless of the substrate temperature, feature sizes, density, and grain size and habit were found to be starkly dependent on this parameter. Figure 41 below shows secondary electron images of $CH_3NH_3PbBr_3$ films deposited on FTO kept at 10, 50, 70 and 95°C.

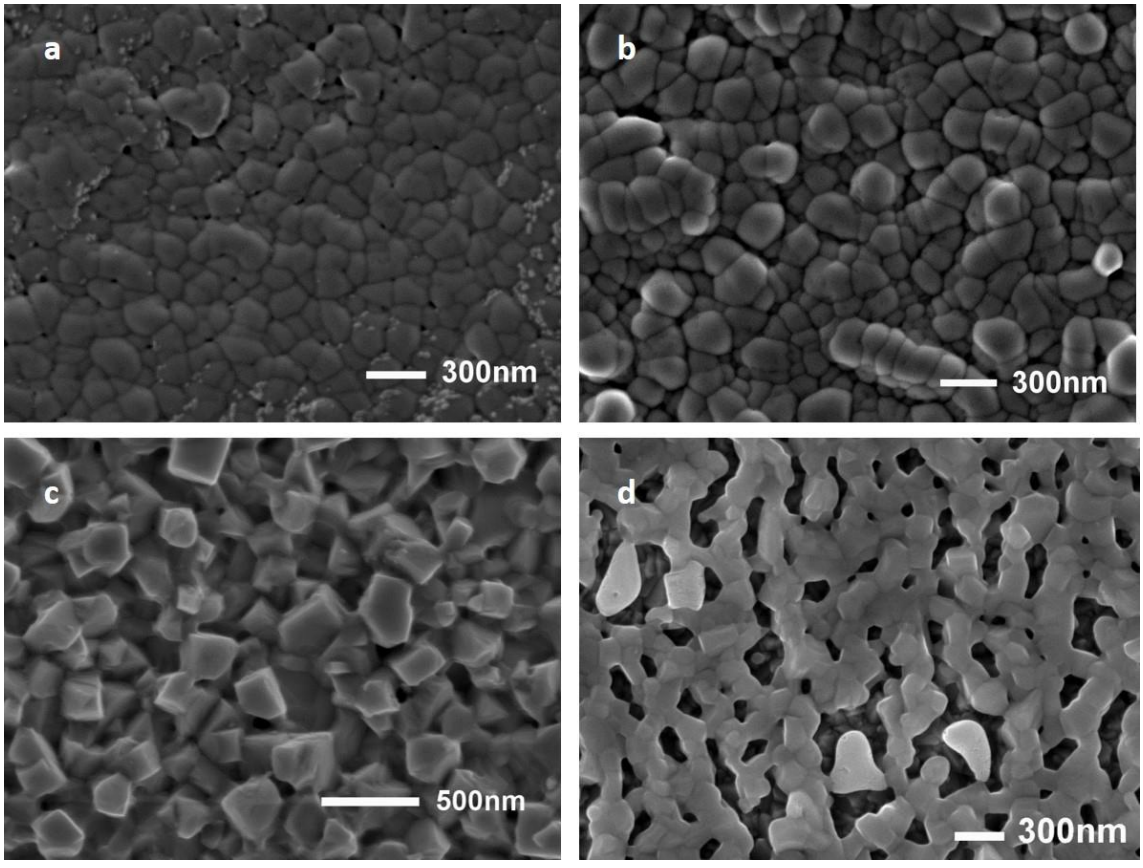

Figure 41 Top-view SEM images of MALI deposited on FTO at a) 10° b)50°C, c)70°C and d) 95°C substrate temperature

The film in a) was deposited at 10°C which is the lowest temperature possible with the setups. It is made up of rounded grains grown closely together and some pin holes are apparent. The grain size is relatively uniform and does not vary significantly. The deposit shown in b), which was deposited at 50°C, shows larger gaps between grains and more defined structures in comparison to a). Further increase of substrate temperature to 70°C, shown in c, leads to the formation of faceted structures and a much rougher film. The material is clearly highly crystalline with narrow grain size distribution. The film in d) was deposited at a substrate temperature of 95°C, which is the highest temperature attainable with the setup. It is clearly discontinuous with large gaps between crystallized features.

Microstructural changes and variations are frequently a result of a variety of factors. While composition is relatively easy to vary, targeted microstructural changes are difficult to obtain and are very difficult to de-couple from composition, local environment, and other factors. It is an observation frequently made in combinatorial materials screening approaches and at the same time a major challenge in library processing as well as a frequently voiced criticism of the high-throughput screening approach in general. It was beyond the scope of this thesis to investigate structure-composition-morphology relationships in sufficient detail in order to provide reliable data regarding this aspect.

5.7 Single-Composition Libraries

The fabrication of the perovskite libraries broadly exploits the same principle as that used by the Zaban group to fabricate the oxide libraries introduced earlier. It relies on the fact that the deposition profile inside a PVD chamber is largely inhomogeneous. Typically, this inhomogeneity poses practical issues, which is why sample holders are typically rotated to compensate for said inhomogeneity. Depositing on a stationary substrate inevitably leads to the formation of non-uniform films most apparent in the formation of thickness gradients across larger surfaces. While an inconvenience at best for most processes and devices relying on uniformly thin films, this effect is largely reproducible in itself and can be used to reliably produce samples perfectly adapted for high throughput research.

While for the oxide libraries prepared by sputter- or pulsed laser deposition presented in the previous sections sufficient thickness gradients could be achieved by simply keeping the substrate steady on the sample holder, adjustments had to be made for the perovskite library preparation. Sufficient thickness gradients for the oxide libraries prepared by sputter- or laser deposition presented in the previous section could be achieved by simply keeping the substrate steady on a sample holder, however adjustments had to be made for the perovskite library preparation.

The reactor used in all evaporation/sublimation experiments is a cold-wall reactor, resulting in relatively large amounts of deposit on its walls. While excessive deposition on reactor walls leads to low deposition efficiencies, the inhomogeneity of the deposition on respective reactor walls could be used to fabricate various library layouts with varying degrees of thickness and composition gradients, depending on their position relative to the sources. The reactor walls could not be heated or actively cooled during deposition which means that all depositions of combinatorial libraries had to be carried out with the substrate at room temperature.

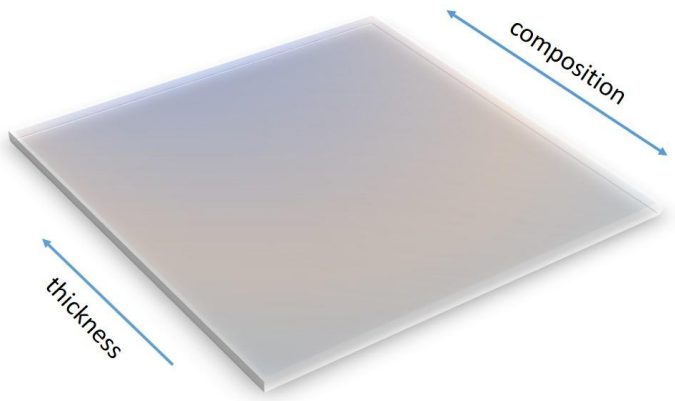

Figure 42 Schematic of a compositional library with thickness gradient

Figure 42 shows a schematic of a compositional library with thickness gradient. It becomes clear that each point on the library will be unique in terms of composition, thickness of individual layers, and the resulting properties. The smaller the defined individual areas of interest, the more precise trends resulting from variations in composition and/or thickness can be studied.

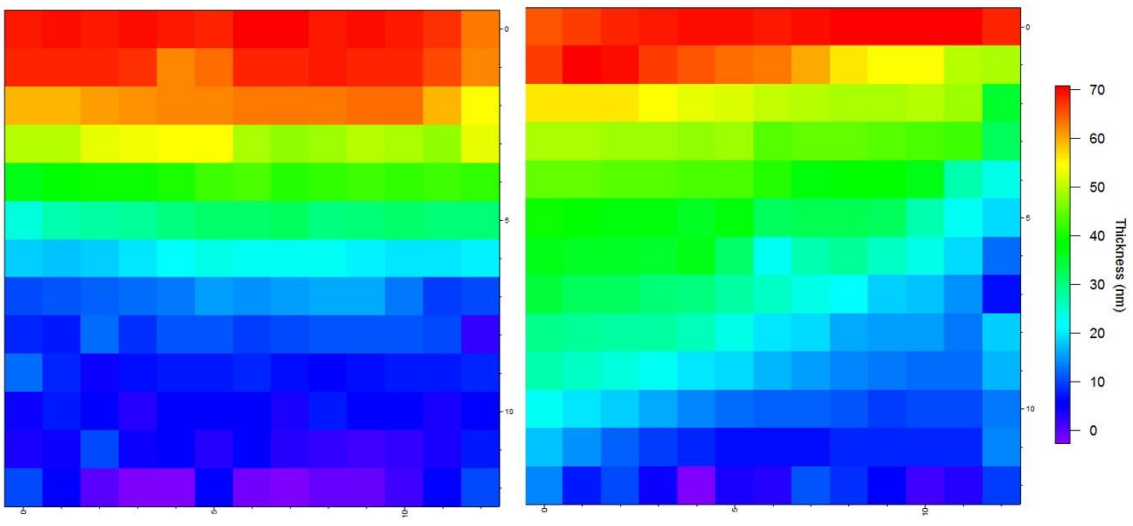

Figure 43 Thickness distribution measured optically on two different MAPbBr3 libraries prepared by vacuum flash evaporation

In some cases, the distribution of film thickness could even be identified with unaided eyes. Precise thickness was measured optically at Bar Ilan University using a homebuilt optical scanner equipped with a white LED, similar to the setup shown in

Figure 36. Results of the optical scanning for thickness determination on two MALBr libraries are presented in Figure 43. Both libraries were deposited during the same deposition cycle on FTO sheets coated with TiO_2, kept at two distinct positions on the reactor walls.

The plots show samples of 7x7cm side length. Each pixel represents a potential solar cell device. All pixels are unique and can be identified by their respective XY coordinates. Successful preparation of thickness gradients was a prerequisite to the fabrication of compositional libraries where pixels are not only unique in terms of thickness of the layer of interest but also in the layer's chemical composition.

Solar cell devices were fabricated from the library presented on the right in the figure above. Spin-coated spiro-MeOTAD served as hole conductor material and sputtered silver was used as the back contact to complete the cell.

.

A mapping of the results for J_{sc} and V_{oc} from jV sweeps performed immediately after cell fabrication are shown in Figure 44.

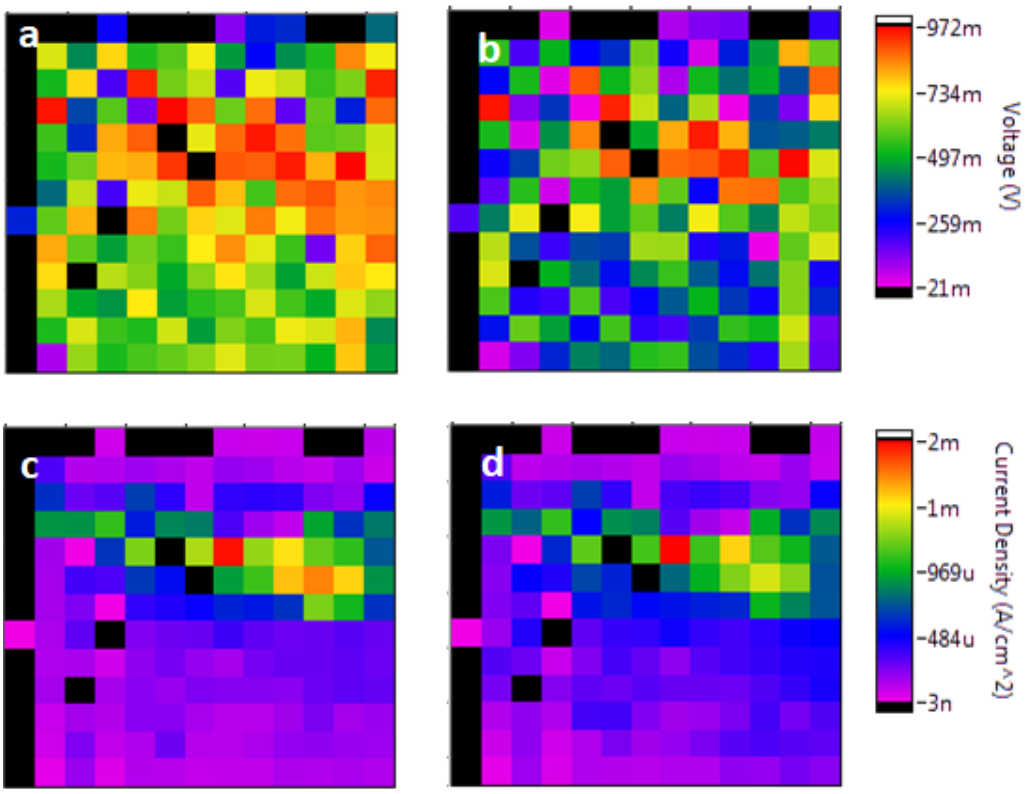

Figure 44 Maps of Voc and Jsc on MALBr library. a+c: forward bias, b+d: reverse bias. Black pixels indicate non-photovoltaic behavior. The cell performance was analyzed using a home-built jV scanner depicted schematically in

Figure 36

Overall performance of the measured devices is low; both voltage and current output are far below values achieved with other deposition means for this perovskite. It has to be taken into consideration that the maximum absorber film thickness in the entire library does not exceed 70nm, therefore low Jsc values are consequently expected.

Despite the overall poor device performance across the entire library, a region of relatively higher performance can be identified in both current and voltage maps. Surprisingly, the pixels with highest current output do not coincide with those with the thickest absorber films.

This behavior could be due to multiple reasons. Changes in absorber material film formation as the film grows thicker on the substrate could prove to be detrimental. The film morphology is not laterally uniform

as discussed in previous sections and shown in images in Figure 40. Varying morphology might also impact HTM-absorber surface wetting.

As the HTM was spin-coated onto the library, thickness gradients of the HTM are probable, particularly at the edges of the relatively large substrates used for library fabrication. It may even be possible that no or insufficient HTM is present on some parts of the sample, leading to direct contact of perovskite and the silver back contact. An indication for this is the fact that a large number of pixels at the edges of the library do not exhibit photovoltaic behavior, indicated in the map by black pixels. Practical issues must also be considered when evaluating the results presented above. The substrates measure 7x7cm and are very large compared to typical lab-scale PSC devices, therefore the handling of the samples can be challenging and damage from mechanical impact is expected particularly around the edges.

Clearly, further experiments as well as more in-depth characterization must be carried out to rule out external factors not related to the perovskite film thickness itself if libraries are to be used in optimization of PSC devices.

5.8 Towards Compositional Libraries

With thickness gradients of the target materials realized, compositional libraries could be fabricated.

More than one perovskite material could be deposited on a single substrate by Using two sources located at opposing sides of the deposition chamber. To the best of my knowledge, this is the first repot of combinatorial perovskite libraries where the combinatorial aspect focuses on the perovskite material itself.

It should be noted that this project cannot be considered completed, the following section should rather be taken as proof-of-concept for the possibility to fabricate perovskite compositional libraries.

Figure 45 shows a photograph of a MALI-MALBr library. In this case, the presence of a compositional gradient can be clearly seen with unaided eyes due to the large difference in optical bandgaps of the two materials. The gradient from the black MALI to orange MALBr appears to be relatively sharp, with an intermediate phase in between.

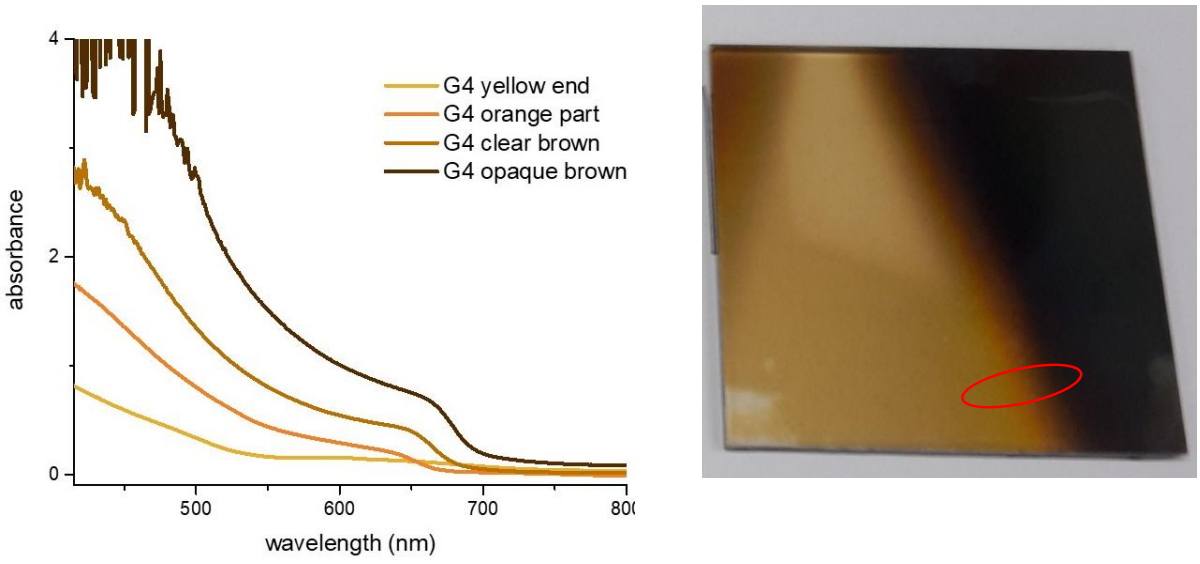

Figure 45 Absorption characteristics measured on single MALI-MALB-library measured in circled area

The region circled in red at the bottom of the library was used to collect UV-visible absorption spectra, which are shown on the left figure panel. The absorption onset shifts gradually with composition, as expected.

Aside from mixed halide libraries such as shown in the figure above, libraries could also be fabricated by mixing two perovskites with varying cations. Figure 46 shows further examples of compositional libraries successfully prepared by Thermal Flash Vacuum Deposition. The three libraries in the top row were fabricated from single crystals of FALBr and MALBr to form a mixed-cation compositional gradient. Color variation indicates the presence of materials of various bandgaps and correspond to the expected for the two materials.

The three libraries in the bottom row were prepared from MALI and MALBr single crystals. The occurrence of the red phase indicates formation of a mixed halide phase. Unfortunately, the libraries were damaged during shipment to Bar Ilan University and could not be analyzed further.

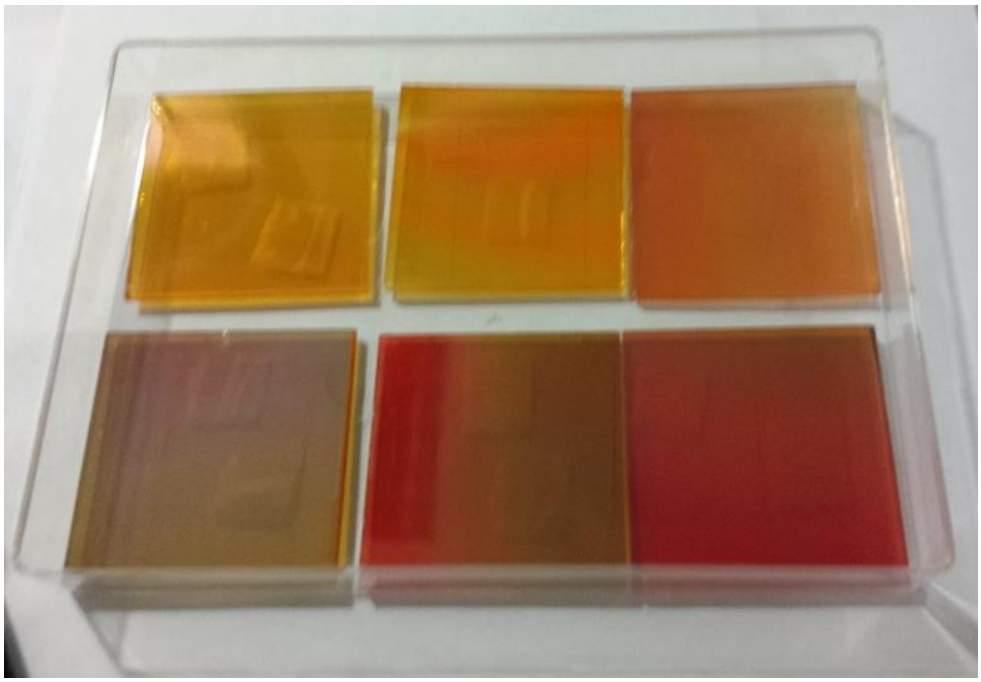

Figure 46 Mixed cation libraries (top row) and mixed halide libraries (bottom row) grown at different positions in chamber

5.9 Advantages and Challenges of Single-source evaporation for PSCs

Single-source evaporation poses multiple advantages over other commonly employed deposition methods such as spin-coating, dip-coating, dual source evaporation or low-vacuum flash evaporation. The most important advantages are listed below:

- No solvents are required for film formation itself
- Solvents can be eliminated altogether by using mechano-synthesis for perovskite fabrication[234,235]
- Precise deposition and formation of complex geometries possible by simple shadow masking
- Only one evaporation rate to be monitored and optimized
- Deposition is fast -> total deposition time typically less than 300s
- PVD is a scalable, industry compatible process with material efficiency increasing with reactor size
- High degree of automation possible
- Once optimized, high degree of reproducibility achievable
- Operation does not require highly trained personnel
- Substrates remain cold-> wide choice of materials available, including plastics
- Large numbers of samples can be processed in parallel

Despite the encouraging results presented in the preceding sections, the optimization and adaptation of TFVD for the fabrication of PSC devices still faces challenges that need to be overcome for successful, large-scale implementation. The most crucial points are listed below:

General limitations

- TFVD is a batch process by design, it is not suitable for continuous fabrication
- Halogens, including Iodine and its ions, pose a practical issue as they corrode metals and can damage deposition equipment rapidly
- Condensation on reactor walls reduces material efficiency dramatically
- Vacuum deposition equipment required poses relatively large initial financial investment
- Solvent-free process should be employed for precursor preparation
- Material from reactor walls should ideally be removed and recycled periodically

Instrument-specific limitations

- The “Minispectros” setup was designed for low-temperature depositions and was not capable of reproducibly producing the very rapid heating required for successful perovskite deposition

- Setup used has a very small deposition chamber and sample holder, further reducing material efficiency

5.10 Future Work

The results presented in the preceding sections show that the fabrication of PSC compositional libraries is possible, quick, and can be implemented without major modifications to standard deposition equipment. Multiple aspects will still have to be targeted in future projects to ensure reliable reproducibility in deposition, film quality and ultimately device library performance.

Difficulties related to the synchronous sublimation of MAX and PbX_2 and other components were found to frequently stem from the thermal source not allowing the fast heating rates required. A special, low-temperature source with exceptionally good linearity in low T regimes was employed in the experiments in this chapter. Modifying this source to a traditional high-temperature source would lead to reduced linearity and consequently thermal overshoot, however it is likely to be better suited for the direct sublimation of hybrid perovskite materials.

Generally speaking, it will be desirable to fabricate the entire device library by PVD processes. This could potentially even be done in the same chamber to save time and to reduce manual labor which is prone to induce non-systematic errors. Hole transport materials, such as CuSCN, as well as metal counter electrodes can be thermally evaporated and, if adequate protection from cross-contamination between n-type and p-type materials is ensured, can even be processed in the same chamber.

In addition to sample and preparation related optimization, data acquisition, processing, and storage should also be adapted to library-based research. This would require large changes to not only infrastructure but also laboratory philosophy.

With regards to acquisition, a number of relevant versatile parameters will have to be identified and collected for each spot on a library. Optical means are well-suited for scanning techniques and a lot of important information can be extracted from these methods e.g. absorption characteristics. Typically, the perovskite layer in a solar cell exhibits high optical densities which may require the use of reflective means rather than transmission-based measurements if data is to be acquired rapidly and with minimal investment. Solutions for absorption measurements based on optical fibers are typically flexible and easy to incorporate into homemade scanners but lack the resolution of a full spectrophotometer.

IV characteristics are relatively simple to measure and a library sample poses no significant practical difference to single devices. Current losses can arise if the metal contact defining the active area of a

library pixel is placed too far away from the anode. This can lead to current underestimation in geometrically large library samples and the implementation of busbars may have to be considered.

Processing device libraries rapidly generates large amounts of data. While obtaining a maximum of information is what makes HTR promising, it can eventually lead to data generated that can no longer be effectively analyzed by individual researchers. Suitable infrastructure for storage and processing has to be developed to harvest the full potential of HTR. The large amount of information available from HTR may be of interest for data mining and machine learning.

5.11 Conclusion

Thermal Flash Vacuum Deposition was developed as simple, scalable, and rapid deposition method for the fabrication of hybrid perovskite thin film libraries for high-throughput research. The process requires minimal investment and can be applied to virtually any solid substrate. Unlike many present deposition processes used in PSC research, TFVD is likely to perform better and more efficiently in larger, industrial size reactors than in the available small deposition chamber. Material libraries with thickness gradients could be fabricated by exploiting naturally occurring inhomogeneity of the deposition profile on cold-wall reactor walls. The same process was used successfully in the fabrication of combinatorial material libraries of hybrid perovskites with varying halide compositions. This is, to the best of my knowledge, the first time a scalable combinatorial approach has been taken to investigate compositional effects on the perovskite layer itself. Implementation of combinatorial materials science to PSC research could significantly improve data quality, increase research output and lead to unexpected discoveries. Aside from this, the process introduced here offers the possibility for a high degree of automation and will allow complete de-coupling of the manual skills of the experimentalist from obtained results. In turn, reproducibility, reliability, and statistical relevance of new discoveries will be significantly improved. Introducing library-based combinatorial research methods in the PSC field may well free a large amount of man-hours that are now dedicated to repetitive tasks associated to sample preparation and allow researchers to explore more materials more easily.

6 Inkjet Printing for HTR

Inkjet printing has become a printing technique with an extremely wide field of applications today. Early research on inkjets and bubbles goes back as far as 1833 when Felix Savart was the first to make the breakup of liquid jets and drop formation his field of theoretical research. The first to describe the possibility to use transient pressure pulses to induce controlled breakup of continuous jets into micro droplets was Lord Rayleigh. His observations laid the foundation for modern inkjet printing. In 1870, Lord Kelvin filed the first patent of the field, describing a *"method to automatically record telegraphic messages by using electrostatic force to direct a stream of ink"*[236].

Today, inkjet printers have become standard home appliances and find uses not only in the printing industry but also in cell research, combinatorial materials science, fabrication of electronic circuits, and a multitude of other fields both in academic research and large-scale industrial applications. While in some fields, such as cell biology, an inkjet printer might be used to precisely dose or deposit cells in a pre-defined pattern, it may just as well be used in printing applications where each print is individual, such as for adding serial numbers to small devices or batch identifications in food processing. The fact that no pre-made, physical printing template is necessary makes inkjet printing highly adaptable and cost-effective. Various research groups have taken up the task of developing printable perovskite inks or even printing full PSC devices.[237–239]

6.1 Parameters and Basic Functioning of Drop-On-Demand Printing

The two main industrially relevant methods of inkjet printing are continuous inkjet (CIJ) and "Drop-On-Demand" (DOD). Thermal inkjet printing relies on significantly different principles and will not be discussed here. For printing perovskite libraries and devices, DOD was found to be the most appropriate method. Briefly, the ink flows through the nozzle orifice, producing a very short jet that eventually forms a single drop before reaching the surface of the substrate. The pressure to eject a drop is most commonly generated using a piezoelectric element to which a voltage pulse is applied. Variation of the waveform of the pulse has to be found for each ink and can differ significantly from printhead to printhead, depending on its geometry. Figure 47a schematically shows droplet generation in DOD. A typical waveform used for some of the perovskite inks formulated in the course of this project is shown in b) and the typical ideal evolution of a single droplet is depicted in panel c).

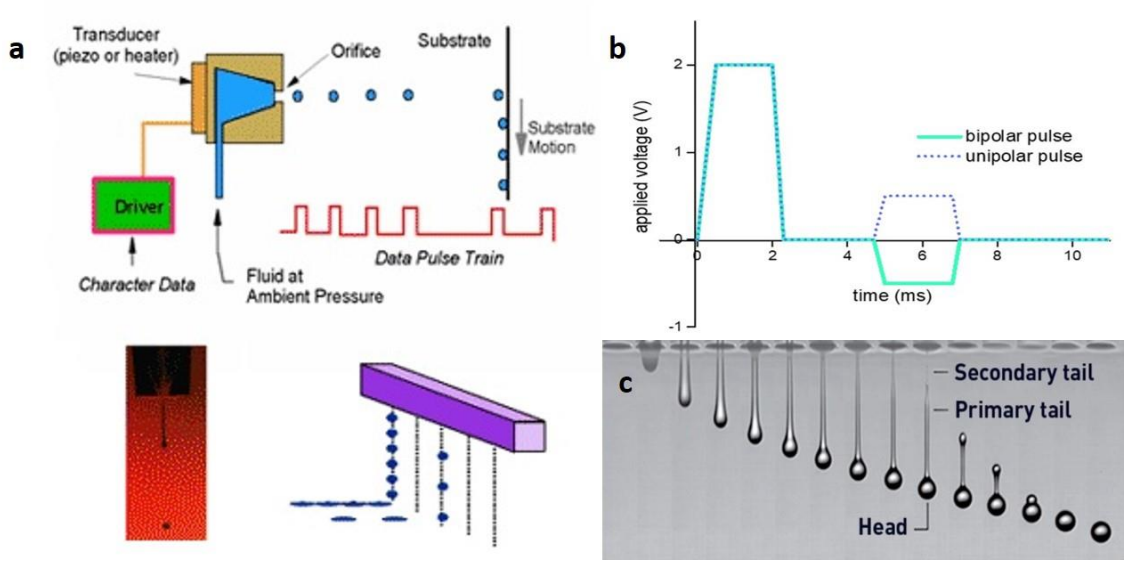

Figure 47 a) Schematic of drop-on-demand inkjet printing technology, reproduced with permission from Wiley Publishing Group b) Example of waveform applied to piezo in DoD printhead c) left –to-right: evolution of droplet from t_0 to t_i.

Regarding the jetting parameter optimization, mainly the following points have to be kept under consideration:

- Droplets should be round
- Volumes should be constant
- Droplets should fall straight to ensure maximum print resolution
- Tails should merge with the droplet before it reaches the substrate
- Falling velocity should be as fast as possible
- Satellite droplets should be avoided
- Spacing in x and y direction has to be optimized separately

6.2 Properties of Jettable Inks

Inkjet printing allows deposition of a wide range of fluids from human cell suspensions, liquid polymers, and colloidal nanoparticle inks to commercial inks for color printing. Despite the variety of liquids printed successfully in industry, R&D, and household printers, ink design is not trivial and liquids for inkjet printing have to fulfil a large number of criteria in order to be jettable in the first place. Some limitations, such as the maximum acceptable particle size in colloidal inks, are printhead-related and can vary significantly from setup to setup., others Other limitations are universal and governed purely by fluid dynamics, including viscosity, surface tension, or surface energy.

To ensure reproducible printhead filling and droplet ejection, relatively low viscosity is required, ranging from 1-20mPas. If the ink viscosity is too low no stable droplet formation will take place and tails and satellites are very likely to form, in turn reducing print resolution and uniformity. Some pure solvents including water, EtOH, CB, GBL and DMF/DMSO mixtures are printable with stable droplet formation without addition of viscosity modifiers. Typical viscosity modifiers for

industrial printing are non-adsorbing polymers such as polyethylene glycol. Although it was not possible to measure the viscosity of the prepared perovskite inks, it can be assumed that they fall into this range. Aside from modifying the composition of an ink, the fluid viscosity can be controlled by altering the temperature. As many organic solvents are volatile, the possibility for adjustment of ink viscosity by thermal means varies greatly from ink to ink.

The addition of colloids and/or polymers in particular can alter the main solvent viscosity significantly and even small alterations in composition can make the fluid impossible to jet. The addition of colloids can lead to the fluid behavior deviating from the typically Newtonian nature of non-polymeric solvents i.e. where $\tau = \eta\dot{\gamma}$ where τ is the shear stress, η the Newtonian viscosity and $\dot{\gamma}$ the applied shear rate, which requires particular attention during jet optimization.

In non-Newtonian fluids, the apparent viscosity η_a depends on the applied shear rate:

$$\tau = \eta_a(\dot{\gamma})\dot{\gamma}$$

The Einstein equation can be used for finding the lower bound for the viscosity for non-interacting particle-based inks when the particle concentration is low:

$$\eta = \eta_0\,(1 + 2.5\phi)$$

With η_0 being the base viscosity of the solvent or carrier liquid, and ϕ the volume fraction of particles added. While the Einstein equation shows that particle addition has a limited effect on the fluid viscosity, the narrow viscosity window acceptable for jetting can easily be exceeded by addition of even relatively small volume fractions of particles. Polymer addition or use of polymeric fluids tends to have more important effects on fluid dynamics but will not discussed here as all inks considered in this thesis are polymer free.

Surface tension γ [$Nm^{-1,}$, Jm^{-2}] is the second dominant physical property that governs the formation of drops and stable jets and which therefore has to fall into a certain known range. Most non-colloidal inkjet inks based on organic solvents have surface tensions from 20-40mNm^{-1}, H_2O with its relatively higher intermolecular energies reaches 72.5mNm^{-1}. Stark deviations from these values can make stable drop formation challenging or even impossible.

A number of dimensionless groups are used to further characterize fluid properties in inkjet printing:

Reynolds number (*Re)* represents the ration between inertial and viscous forces in a moving fluid:

$$Re = \frac{\rho V d}{\eta}$$

Where ρ is the density of the fluid,

V is the fluid velocity

d is a characteristic length, such as nozzle or jet diameter

η is the fluid viscosity

The Weber number (*We)* depends on the ratio between inertia and surface tension:

$$We = \frac{\rho d V^2}{\gamma}$$

Where γ is the surface tension

The Ohnesorg number (*Oh) (or Z=1/Oh)* allows to remove the influence of velocity on the two aforementioned dimensionless groups:

$$Oh = \frac{\sqrt{We}}{Re} = \frac{\eta}{\sqrt{\gamma \rho d}}$$

If the Ohnesorg number is too high, i.e. Oh>1, the separation of a drop will be prevented through viscous forces, while a low Ohnesorg number below 0.1 usually leads to the formation of undesired satellite drops. Figure 48 below illustrates the narrow parameter space a fluid has to fall into in order to be reproducibly printable.

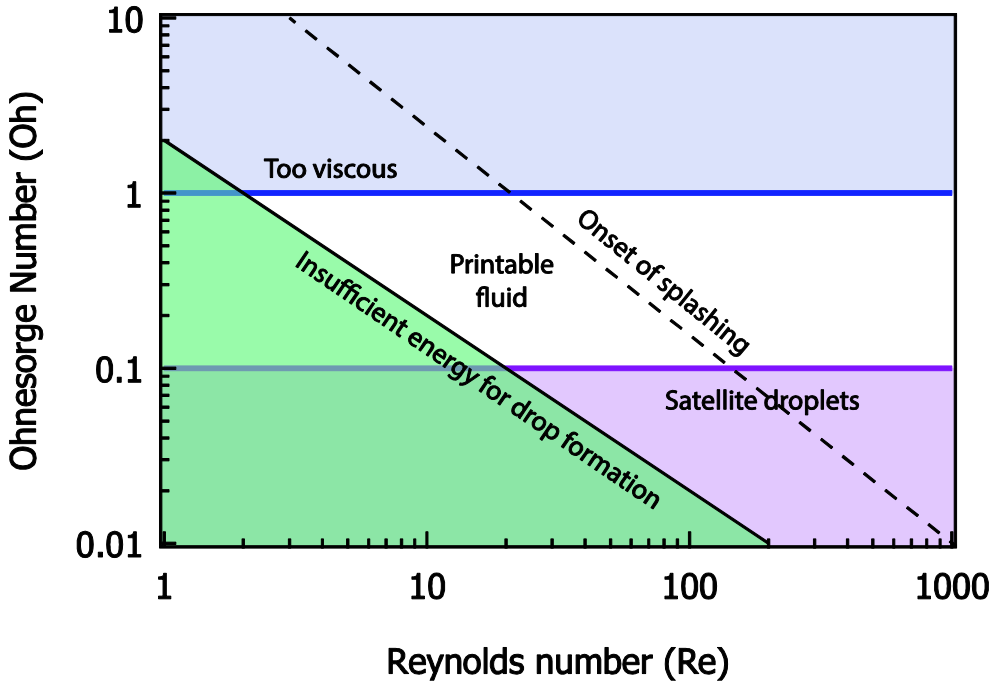

Figure 48 Graphic representation of printable fluid region considering Ohnesorg and Reynold's numbers

6.3 Ink Composition

The components of typical inks can be separated in two groups; namely components that are present to ensure printability and those that actually represent the components that are meant to be printed. Into the first category fall solvents, carrier fluids, de-foaming agents, humectants, viscosity modifiers, surfactants, biocides and auxiliary solvents. A number of examples are given in Table 5.

The second category of ink components may only make up a relatively small weight fraction. Today, printed materials range from dyes, pigments, and conductive carbon inks to animal or even human cells. In colloidal inks, such as perovskite precursors, the colloid size has to match the size diameter of the printhead nozzle. Empirically recommended are colloid sizes not exceeding 1/10 of the nozzle diameter. Typical printhead nozzle diameters for research printing range from 10 to 80µm, allowing relatively large particles to pass without clogging the nozzle. To ensure reproducible print resolution, the particle size distribution should be uniform and stable, and aggregation has to be avoided.

Colloidal inks are most commonly pigment-polymer dispersions, which allow highly colored, light-fast and stable prints.

Table 5 Typical ink composition, adapted from [240]

Component	**Amount (wt%)**	**Purpose**
Pigment	2-6	Color/active material
Diethylene Glycol	5-15	Water-miscible solvent
Glycerol	0-10	Humectant
2-Pyrollidone	0-10	Humectant
Surfynol 465	0.5-2	Surfactant
Proxel GXL	0.2	Biocide
Water	Balance	Solvent

Aside from rheological properties discussed above, inks should fulfil a multitude of further characteristics, e.g. suitable volatility, good surface wetting as well as a long shelf life.

6.4 Challenges and advantages in printing perovskite solar cells

6.4.1 Ink Design: Particles in Suspension vs. Precursor Ink

The fabrication of jettable perovskite inks poses several unique challenges. Theoretically, two approaches exist for preparing ink for perovskite printing. One is to prepare a colloid ink containing already crystallized, dispersed nanoparticles of the target material in an inert, volatile carrier liquid. Humectants and other auxiliary components might be added in order to ensure a long shelf-life and reproducible print performance. This approach would require uniform particles to be synthesized, at best in a solvent-free process such as dry-milling. The particle size would not only be restricted by the printhead nozzle diameter but also by the maximum film thickness desired. It is not clear if such an approach would actually lead to the formation of continuous films and which treatments (solvent vapor, heating) would be required to induce fusing of the deposited particles.

Another approach to ink design for perovskite printing is the use of one or several precursor inks similar to the spin coating precursors used in many groups. Complex compositions can be formed from precursor inks based on lead halides, inorganic and organic iodides and bromides, and a range of polar solvents.

The precursor ink approach is used to fabricate devices with the highest reported PCEs to date. Some inks have been reported to be stable for months[240].

In this case, the perovskite material would form after deposition on the substrate. Heating will be necessary to achieve crystallization. The precursor approach allows for complex uniform compositions with multiple cations and mixed-halides to be obtained and has been optimized very successfully for device preparation by spin-coating.

6.4.2 Precursor Ink Optimization

Perovskite precursor solutions are typically highly concentrated solutions containing solute as well as dispersed colloidal components. Details about the colloidal nature of the perovskite precursors are discussed in Chapter 1.

Perovskite precursor solutions tend to crystallize very rapidly even at moderate temperatures which can pose some practical issues such as clogged printhead nozzles, but also leads to difficulties in optimization of x-y-spacing of the print. Rapid crystallization in heavily particle-laden liquids generally makes obtaining uniform films challenging due to the Coffee Ring Effect, which is a common occurrence in sessile droplet dying, as occurs in inkjet printing.

For many inkjet printing inks, the ink design can be approached on the basis that all or most variables such as particle sizes, size distribution, chemical composition and components are known. Typically, a carrier liquid would be selected based on rheological characteristics, toxicity as well as substrate compatibility, surfactants, humectants and stabilizers would be added systematically, as briefly outlined above. For inert colloids, a vast range of carrier liquids exists and adjustment of viscosity can often be achieved by addition of polymers. In the case of perovskite precursor inks, ink design does not allow many degrees of freedom.

In the present case, the selection of solvent/carrier liquid is limited to DMF, DMSO and γ-butyrolactone and their mixtures. Other solvents typically are not able to dissolve sufficient concentrations of the precursor components to fabricate thick enough layers for applications desiring maximum absorption in the visible region. While DMF is undesirable in large-scale applications due to toxicity as well as corrosive nature, γ-butyrolactone possesses low vapor pressure in standard conditions which results in very slow drying rates. Inks based on acetonitrile (ACN) have been reportedly fabricated by bubbling methylammonium gas through a concentrated PbI_2-ACN mixture[241]. This composite MA-ACN solvent has been promoted as environmentally superior to DMF-DMSO based solutions, a detailed discussion on solvent ecotoxicity and environmental performance can be found in Chapter 2. DMSO is commonly regarded as overall environmentally favorable solution, however, its high surface made it difficult to jet the solvent alone. Mixtures of DMSO and GBL/DMF were successfully jetted.

The main complication in perovskite ink composition lies within the (unknown) nature of the colloid. As the halide salts are actually not fully soluble in either solvent discussed at concentrations typically required for the formation of optically dense films, the precursor is actually a colloidal suspension, as can be demonstrated by a simple Tyndall test (see Chapter 1). Considering the Einstein equation discussed above, the particle fractions do substantially alter the rheological properties of any liquid. While the equation is expressly to be applied to systems with low particle content and assumes non-interaction, it demonstrates a further complication in ink design for hybrid perovskites; as the particle fractions are not known and interactions in the colloid have, to the best of my knowledge, not been fully understood, precise predictions on the ink's rheological behavior are difficult to make. The high optical density (>4) of

lead iodide-based inks makes particle size distribution analysis challenging, and the unknown optical properties of the colloidal species are likely to induce imprecise results.

The shelf-life of perovskite inks appears to depend on their concentrations. Inks with concentrations above 0.8M tending to form elongated, needle-like structures after being left undisturbed for multiple days, particularly in the case of DMF-only based precursors. A long shelf-life is highly desirable for the printing optimization as the process is relatively slow and small variations in compositions may alter the ink behavior unexpectedly. Furthermore, the formation of large structures is highly problematic as their presence easily leads to nozzle clogging and/or alteration of the jetting behavior if they deposit near the orifice.

6.4.3 Morphology

Figure 49 shows a DMF based ink consisting only of PbI_2 and CH_3NH_3I on a non-pre-treated planar NiO_x surface. [7] The coverage is clearly not uniform, and the deposit exhibits typical Coffee Ring patterns.

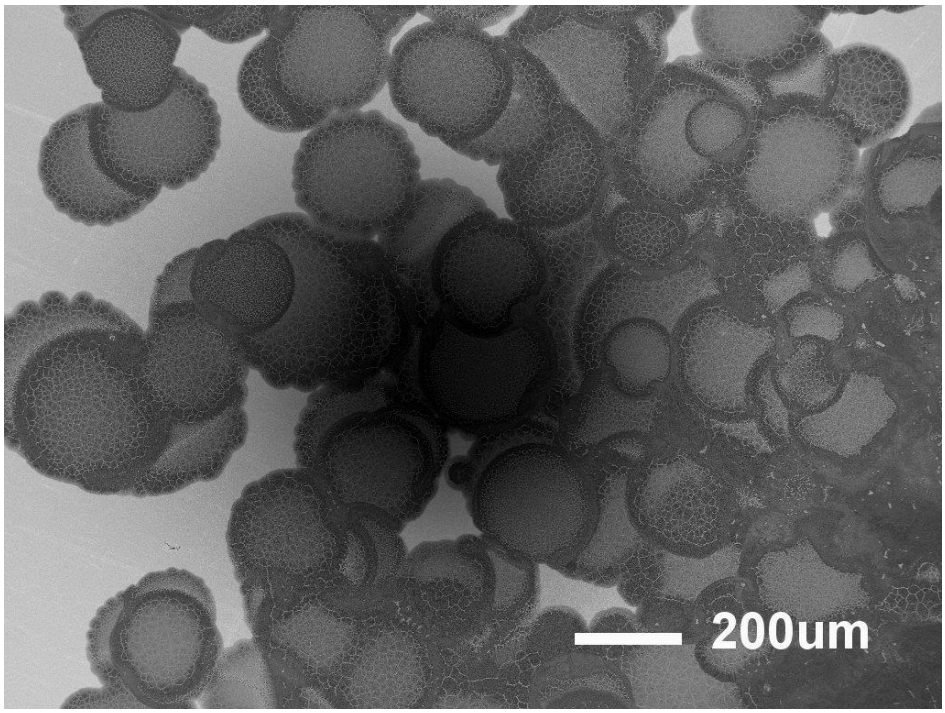

Figure 49 Typical Coffee Ring formation on edges of film, perovskite precursor ink printed on NiOx. Dark region in center due to SE detector positioning

Coffee Rings are characteristic of deposits of colloidal/particulate suspensions and are the result of multiple phenomena. Masking the original shape of the droplet, they are produced by particle transport by radial flow moving outwards form the center to regions with higher evaporation rates, i.e. to the contact line. Near the contact line, the concentration eventually exceeds saturation and typical ring

[7] For printing parameters, XRD patterns of printed films and print-speed-morphology relationship please see corresponding section of the annex

patterns are formed. Thickness of the (solid) ring is dependent on the solvent(s) evaporation rate(s). Coffee Rings typically do not occur in small droplets with diameters <10µm where complete evaporation of the solvent typically occurs before the radial outwards particle transport becomes relevant. [242]

The presence of Coffee Rings is not desirable for applications in PSC devices which require complete and pin hole free coverage in order to avoid recombination centers between the ETL and HTM. Multiple strategies can be used to overcome or reduce the effect, including the application of an AC electric field through the apex and the substrate ("Electrowetting"), reduction of droplet size, or modification of droplet evaporation flux. Electrowetting is not suitable for industrial applications and was discarded. In order to modify the surface-liquid interaction, both ink and substrate surface can be targeted.

Substrate pre-treatment

Film formation and homogeneity could be improved by treating the surfaces immediately prior to ink deposition.

Figure 50 shows electron images of films deposited after pre-treatments, with a) as control (i.e. no treatment except for heating to 450°C for 5min which was done to all samples). Sample b) was subjected to an O_3 treatment before printing. Sample c) was dipped into anisole (99%, Arcos) and left to dry naturally before ink deposition. This same process was used on sample d) with chlorobenzene. All substrates were printed at 115°C platen temperature with the same ink and jet setup.

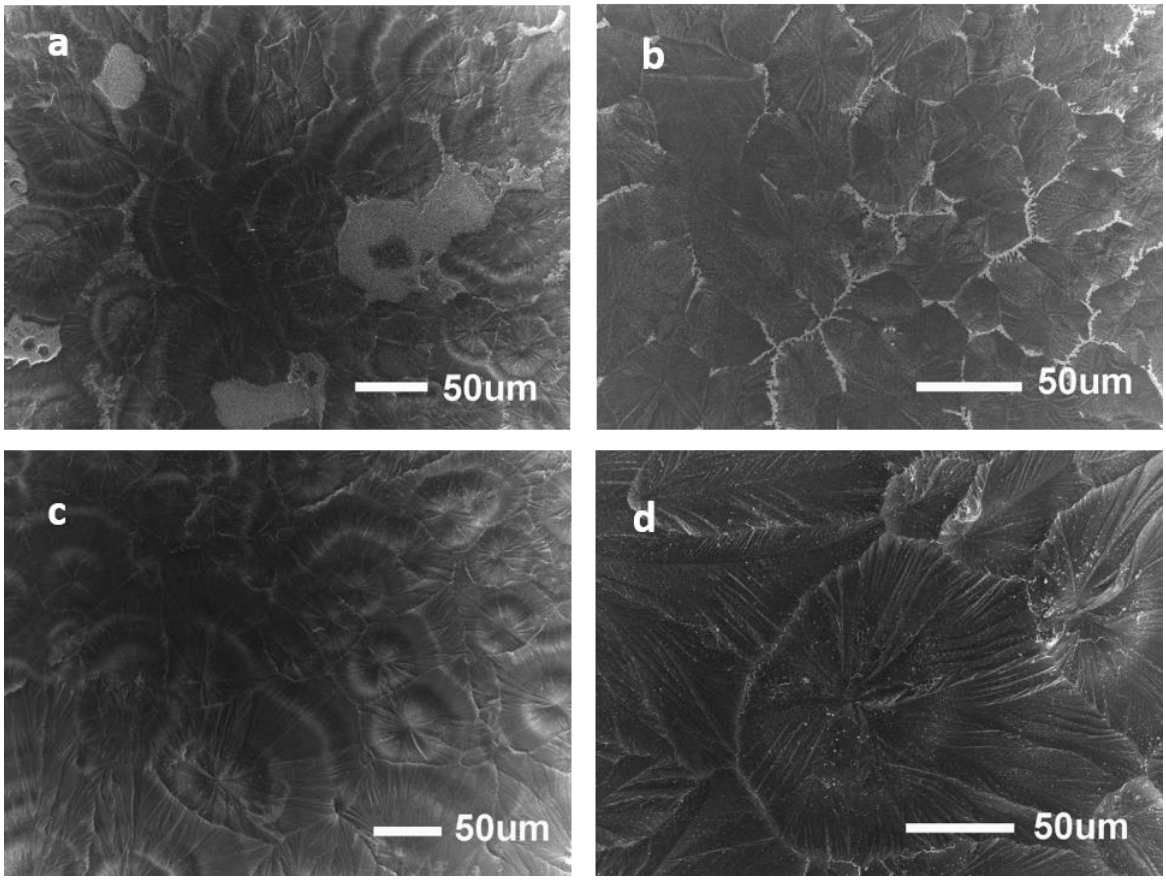

Figure 50 secondary electron images of inkjet printed films with various pre-treatments: a) control-no treatment b) ozone c) anisole d) chlorobenzene

Ink Modification

Figure 52 shows perovskite thin films printed from 0.5M equimolar PbI_2-MAI inks with two different solvent compositions. Panels a and c show the same substrate printed with a DMF-DMSO-GBL mixture as the solvent. Images b and d show the same substrate, printed with GBL-based ink. The samples show large differences in morphology. The single-solvent ink led to poor coverage and still shows signs of coffee stains. The film produced from the mixed solvent system does notproduce continuous coverage either, but shows very different morphological features.

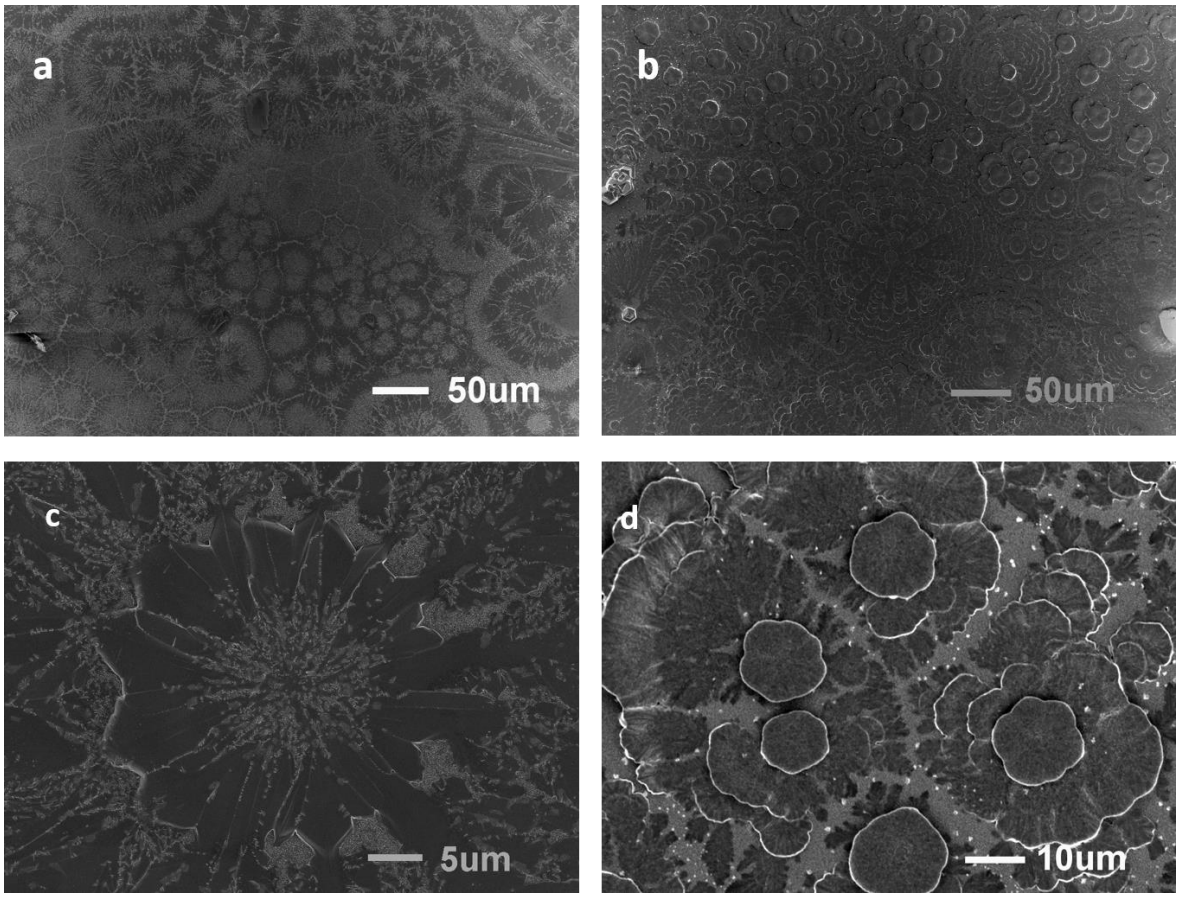

Figure 51 secondary electron images of inkjet printed films deposited from GBL-DMSO-DMF-mixed solvent ink (a+c) and GBL based ink (b+d) on planar TiO_2

The importance of controlling solvent evaporation in inkjet printing is well known and one of the most important aspects of ink design. As the boiling points in the mixed solvent system used here differ significantly (208°C for GBL, 189°C for DMSO and 154°C for DMF under standard conditions), the evaporation of the solvent is likely occurring in multiple stages, with the evaporation rate of the most volatile solvent controlling the evaporation rate in the first stage. The morphology is likely differing depending on whether the system leads to a pinned or moving contact line during drying.

Small additions of DMF to GBL based inks could be observed to already significantly impact the morphology of printed $CH_3NH_3PbI_3$ films, as depicted in the electron images in Figure 52.

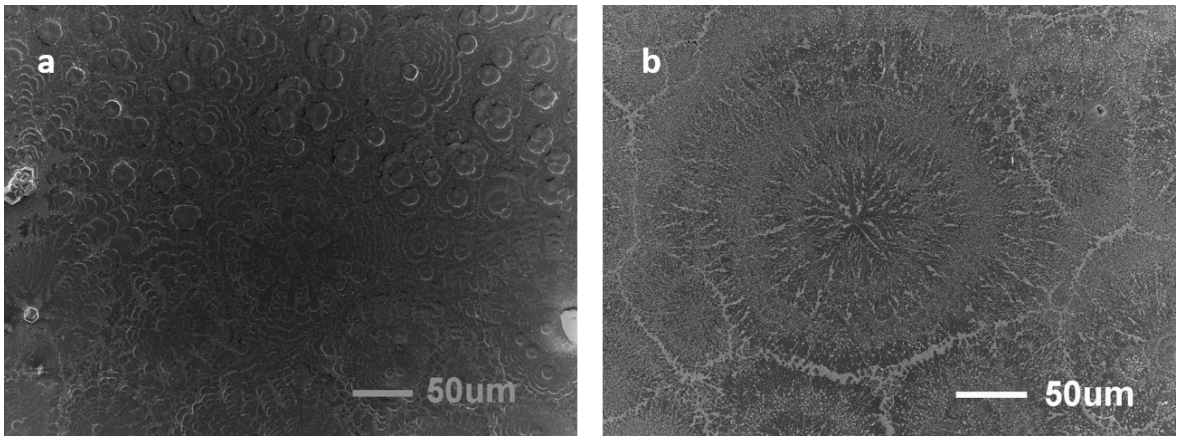

Figure 52 electron images of films printed from a) GBL-based ink and b) 90%GBL and 10% DMF

6.5 Strategies for Compositional Library Printing

Several approaches are promising for the fabrication of combinatorial perovskite libraries by inkjet printing. The possibility for implementing these strategies is likely to be limited by the specifications of the inkjet printer available and options for modifications on existing setups.

In commercial color inkjet printers, different colors are achieved through combinations of several color inks, commonly magenta, cyan, yellow and black. By printing defined numbers of droplets of the color precursors and varying their ratios in number and spacing, colors printable from these basic inks cover the entire visible spectrum and represent thousands of combinations.

The same approach used in standard office printers to generate different colors could theoretically be used to print combinations of multiple perovskite inks. Good compatibility of the various precursor inks is likely required in order for this approach to be successful. Inks should be completely miscible and exhibit very similar microfluidic characteristics in order to avoid liquid phase separation during drying of the deposited liquid film. Generation of Marangoni flows due to differences in fluid viscosities and evaporation rates can lead to non-uniform particle distribution in a drying droplet and can be detrimental to homogeneous film formation. [242]

In the setup available for the present project, printing from two printheads simultaneously is not possible; a different approach has to be taken for library printing.

Figure 53 schematically shows a possible approach to printing compositional libraries using only one printhead at a time. The green background in the three exemplary pixels represents a primary precursor ink deposited first. The primary ink is printed until continuous liquid coverage of the pixel. Blue dots represent the secondary ink used to vary the composition of the final film, printed into the still liquid primary ink. By varying the amount of secondary ink per pixel, multiple variations of for example halides can be achieved. In the suggested approach, the amount of secondary ink per pixel is varied by tuning the x-y-spacing of droplets deposited on top of the primary ink.

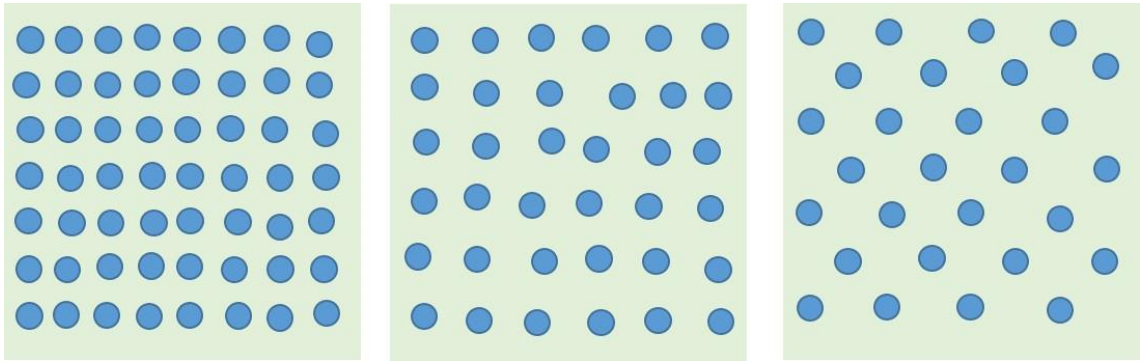

Figure 53 Schematic approach to varying composition using only one printhead: green: primary ink, blue: secondary ink, printed with varying XY-spacing on top of primary ink

High boiling point solvents allow for longer mixing time and might may advantageous. Although this process cannot produce the combinatorial gradients shown in the previous chapter on vacuum-deposited thin films, it can generate arrays of defined ink combinations and film compositions. While possibly requiring more area to achieve the same number of combinations as in vacuum-deposited libraries, the advantage of an array-based library over one with combinatorial gradients is that the entire pixel possesses the same composition. This may simplify interpretation of results. Small pixels are advantageous here in order to reduce the difference in time until crystallization during heating across the library. Rapid over-printing with an anti-solvent may be advantageous in reducing such effects.

Similar strategies might be used to produce not only combinatorial perovskite libraries but also to assess optimum doping in hole transport materials.

6.6 Conclusion

Hybrid organic-inorganic perovskites typically used in PV applications can be inkjet printed. The method is scalable and the preparative outcome is assumed to be independent of the printer operator. The process is very material efficient with low amounts of solvent waste generated during operation compared to spin-coating or dip-coating. A high degree of automation is possible. Surface-ink interaction can be improved by treating the substrate with an anti-solvent and O_3. IJP is a versatile method that allows sample preparation without the need for physical masks. The method is thought to be suitable for the preparation of combinatorial libraries for HTR, but much optimization work will be required until efficient solar cell devices can be fully prepared using this method.

7 Annex

7.1 Single Crystal XRD

STOE XRED32 1.57 23-Jul-2016 15:05

Input File(s) : D:\Kunden\Jeanette\OneToOnePointTwoBromine\MrSoSo.x

Cell Parameters : 5.9243(9), 5.9243(9), 5.9243(9), 90.00, 90.00, 90.00

Cell Volume : 207.93(5)

Laue Symmetry : Cubic m 3 Lattice : Primitive

Chemical Formula : C1 H6 N1 Pb1 Br3

Molecular Weight : 479.0 Z = 1 Volume/Atom = 34.7

Density (calc.) : 3.83 Mg/m^3

Absorption Coef. : 34.68 mm^-1

Number of reflections read : 3420 Rejected : 36 (overflowed, Lorentz zone)

Residual reflections used : 3384

Minimum and maximum 2Theta : 6.9, 72.9

Minimum and maximum H,K,L : -9,-9,-9 9,9,9

Avg. I/Sigma for all data : 43.63

Number of unique reflections : 208

Completeness of data set [%] : 97.7 Redundancy : 16.27

R(int) = 0.1415 (3382 contributors) R(Sigma) = 0.0222

Average I/Sigma vs. 2Theta

2Theta	6.9	29.9	37.9	45.2	51.0	55.4	59.0	62.7	66.3	70.0	72.9
Resol.	5.92	1.38	1.09	0.93	0.83	0.76	0.72	0.68	0.65	0.62	0.60
N(Refl)	326	322	409	358	333	337	366	345	445	143	
I/Sigma	122.97	93.89	67.41	42.98	28.73	24.77	21.17	12.73	7.84	5.75	
Completeness	100.0	100.0	100.0	100.0	100.0	100.0	100.0	100.0	100.0	66.7	
Redundancy	13.6	16.1	17.0	17.0	17.5	16.9	15.9	17.3	16.5	14.3	

R(int) 0.108 0.114 0.158 0.167 0.181 0.183 0.188 0.206 0.221 0.270

I/Sigma < 0 2 4 8 16 32 64 128 256 512

N(Refl) 5 26 98 459 1137 1961 2655 3147 3365 3384

Percent 0.1 0.8 2.9 13.4 33.2 57.3 77.6 92.0 98.4 98.9

Absorption Correction : Numerical

Absorption Coefficient : 34.68 mm^-1

Min and max Transmission : 0.0089, 0.0503

Crystal Faces

N	H	K	L	D [mm]
1	4	4	1	0.1300
2	1	3	-5	0.1100
3	0	-1	-4	0.1300
4	0	1	4	0.1400
5	-1	-3	5	0.2020
6	1	-6	0	0.1000
7	0	-4	-1	0.1140
8	-7	-1	0	0.1500
9	-7	2	1	0.1400
10	6	0	-5	0.1650
11	5	-3	0	0.1600
12	-4	6	-3	0.1900
13	-3	-1	-6	0.1630
14	4	4	-1	0.1260
15	1	0	0	0.1650
16	0	3	4	0.1610
17	-7	6	-1	0.1820
18	2	3	-11	0.1030

131 Inconsistent Equivalents (ESD > 4 * Sigma)

H	K	L	Mean Int.	Sigma	ESD	N
0	0	2	10000.0	36.1	1507.9	6
0	2	4	3716.9	18.4	682.2	11
0	2	2	7213.7	27.6	1003.0	12
0	0	4	5304.1	21.4	711.8	6
0	1	4	3145.2	17.5	545.2	11
2	0	4	3832.7	18.8	511.2	11
2	2	2	5280.3	23.0	611.7	8
0	0	6	2259.9	16.9	422.5	6
1	0	4	3350.8	18.1	441.9	11
1	2	4	2521.8	16.3	378.3	22
1	0	2	4178.9	24.2	556.1	11
1	1	4	1894.6	15.2	339.5	24
2	1	4	2533.5	17.0	361.5	23
0	2	6	1619.2	15.9	332.5	12

0	4	4	1663.5	15.3	317.7	12
2	1	5	455.6	11.5	237.7	23
2	2	4	2543.2	16.4	337.7	22
1	2	2	3823.8	20.3	417.1	22
1	2	6	1322.2	14.5	287.1	22
0	1	6	1814.2	15.9	310.0	12
0	0	1	3937.2	33.8	624.7	6
2	0	8	478.8	15.4	282.3	13
1	0	6	1896.7	15.9	292.7	12
0	1	2	4318.3	24.3	443.0	12
2	0	6	1670.7	15.6	276.8	11
0	0	3	2615.1	17.9	309.1	6
1	1	6	1493.6	15.5	265.9	24
2	2	6	1122.2	14.3	243.5	20
0	2	3	2303.8	16.6	279.0	12
0	3	6	948.4	13.6	225.1	10
2	0	3	2252.3	16.3	267.7	12
2	1	6	1359.2	14.7	241.5	22
3	4	4	734.1	12.4	201.7	18
1	4	4	1363.2	14.2	229.2	22
0	3	4	1671.8	15.5	250.4	12
2	2	3	1918.3	15.1	237.1	22
2	4	4	1209.2	13.4	193.8	18
0	4	6	718.5	13.8	198.3	10
1	3	6	850.5	13.9	193.5	22
1	1	2	1681.5	16.2	224.1	21
3	0	6	1013.7	15.0	198.3	12
3	0	4	1701.7	15.4	201.6	12
2	3	6	739.5	13.8	171.4	21
2	3	4	1323.2	14.2	175.6	22
0	1	1	1739.0	21.5	263.1	12
0	2	5	802.2	13.4	159.1	12
1	4	6	649.9	14.2	165.5	22
1	3	4	1158.9	13.6	159.4	22
3	2	4	1311.1	13.6	152.7	20
3	1	6	859.4	14.1	158.1	22

etc.

STOE XRED32 1.57 19-Jul-2016 19:03

Input File(s) : D:\Kunden\Jeanette\OneToOneBromine\MrCUBE.x

Cell Parameters : 5.9343(5), 5.9343(5), 5.9343(5), 90.00, 90.00, 90.00

Cell Volume : 208.98(3)

Laue Symmetry : Cubic m 3 Lattice : Primitive

Chemical Formula : C1 H6 N1 Br3 Pb1

Molecular Weight : 479.0 Z = 1 Volume/Atom = 34.8

Density (calc.) : 3.81 Mg/m^3

Absorption Coef. : 34.50 mm^-1

Number of reflections read : 3399 Rejected : 33 (overflowed, Lorentz zone)

Residual reflections used : 3366

Minimum and maximum 2Theta : 6.9, 72.7

Minimum and maximum H,K,L : -9,-8,-9 9,9,9

Avg. I/Sigma for all data : 31.80

Number of unique reflections : 211

Completeness of data set [%] : 99.1 Redundancy : 15.95

R(int) = 0.1422 (3363 contributors) R(Sigma) = 0

Average I/Sigma vs. 2Theta

2Theta	6.9	29.8	37.8	45.1	50.2	55.3	58.9	62.5	66.2	69.8	72.7
Resol.	5.93	1.38	1.10	0.93	0.84	0.77	0.72	0.68	0.65	0.62	0.60
N(Refl)	326	320	324	402	372	329	375	331	440	147	
I/Sigma	104.79	72.52	47.54	34.86	17.28	15.06	12.28	6.76	3.80	2.41	
Completeness	100.0	100.0	100.0	100.0	100.0	100.0	100.0	100.0	100.0	86.7	
Redundancy	13.6	16.0	17.1	16.8	17.7	16.5	16.3	16.5	16.3	11.3	
R(int)	0.168	0.113	0.112	0.119	0.120	0.126	0.135	0.169	0.265	0.359	

I/Sigma	< 0	2	4	8	16	32	64	128	256	512

N(Refl) 6 149 471 991 1722 2377 2847 3220 3357 3366

Percent 0.2 4.4 13.9 29.2 50.7 69.9 83.8 94.7 98.8 99.0

Absorption Correction : None

69 Inconsistent Equivalents (ESD > 4 * Sigma)

H	K	L	Mean Int.	Sigma	ESD	N
0	2	2	7461.7	31.7	2503.9	12
0	0	4	4452.7	22.2	1346.3	5
0	0	2	10000.0	40.9	2259.5	6
1	0	2	4246.7	27.2	1181.8	12
0	1	2	4136.0	27.2	1110.3	12
0	0	3	2230.5	18.8	556.1	6
0	1	4	2650.0	18.7	538.9	12
0	2	3	2030.3	17.0	428.4	10
1	2	2	3947.8	23.0	576.4	22
1	0	4	2602.2	18.5	457.8	12
2	0	3	2029.1	17.8	428.3	12
0	0	6	1774.3	17.3	378.3	6
2	0	4	2973.8	19.5	417.8	12
1	1	4	1601.3	16.4	349.6	23
0	1	1	1744.9	25.4	533.4	12
1	2	4	2159.7	17.3	358.7	20
2	1	4	2076.3	17.7	360.0	24
2	2	4	2224.5	17.7	357.6	22
0	0	1	3601.8	37.7	715.3	6
0	2	4	3043.9	18.3	326.7	10
1	1	2	1652.0	18.9	302.6	24
0	1	6	1423.0	16.2	256.0	10
0	3	4	1351.2	14.8	215.8	10
1	0	6	1426.4	16.8	235.2	12
2	2	3	1731.9	16.4	227.1	23
2	2	2	5486.9	25.7	323.7	8
0	4	4	1313.6	14.9	173.2	9
0	2	6	1209.2	15.1	173.6	10
1	1	6	1142.1	16.1	184.7	24
3	0	4	1326.8	16.2	184.9	12
2	2	6	796.3	14.9	163.3	22
0	0	5	654.6	14.6	157.2	6

1	2	3	946.7	14.3	142.3	21
1	2	6	977.0	15.3	150.8	22
1	0	3	700.7	14.0	137.1	12
2	1	6	972.3	15.6	147.8	24
2	1	3	923.2	14.5	128.4	23
0	3	3	592.3	12.5	108.1	10
3	2	4	1098.4	15.2	130.9	22
2	3	4	1090.0	14.8	124.4	21
2	0	6	1181.3	16.3	131.7	12
3	1	4	929.2	14.5	114.8	22
1	3	4	971.5	14.7	116.3	21
2	2	5	528.7	13.3	105.0	21
0	3	6	675.9	14.6	107.1	10
0	1	3	698.3	14.3	105.2	12
1	3	6	585.6	14.1	100.2	20
1	4	4	1098.9	15.1	101.5	22
0	2	5	589.9	13.2	86.7	10
3	2	6	510.5	14.4	91.9	20

etc.

STOE XRED32 1.57 14-Jun-2016 16:15

Input File(s) : D:\Kunden\Jeanette\MAPbBr3\MrIrregolare.x

Cell Parameters : 5.9251(6), 5.9251(6), 5.9251(6), 90.00, 90.00, 90.00

Cell Volume : 208.01(4)

Laue Symmetry : Cubic m 3 Lattice : Primitive

Chemical Formula : C1 N1 H3 Pb1 Br3

Molecular Weight : 476.0 Z = 1 Volume/Atom = 34.7

Density (calc.) : 3.80 Mg/m^3

Absorption Coef. : 34.66 mm^-1

Number of reflections read : 3410 Rejected : 32 (overflowed, Lorentz zone)

Residual reflections used : 3378

Minimum and maximum 2Theta : 6.9, 72.8

Minimum and maximum H,K,L : -9,-9,-9 9,9,7

Avg. I/Sigma for all data : 44.82

Number of unique reflections : 209

Completeness of data set [%] : 98.1 Redundancy : 16.16

R(int) = 0.0569 (3377 contributors) R(Sigma) = 0.0193

Average I/Sigma vs. 2Theta

2Theta	6.9	29.9	37.9	45.9	51.7	56.1	60.5	64.1	67.8	71.4	72.8
Resol.	5.93	1.38	1.09	0.91	0.81	0.76	0.71	0.67	0.64	0.61	0.60
N(Refl)	324	327	447	337	375	431	357	364	383	33	
I/Sigma	151.11	105.46	65.06	42.70	24.92	18.44	11.29	5.46	2.86	1.97	
Completeness	100.0	100.0	100.0	100.0	100.0	100.0	100.0	100.0	100.0	55.6	
Redundancy	13.5	16.4	17.2	16.0	17.9	17.2	17.0	15.2	17.4	6.6	
R(int)	0.041	0.042	0.053	0.057	0.085	0.115	0.182	0.289	0.460	0.443	

I/Sigma	< 0	2	4	8	16	32	64	128	256	512
N(Refl)	31	237	487	856	1421	2033	2643	3084	3320	3377
Percent	0.9	7.0	14.3	25.1	41.7	59.6	77.5	90.4	97.4	99.0

Absorption Correction : Numerical

Absorption Coefficient : 34.66 mm^-1

Min and max Transmission : 0.0237, 0.1431

Crystal Faces

N	H	K	L	D [mm]
1	1	2	1	0.1430
2	2	3	-3	0.2880
3	-6	-7	0	0.1590
4	5	2	4	0.0640
5	-2	-7	3	0.1830
6	-5	-1	-6	0.0330
7	4	1	3	0.0600
8	10	-1	3	0.0940
9	3	1	4	0.1000
10	2	-1	-2	0.1750
11	-6	1	-5	0.0160
12	-6	5	1	0.0300
13	0	-7	-2	0.1180

51 Inconsistent Equivalents (ESD > 4 * Sigma)

H	K	L	Mean Int.	Sigma	ESD	N
0	0	2	10000.0	26.3	667.5	6
0	0	6	947.2	6.4	104.0	4
0	2	2	6247.6	17.5	256.8	12
0	1	4	2046.7	9.3	124.4	10
0	0	1	4163.8	23.7	311.3	5
0	2	4	2297.8	9.4	108.7	10
1	0	4	2065.7	10.1	112.4	11
0	1	2	3634.3	15.6	171.2	11
0	0	4	3336.9	12.3	133.1	6
2	0	4	2373.0	10.5	106.4	12
1	2	4	1572.3	8.7	86.2	22
0	3	4	991.1	7.8	76.0	12
2	2	2	4139.7	13.7	125.3	8
2	1	4	1585.9	8.8	78.2	22
1	1	6	638.5	6.5	54.9	20
2	0	3	1574.1	9.3	78.8	12
1	0	2	3625.1	15.5	126.7	12
1	2	6	598.1	6.6	53.8	20
0	2	6	711.5	6.7	52.4	10
1	0	6	777.0	6.9	52.7	9
0	1	6	799.3	7.0	53.6	10
1	1	4	1215.3	8.2	61.3	21
0	2	3	1572.7	9.5	69.2	11
2	0	6	701.7	6.9	50.2	8
2	1	6	605.7	6.6	47.5	21

2	2	4	1655.4	9.0	63.3	22
1	2	2	2946.2	12.5	85.9	24
2	2	3	1324.3	8.7	57.4	23
0	4	4	931.8	7.6	50.0	11
1	3	4	684.2	7.0	45.1	22
1	4	4	774.3	7.4	45.5	22
3	0	4	1003.6	8.3	50.5	11
2	2	6	526.4	6.7	40.3	22
0	1	3	610.4	6.7	40.1	10
3	1	4	693.8	7.3	41.8	24
1	3	6	374.3	6.0	34.4	20
2	0	5	441.2	6.8	37.3	12
3	2	4	800.9	7.5	40.7	23
4	1	6	288.9	6.6	34.2	21
0	3	6	428.6	6.2	30.8	10
0	2	8	172.0	6.2	29.4	10
2	4	4	701.8	7.5	34.8	23
3	0	8	104.7	6.2	28.5	10
0	0	8	237.3	5.3	23.6	4
0	3	3	432.9	6.6	29.6	11
0	0	5	419.1	6.6	28.9	6
1	2	5	293.5	6.1	25.9	22
0	0	3	1851.5	10.7	45.0	6
1	0	3	618.7	7.5	31.1	12
0	2	5	416.0	6.1	25.4	10

etc.

STOE XRED32 1.57 03-Oct-2016 12:04

Input File(s) : D:\Kunden\Jeanette\FourToSixFromBromine\MrKute.x

Cell Parameters : 5.9276(5), 5.9276(5), 5.9276(5), 90.00, 90.00, 90.00

Cell Volume : 208.28(3)

Laue Symmetry : Cubic m 3 Lattice : Primitive

Chemical Formula : C1 H6 N1 Br3 Pb1

Molecular Weight : 479.0 Z = 1 Volume/Atom = 34.7

Density (calc.) : 3.82 Mg/m^3

Absorption Coef. : 34.62 mm^-1

Number of reflections read : 3298 Rejected : 22 (overflowed, Lorentz zone)

Residual reflections used : 3276

Minimum and maximum 2Theta : 6.9, 72.8

Minimum and maximum H,K,L : -9,-7,-7 9,9,9

Avg. I/Sigma for all data : 42.32

Number of unique reflections : 209

Completeness of data set [%] : 98.1 Redundancy : 15.67

R(int) = 0.0549 (3275 contributors) R(Sigma) = 0.0223

Average I/Sigma vs. 2Theta

2Theta	6.9	29.9	37.9	45.1	51.0	55.3	59.0	62.6	66.3	69.9	72.8
Resol.	5.93	1.38	1.10	0.93	0.83	0.77	0.72	0.68	0.65	0.62	0.60
N(Refl)	314	315	401	344	329	316	364	318	433	142	
I/Sigma	130.50	93.33	65.11	38.52	25.04	22.41	18.68	10.64	6.35	4.64	
Completeness	100.0	100.0	100.0	100.0	100.0	100.0	100.0	100.0	100.0	73.3	
Redundancy	13.1	15.8	16.7	16.4	17.3	15.8	15.8	15.9	16.0	12.9	
R(int)	0.057	0.047	0.047	0.051	0.057	0.058	0.061	0.087	0.130	0.177	

I/Sigma	< 0	2	4	8	16	32	64	128	256	512
N(Refl)	1	11	181	601	1252	1993	2612	3035	3258	3276
Percent	0.0	0.3	5.5	18.2	38.0	60.4	79.2	92.0	98.8	99.3

Absorption Correction : Numerical

Absorption Coefficient : 34.62 mm^-1

Min and max Transmission : 0.0025, 0.0497

Crystal Faces

N	H	K	L	D [mm]
1	1	0	0	0.1430
2	-1	0	0	0.1300
3	0	-1	0	0.1680
4	0	1	0	0.1200
5	0	0	1	0.0940
6	0	0	-1	0.1170
7	-1	-1	0	0.1970
8	7	1	4	0.1550
9	2	9	4	0.1290

50 Inconsistent Equivalents (ESD > 4 * Sigma)

H	K	L	Mean Int.	Sigma	ESD	N
0	0	2	10000.0	35.7	803.1	6
1	0	4	2397.1	13.5	212.7	12
2	0	4	2727.1	13.9	213.1	11
0	1	4	2372.6	12.6	169.6	11
2	2	2	4742.9	18.6	249.6	8
0	0	1	4459.6	40.9	545.5	5
0	2	4	2730.4	14.0	175.5	12
0	1	2	4069.5	21.2	264.1	12
1	0	2	4091.7	21.6	246.0	12
0	2	2	6727.1	20.8	236.3	10
2	2	4	1935.4	13.2	141.0	24
1	2	2	3461.4	17.0	175.4	23
1	1	4	1416.4	10.7	100.8	18
0	0	4	3719.4	14.0	120.5	6
3	0	4	1151.4	9.3	76.6	10
1	4	4	912.9	9.0	71.3	20
2	0	3	1841.4	11.8	91.6	9
0	2	3	1834.1	11.8	91.5	9
0	1	1	1593.7	16.5	128.0	10
2	1	4	1883.1	12.7	96.9	23
1	2	4	1886.8	12.3	94.2	23
0	3	4	1151.3	9.4	69.8	10
2	2	3	1599.6	12.3	91.1	24
0	4	4	1075.8	9.3	68.6	10

1	1	2	1571.5	13.9	95.5	24
0	2	6	829.8	8.4	54.4	12
1	0	6	926.1	7.7	48.4	12
1	3	4	825.2	9.3	57.6	19
0	0	3	2003.5	13.4	77.6	6
1	2	6	707.4	8.2	46.5	24
2	0	6	838.0	8.4	47.2	10
0	1	6	925.3	7.7	41.5	12
3	2	4	956.0	10.5	55.0	21
0	0	6	1135.2	7.9	41.3	6
2	0	5	491.5	8.7	44.1	10
2	1	6	708.5	8.5	42.5	23
1	1	6	764.1	7.6	37.5	23
0	3	6	507.8	7.5	36.3	9
1	0	3	743.4	11.5	54.2	12
3	1	4	815.5	9.3	43.6	20
0	2	5	495.2	8.7	40.0	11
3	0	6	522.8	8.2	37.4	9
2	3	4	944.7	10.4	46.9	21
2	1	3	849.8	10.5	47.4	22
1	2	3	847.3	10.5	45.1	22
0	3	5	270.8	7.5	32.3	10
0	4	6	359.9	7.8	32.9	10
0	1	3	729.1	10.9	46.0	12
4	0	5	361.4	7.5	31.0	10
3	1	6	445.2	7.9	31.8	17

STOE XRED32 1.57 08-Jul-2016 11:09

Input File(s) : D:\Kunden\Jeanette\NineOne\MrKut.x

Cell Parameters : 5.9252(5), 5.9252(5), 5.9252(5), 90.00, 90.00, 90.00

Cell Volume : 208.02(3)

Laue Symmetry : Cubic m 3 Lattice : Primitive

Chemical Formula : C1 H6 N1 Br3 Pb1

Molecular Weight : 479.0 Z = 1 Volume/Atom = 34.7

Density (calc.) : 3.82 Mg/m^3

Absorption Coef. : 34.66 mm^-1

Number of reflections read : 3395 Rejected : 35 (overflowed, Lorentz zone)

Residual reflections used : 3360

Minimum and maximum 2Theta : 6.9, 72.8

Minimum and maximum H,K,L : -9,-9,-8 9,9,9

Avg. I/Sigma for all data : 44.33

Number of unique reflections : 208

Completeness of data set [%] : 97.7 Redundancy : 16.15

R(int) = 0.0618 (3359 contributors) R(Sigma) = 0.0214

Average I/Sigma vs. 2Theta

2Theta	6.9	29.9	37.9	45.2	50.3	55.4	59.0	62.7	66.3	69.9	72.8
Resol.	5.93	1.38	1.09	0.93	0.84	0.76	0.72	0.68	0.65	0.62	0.60
N(Refl)	322	325	322	405	376	327	375	331	439	138	

I/Sigma 130.47 96.19 66.66 51.06 26.54 24.17 20.38 12.08 7.31 5.73

Completeness 100.0 100.0 100.0 100.0 100.0 100.0 100.0 100.0 100.0 66.7

Redundancy 13.4 16.3 16.9 16.9 17.9 16.4 16.3 16.5 16.3 13.8

R(int) 0.048 0.055 0.065 0.071 0.076 0.084 0.092 0.128 0.143 0.153

I/Sigma < 0 2 4 8 16 32 64 128 256 512

N(Refl) 0 5 105 500 1155 1970 2630 3103 3340 3360

Percent 0.0 0.1 3.1 14.7 34.0 58.0 77.5 91.4 98.4 99.0

Absorption Correction : Numerical

Absorption Coefficient : 34.66 mm^-1

Min and max Transmission : 0.0108, 0.0662

Crystal Faces

N	H	K	L	D [mm]
1	0	-1	0	0.1230
2	-1	0	0	0.1280
3	0	0	1	0.0750
4	0	0	-1	0.0710
5	2	3	-6	0.1170
6	-1	7	2	0.1400
7	0	1	0	0.1530
8	6	1	3	0.1150
9	7	-3	2	0.0930
10	5	-1	3	0.0850
11	3	2	6	0.1190
12	6	4	-1	0.1640
13	4	-1	-4	0.0990
14	3	1	-7	0.0840

63 Inconsistent Equivalents (ESD > 4 * Sigma)

H	K	L	Mean Int.	Sigma	ESD	N
2	2	2	5590.6	23.1	492.7	8
0	0	4	4408.2	17.0	272.9	6
0	0	2	10000.0	35.2	532.6	6
2	2	3	1969.1	13.6	192.5	19

0	1	4	2912.7	15.2	210.0	12
2	2	4	2412.1	14.0	190.6	20
1	0	4	2927.3	15.5	205.2	12
0	0	6	1447.6	10.5	123.1	6
0	4	4	1437.1	12.4	142.4	10
0	1	2	4448.8	23.4	265.0	11
1	2	2	3835.9	19.0	214.0	21
2	0	4	3302.9	16.8	189.4	12
0	2	4	3219.4	16.1	180.6	12
0	2	3	2253.7	15.3	170.0	12
1	0	6	1193.0	10.2	108.5	12
0	2	2	7292.1	25.6	255.4	11
1	2	4	2285.2	14.5	143.1	23
2	1	4	2295.1	14.8	141.6	24
3	2	4	1198.7	12.0	107.1	22
1	1	2	1888.9	17.2	151.9	24
1	4	8	102.2	7.9	68.8	21
0	1	6	1183.2	10.3	83.6	12
2	0	6	1074.5	10.4	83.9	12
1	1	6	977.4	10.0	79.7	22
2	2	6	807.8	10.8	84.5	24
1	0	2	4548.3	24.0	185.9	12
1	1	4	1765.1	13.4	101.8	24
0	2	6	1076.3	10.4	76.4	12
0	0	1	4655.6	39.9	292.5	6
2	3	4	1183.5	11.8	86.1	21
2	1	6	916.2	10.5	75.9	24
1	2	6	922.1	10.3	74.4	24
0	3	4	1452.4	13.1	90.3	12
2	4	4	1041.0	11.3	77.1	22
3	0	6	676.3	10.7	70.1	12
1	4	4	1161.1	11.9	77.2	20
3	1	4	1023.7	11.6	73.1	21
3	0	4	1463.5	13.2	79.5	11
0	0	5	624.6	9.1	53.7	6
2	0	3	2237.2	15.5	90.6	12
0	0	8	416.9	8.6	50.1	6
1	3	4	1021.0	11.7	66.3	21
0	0	3	2436.2	15.7	88.8	5
3	3	4	682.5	10.3	57.8	19
3	4	4	676.8	10.1	54.3	18
4	4	4	514.2	9.8	52.1	6
2	3	3	743.2	11.3	59.1	22
0	1	8	375.1	8.4	43.3	12

1	3	6	583.5	9.6	46.8	22
2	2	5	581.9	10.1	48.8	21

etc.

Figure S 1 Mixed halide single crystal, x=066, indexed

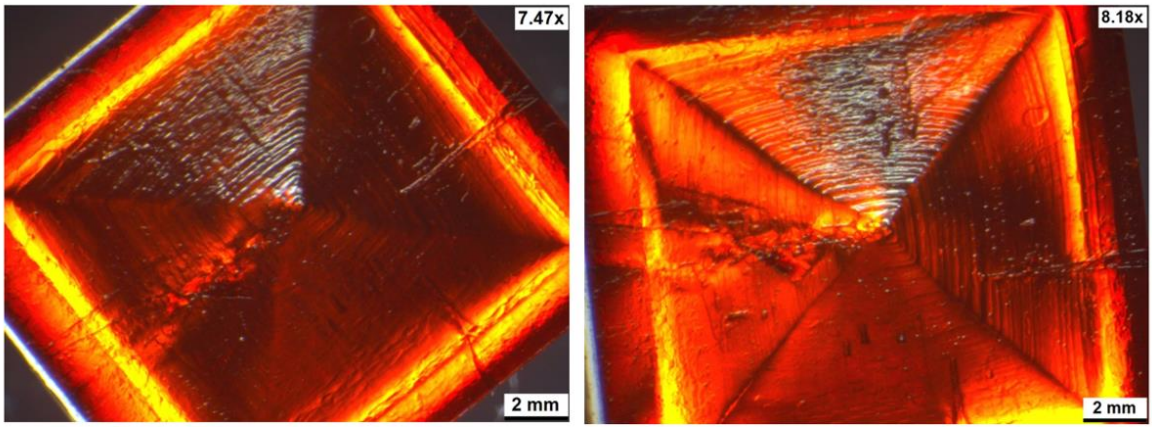

Figure S 2 Optical microscopy image of mixed halide single crystal, x=2.7, under polarized light

7.2 X-Ray Fluorescence on single crystals

Table 6 Results of X-ray fluorescence on freshly prepared crystals

Nominal composition	Pb (atomic %)*	I (atomic %)*	Br (atomic %)*
$(MA)PbI_3$	25	75	-
$(MA)PbI_{2.9}Br_{0.1}$			
$(MA)PbI_{2.66}Br_{0.33}$	24	67	9
$(MA)PbI_{2.33}Br_{0.66}$	24	55	21
$(MA)PbI_{2.5}Br_{0.5}$	24	60	15
$(MA)PbI_{0.3}Br_{2.7}$	24	1.6	74
$(MA)PbI_{0.1}Br_{2.9}$	24	1	75

*atomic percent in inorganic portion of sample

7.3 XRD patterns of inkjet printed thin films

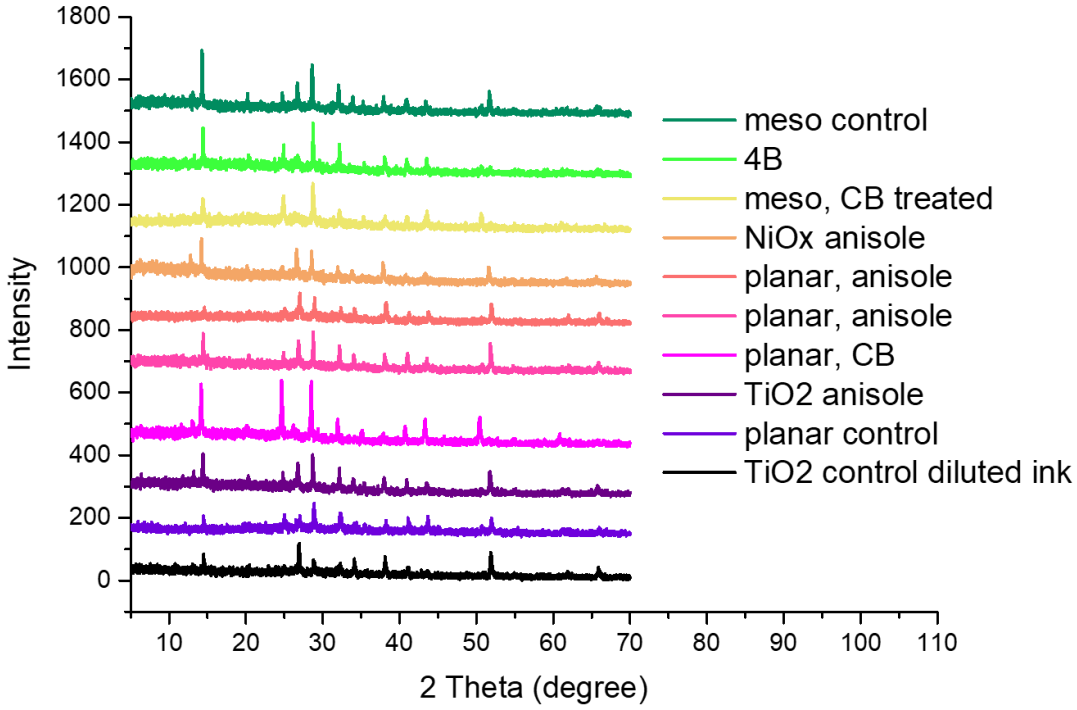

Figure S 3 XRD patterns of inkjet printed thin films on various substrates

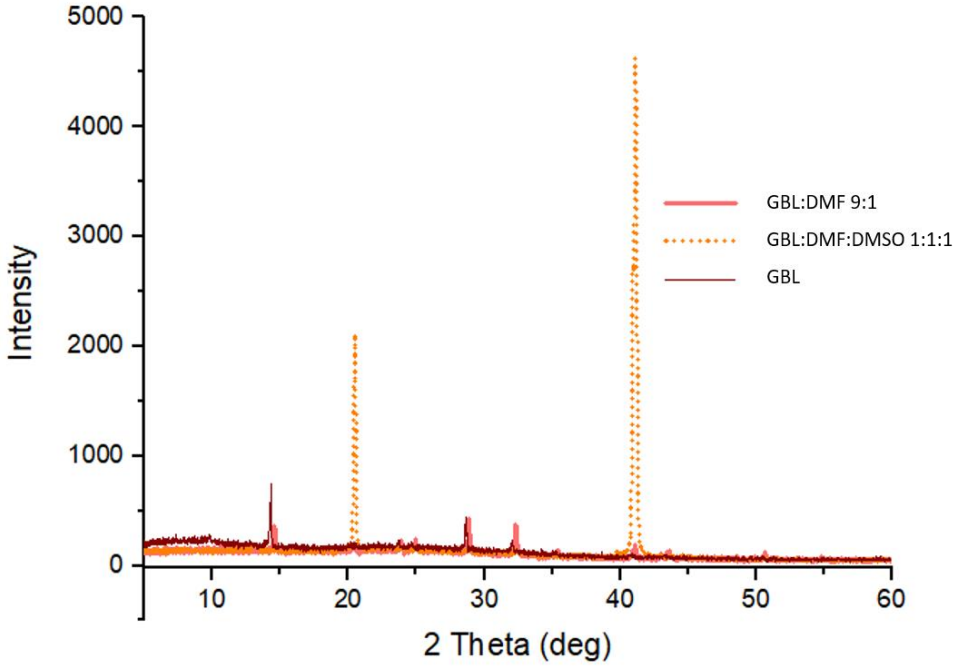

Figure S 4 XRD patterns of films printed on glass with various precursor solvent combinations

7.4 Jet setup for precursor inks

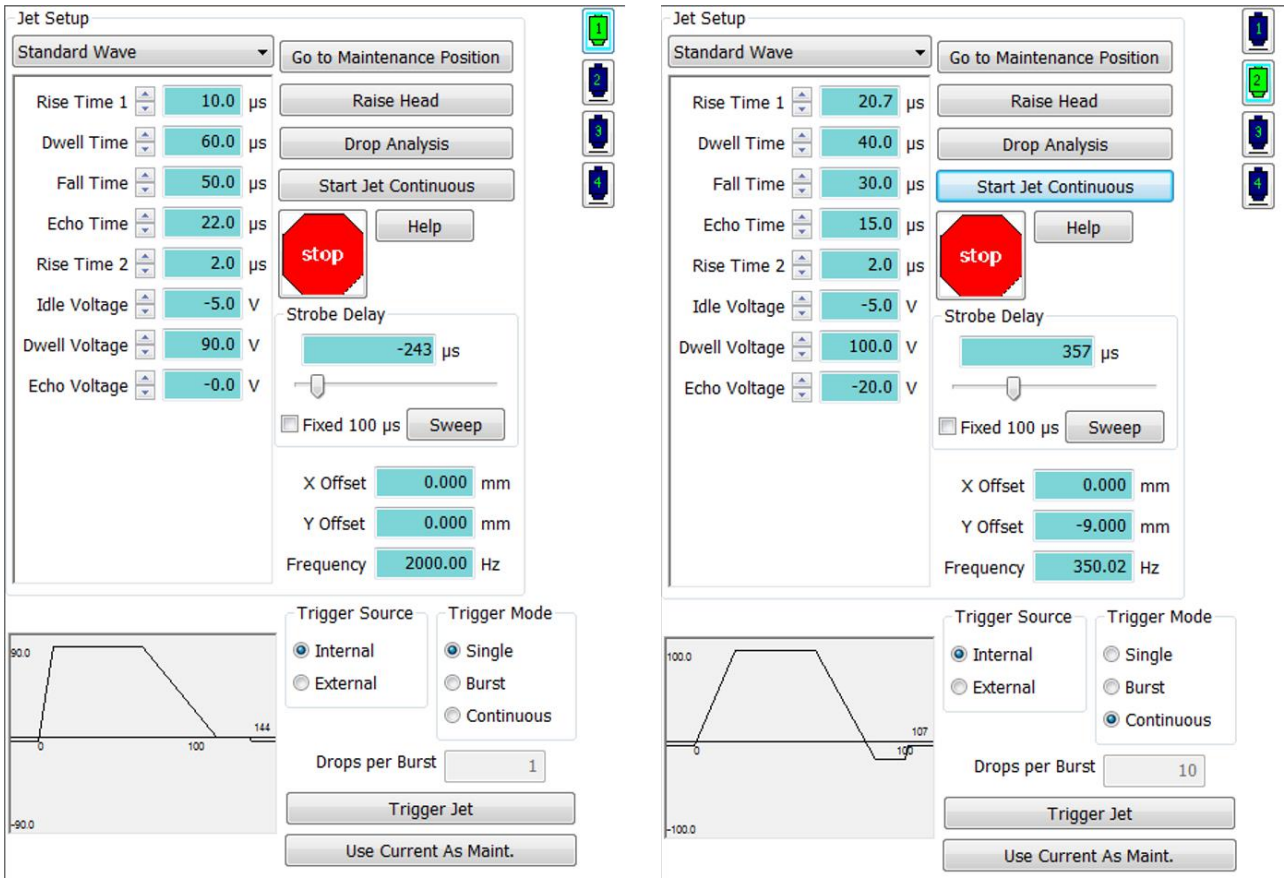

Figure S 5 Jet setups for $CH_3NH_3PbI_3$ precursor (jet 1) and $CH_3NH_3PbBr_3$ (jet 2)

7.5 Optimized Drop Shape

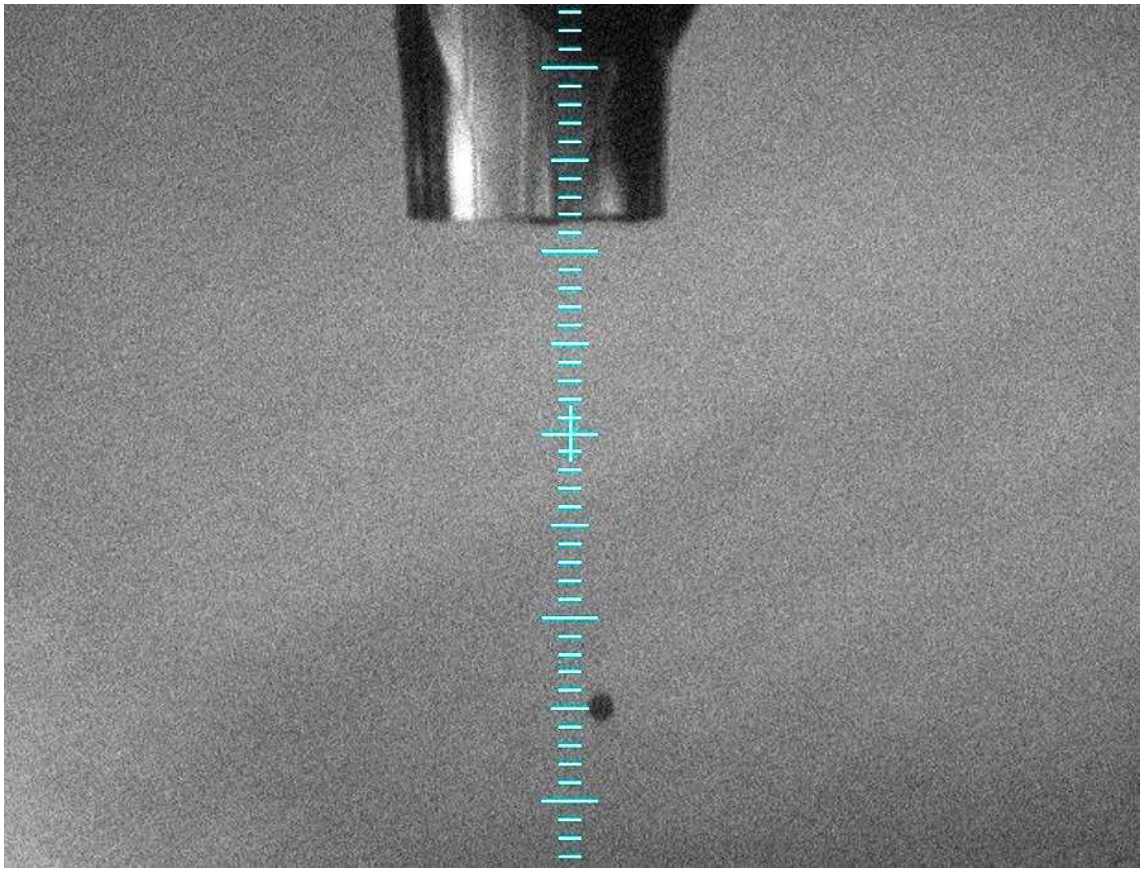

Figure S 6 Photograph of droplet according to parameters for jet 1 presented above, nozzle diameter 80µm

Drop volume 9pL

Drop velocity 4.90m/s

7.6 Print Speed and Morphology

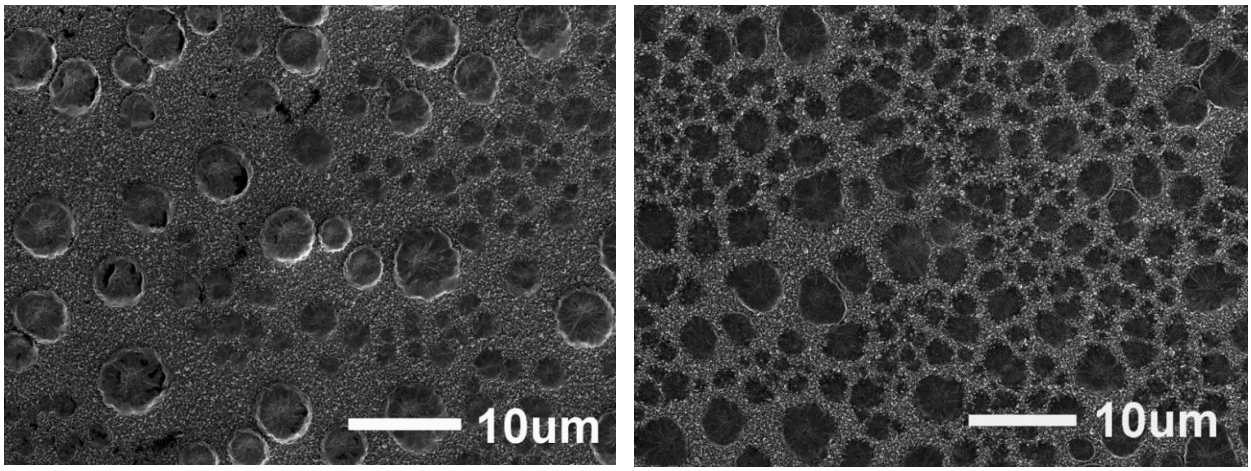

Figure S 7 Secondary electron images of perovskite printed on the fly at 30mm/s (left) and 50mm/s (right), printed on mesoporous TiO_2

8 Bibliography

1. Poglitsch A., W. D. Dynamic disorder in methlyammoniumtrihalogenplumbates observed by millimeter wave spectroscopy.pdf. *J. Chem. Phys.* **87,** 6373–6378 (1987).

2. Weber, D. CH3NH3PbX 3, ein Pb(II)-System mit kubischer Perowskitstruktur. *Zeitschrift für Naturforsch. B* **33,** 1443–1445 (1978).

3. Mitzi, D. B. Organic-inorganic perovskites containing trivalent metal halide layers: the templating influence of the organic cation layer. *Inorg. Chem.* **39,** 6107–13 (2000).

4. Mitzi, D. B. & Liang, K. Synthesis , Resistivity , and Thermal Properties of the Cubic Perovskite NH 2 CH ˛ NH 2 SnI 3 and Related Systems. *J. solid-state Chem.* **381,** 376–381 (1997).

5. Mitzi, D. B., Dimitrakopoulos, C. D. & Kosbar, L. L. Structurally Tailored Organic - Inorganic Perovskites : Optical Properties and Solution-Processed Channel Materials for Thin-Film Transistors. *Chem. Mater.* **13,** 3728–3740 (2001).

6. Mitzi, D. B. Conducting Tin Halides with a layered organic-based perovskite structure. *Nature* 467 (1994).

7. Kojima, A., Teshima, K., Shirai, Y. & Miyasaka, T. Organometal halide perovskites as visible-light sensitizers for photovoltaic cells. *J. Am. Chem. Soc.* **131,** 6050–1 (2009).

8. Im, J.-H., Lee, C.-R., Lee, J.-W., Park, S.-W. & Park, N.-G. 6.5% Efficient Perovskite Quantum-Dot-Sensitized Solar Cell. *Nanoscale* **3,** 4088 (2011).

9. Kim, H.-S. *et al.* Lead iodide perovskite sensitized all-solid-state submicron thin film mesoscopic solar cell with efficiency exceeding 9%. *Sci. Rep.* **2,** 591 (2012).

10. Michael M. Lee, Joel Teuscher, Tsutomu Miyasaka, Takurou N. Murakami, H. J. S. Efficient Hybrid Solar Cells Based on Meso-Superstructured Organometal Halide Perovskites. *Science (80-.).* **338,** 643–648 (2012).

11. Burschka, J. *et al.* Sequential deposition as a route to high-performance perovskite-sensitized solar cells. *Nature* **499,** 316–320 (2013).

12. Liu, M., Johnston, M. B. & Snaith, H. J. Efficient planar heterojunction perovskite solar cells by vapour deposition. *Nature* **501,** 395–8 (2013).

13. Shi, D. *et al.* Low trap-state density and long carrier diffusion in organolead trihalide perovskite single crystals. *Science (80-.).* **347,** 519–522 (2015).

14. Sum, T. C. & Mathews, N. Advancements in Perovskite Solar Cells: Photophysics behind the Photovoltaics. *Energy Environ. Sci.* 2518–2534 (2014). doi:10.1039/c4ee00673a

15. Grätzel, M. The light and shade of perovskite solar cells. *Nat. Mater.* **13,** 838–842 (2014).

16. Galagan, Y., Coenen, E. W. C., Verhees, W. J. H. & Andriessen, R. Towards scaling up of perovskite solar cells and modules. *J. Mater. Chem. A Mater. energy Sustain.* **4,** 5700–5705 (2016).

17. Kim, H., Im, S. H. & Park, N. Organolead Halide Perovskite : New Horizons in Solar Cell Research. *J. Phys. Chem. C* **118,** 5615–5625 (2014).

18. Niu, G., Guo, X. & Wang, L. Review of recent progress in chemical stability of perovskite solar cells. *J. Mater. Chem. A* **3,** 8970–8980 (2015).

19. Yin, S. W., Ji-Hui, Y., Kang, J. & Yan, Y. Halide perovskite materials for solar cells:a theoretical review. *J. Mater. Chem. A* **3,** 8926–8942 (2015).

20. Docampo, P. *et al.* Lessons learned: From dye-sensitized solar cells to all-solid-state hybrid devices. *Adv. Mater.* **26,** 4013–4030 (2014).

21. Grätzel, M. The Rise of Highly Efficient and Stable Perovskite Solar Cells. *Acc. Chem. Res.* **50,** 487–491 (2017).

22. Green, M. A., Emery, K., Hishikawa, Y., Warta, W. & Dunlop, E. D. Solar cell ef fi ciency tables (Version 45). *Prog. Photovoltaics* 1–9 (2015). doi:10.1002/pip

23. Oxford PV. Oxford PV-tandem cells. Available at: http://www.oxfordpv.com/Tandem-perovskite-solar-cells. (Accessed: 20th March 2017)

24. Noel, N. K. *et al.* Lead-free organic–inorganic tin halide perovskites for photovoltaic applications. *Energy Environ. Sci.* **7,** 3061–3068 (2014).

25. Giustino, F. & Snaith, H. J. Toward Lead-Free Perovskite Solar Cells. *ACS Energy* **1,** 1233–1240 (2016).

26. Cortecchia, D. *et al.* Lead-Free MA2CuClxBr4-x Hybrid Perovskites. *Inorg. Chem.* **55,** 1044–1052 (2016).

27. European Parliament. Directive 2011/65/EU of the European Parliament and of the Council of 8 June 2011 on the restriction of the use of certain hazardous substances in electrical and electronic equipment (RoHS). *Off. J. Eur. Union* **54,** 88–110 (2011).

28. Yun, J. S. *et al.* Benefit of Grain Boundaries in Organic − Inorganic Halide Planar Perovskite Solar Cells. *J. Phys. Chem. Lett.* **6,** 875–880 (2015).

29. Sherkar, T. S. *et al.* Recombination in Perovskite Solar Cells :Significance of Grain Boundaries, Interface Traps, and Defect Ions. *ACS Energy Lett.* **2,** 1214–1222 (2017).

30. Yang, M. *et al.* Do grain boundaries dominate non-radiative recombination in CH3NH3PbI3 perovskite thin films? *Phys. Chem. Chem. Phys.* **19,** 5043–5050 (2017).

31. Chu, Z. *et al.* Impact of grain boundaries on ef fi ciency and stability of organic-inorganic trihalide perovskites. *Nat. Commun.* **8,** 2230

32. Weber, D. Das Perowskitsystem CH3NH3[PbnSn1-nX3] (X=Cl,Br,I). *Z. Naturforsch.* **34b,** 939–941 (1979).

33. Nayak, P. K. *et al.* Mechanism for rapid growth of organic–inorganic halide perovskite crystals. *Nat. Commun.* **7,** 1–8 (2016).

34. International Renewable Energy Agency. *End-of-Life Management Solar Photovoltaic Panels*. (2016).

35. Kardarian, K. *et al.* Solar Energy Materials & Solar Cells Effect of Mg doping on Cu 2 O thin fi lms and their behavior on the TiO 2 / Cu 2 O heterojunction solar cells. **147,** 27–36 (2016).

36. Kupfer, B. *et al.* Thin film Co3O4/TiO2 heterojunction solar cells. *Adv. Energy Mater.* **5,** 2–6 (2015).

37. Woo, S. I. *et al.* Current Status of Combinatorial and High-Throughput Methods for Discovering New Materials and Catalysts. *QSAR&Combinatorial Sci.* **1,** (2005).

38. Watanabe, M. *et al.* High-Throughput Screening for Combinatorial Thin-Film Library of Thermoelectric Materials. 175–178 (2008).

39. Kirsten, G. & Maier, W. F. Strategies for the discovery of new catalysts with combinatorial chemistry. *Appl. Surf. Sci.* **223,** 87–101 (2004).

40. Jacobsson, J. T. *et al.* Exploration of the compositional space for mixed lead halogen perovskites for high efficiency solar. *Energy Environ. Sci.* **9,** 1706–1724 (2016).

41. G., K. M. Semiconducting Tin and Lead Iodide Perovskites with Organic Cations: Phase Transitions, High Mobilities, and Near-Infrared Photoluminescent Properties. *Inorg. Chem.* **52,** 9019 (2013).

42. Noh, J. H., Im, S. H., Heo, J. H., Mandal, T. N. & Seok, S. Il. Chemical Management for Colorful, E ffi cient, and Stable Inorganic − Organic Hybrid Nanostructured Solar Cells. *Nano Lett.* **13,** 1764–1769 (2013).

43. Stranks, S. D. *et al.* Electron-hole diffusion lengths exceeding 1 micrometer in an organometal trihalide perovskite absorber. *Science* **342,** 341–344 (2013).

44. Mei, a. *et al.* A hole-conductor-free, fully printable mesoscopic perovskite solar cell with high stability. *Science (80-.).* **345,** 295–298 (2014).

45. Research Cell Efficiency Records 2014 National Renewable Energy Laboratory. 2014 (2014).

46. Park, N.-G. Organometal Perovskite Light Absorbers Toward a 20 % E ffi ciency Low-Cost Solid-State Mesoscopic Solar Cell. *J. Phys. Chem. Lett.* **4,** 2423–2429 (2013).

47. Snaith, H. J. Perovskites : The Emergence of a New Era for Low-Cost , High-. *J. Phys. Chem. Lett.* **4,** 3623–3630 (2013).

48. Bi, D. *et al.* Using a two-step deposition technique to prepare perovskite (CH3NH3PbI3) for thin film solar cells based on ZrO2 and TiO2 mesostructures. *RSC Adv.* **3,** 18762 (2013).

49. Chen, Q. *et al.* Planar Heterojunction Perovskite Solar Cells via Vapor-Assisted Solution Process. *J. Am. Chem. Soc.* **136,** 622–625 (2014).

50. Stoumpos, C. C., Malliakas, C. D. & Kanatzidis, M. G. Semiconducting Tin and Lead Iodide Perovskites with Organic Cations: Phase Transitions, High Mobilities, and Near-Infrared Photoluminescent Properties. *Inorg. Chem.* **52,** 9019–9038 (2013).

51. Yang, S. *et al.* Formation mechanism of freestanding CH3NH3PbI3 functional crystals: In situ transformation vs dissolution-crystallization. *Chem. Mater.* **26,** 6705–6710 (2014).

52. Kollek, T. *et al.* Porous and Shape-Anisotropic Single Crystals of the Semiconductor Perovskite CH3 NH3 PbI3 from a Single-Source Precursor. *Angew. Chem. Int. Ed. Engl.* 1–7 (2014). doi:10.1002/anie.201408713

53. Pisoni, A., Baris, O. S., Spina, M. & Gaa, R. Ultra-Low Thermal Conductivity in Organic − Inorganic Hybrid. *J. Phys. Chem. Lett.* **5,** 2488–2492 (2014).

54. Spina, M., Gaal, R. & Gachet, D. Nanowires of Methylammonium Lead Iodide (CH 3 NH 3 PbI 3) Prepared by Low Temperature Solution-Mediated Crystallization. *Nanoscale* (2014). doi:dx.doi.org/10.1021/nl5020684

55. Im, J.-H., Jang, I.-H., Pellet, N., Grätzel, M. & Park, N.-G. Growth of CH3NH3PbI3 cuboids with controlled size for high-efficiency perovskite solar cells. *Nat. Nanotechnol.* 1–6 (2014). doi:10.1038/nnano.2014.181

56. Schmidt, L. C. *et al.* Nontemplate Synthesis of CH 3 NH 3 PbBr 3 Perovskite Nanoparticles. *J. Am. Chem. Soc.* **136,** 850–853 (2014).

57. Jeon, N. J. *et al.* Solvent engineering for high-performance inorganic-organic hybrid perovskite solar cells. *Nat. Mater.* **13,** 1–7 (2014).

58. Heo, J. H. *et al.* Efficient inorganic–organic hybrid heterojunction solar cells containing perovskite compound and polymeric hole conductors. *Nat. Photonics* 1–6 (2013). doi:10.1038/NPHOTON.2013.80

59. Baikie, T. *et al.* Synthesis and crystal chemistry of the hybrid perovskite (CH3NH3)PbI3 for solid-state sensitised solar cell applications. *J. Mater. Chem. A* **1,** 5628 (2013).

60. Luminy, C. Crystallization Mechanisms in Solution. *J. Cryst. Growth* **90,** 14–30 (1988).

61. Jackson, K. A. *Kinetic Processes: Crystal Growth, Diffusion and Phase Transitions in Materials*. (WILEY-VCH, 2010).

62. Yan, K. *et al.* Hybrid Halide Perovskite Solar Cell Precursors: Colloidal Chemistry and Coordination Engineering behind Device Processing for High Efficiency. *J. Am. Chem. Soc.* **137,** 4460–4468 (2015).

63. Noh, J. H., Im, S. H., Heo, J. H., Mandal, T. N. & Seok, S. Il. Chemical Management for Colorful, Efficient, and Stable Inorganic-Organic Hybrid Nanostructured Solar Cells. *Nano Lett.* **13,** 1764–1769 (2013).

64. Bi, D. *et al.* Efficient luminescent solar cells based on tailored mixed-cation perovskites. *Sci. Adv.* **2,** e1501170–e1501170 (2016).

65. Serrano-Lujan, L. *et al.* Tin- and lead-based perovskite solar cells under scrutiny: An environmental perspective. *Adv. Energy Mater.* **5,** 1–5 (2015).

66. Espinosa, N., Serrano-Lujan, L., Urbina, A. & Krebs, F. C. Solution and vapour deposited lead perovskite solar cells: Ecotoxicity from a life cycle assessment perspective. *Sol. Energy Mater. Sol. Cells* **137,** 303–310 (2015).

67. Gong, Jian, Darling, Seth B., Y. F. Perovskite photovoltaics: life-cycle assessment of energy and environmental impacts. *Energy Environ. Sci.* **8,** 1953–1968 (2015).

68. Zhang, J., Gao, X., Deng, Y., Li, B. & Yuan, C. Life Cycle Assessment of Titania Perovskite Solar Cell Technology for Sustainable Design and Manufacturing. *ChemSusChem* **8,** 3882–3891 (2015).

69. Babayigit, A. *et al.* Assessing the toxicity of Pb- and Sn-based perovskite solar cells in model organism Danio rerio. *Sci. Rep.* **6,** 18721 (2016).

70. Fabini, D. Quantifying the Potential for Lead Pollution from Halide Perovskite Photovoltaics. *J. Phys. Chem. Lett.* **6,** 3546–3548 (2015).

71. Hailegnaw, B., Kirmayer, S., Edri, E., Hodes, G. & Cahen, D. Rain on methylammonium lead iodide based perovskites: Possible environmental effects of perovskite solar cells. *J. Phys. Chem. Lett.* **6,** 1543–1547 (2015).

72. United States Environmental Protection Agency. *Technical Note – Estimating Lead (Pb) Emissions from Coal Combustion Sources*. (2011).

73. *CRC Handbook of Chemistry and Physics*. **84,** (2003).

74. Photovoltaic Solar Energy Department-National Renewable Energy Centre Fundacion Chile. *First Solar CdTe Photovoltaic Technology : Environmental , Health and Safety Assessment Final Report*. (2013).

75. Takahashi, Y. *et al.* Charge-transport in tin-iodide perovskite CH3NH3SnI3: origin of high conductivity. *Dalton Trans.* **40,** 5563–8 (2011).

76. Knutson, J. L., Martin, J. D. & Mitzi, D. B. Tuning the band gap in hybrid tin iodide perovskite semiconductors using structural templating. *Inorg. Chem.* **44,** 4699–705 (2005).

77. R.L.Moss, E.Tzimas, H.Kara, P.Willis, J. K. *European Commission-Critical Metals in Strategic Energy Technologies: Assessing Rare Metals as Supply-Chain Botlenecks in Low-Carbon Energy Technologies*. (2011). doi:10.2790/35716

78. Oakdene Hollins. *Material Security Ensuring resource availability for the UK economy*. (2008).

79. European Commission: Ad hoc working group on defining critical raw materials. *Report on critical raw materials for the EU*. (2014).

80. Gong, J., Darling, B. & You, F. Perovskite Photovoltaics : Life-Cycle Assessment of Energy and Environmental Impacts Supporting Information. *Energy Environ. Sci.* 1–22 (2015).

81. UNEP. *Environmental Risks and Challenges of Anthropogenic Metals Flows and Cycles*. (2013).

82. UNEP. *Assessing the Environmental Impacts of Consumption and Production*. (2010).

83. V2.2, E. No Title.

84. Binek, A. *et al.* Recycling Perovskite Solar Cells To Avoid Lead Waste. *Appl. Mater. Interfaces* **8,** 12881–12886 (2016).

85. Bodamer, G. W., Kunin, R. & Co, H. Behavior of Ion Exchange Resins in Solvents Other Than Water-Swelling and Exchange Characteristics. *Ind. Eng. Chem.* **45,** (1953).

86. Hubicki, Z. & Kołodyńska, D. in (2012).

87. Poll, C. G., Pickup, D. M., Chadwick, A. V, Riley, D. J. & Payne, D. J. Electrochemical recycling of

lead from hybrid organic – inorganic perovskites using deep eutectic solvents. *Green Chem.* **18,** 2946–2955 (2016).

88. Latunussa, C. E. L., Ardente, F., Andrea, G. & Mancini, L. Life Cycle Assessment of an innovative recycling process for crystalline silicon photovoltaic panels. *Sol. Energy Mater. Sol. Cells* 1–11 (2016). doi:10.1016/j.solmat.2016.03.020

89. Kang, S., Yoo, S., Lee, J., Boo, B. & Ryu, H. Experimental investigations for recycling of silicon and glass from waste photovoltaic modules. *Renew. Energy* **47,** 152–159 (2012).

90. Fthenakis, V. M. End-of-life management and recycling of PV modules. *Energy Policy* **28,** 1051–1058 (2000).

91. Doi, T. *et al.* Experimental study on PV module recycling with organic solvent method. **67,** (2001).

92. Berger, W., Simon, F., Weimann, K. & Alsema, E. A. Resources , Conservation and Recycling A novel approach for the recycling of thin film photovoltaic modules. *"Resources, Conserv. Recycl.* **54,** 711–718 (2010).

93. The European Commission. Draft: Commission Regulation Directive 2009/125/EC of the European Parliament and of the Council with regard to ecodesign requirements for electronic displays, repealing Regulation (EC) No 642/2009 with regard to ecodesign requirements for televisions and. (2016).

94. Capello, C., Fischer, U. & Hungerbu, K. What is a green solvent ? A comprehensive framework for the environmental assessment of solvents. *Green Chem.* **9,** 927–934 (2007).

95. Wang, J. *et al.* Highly Efficient Perovskite Solar Cells Using Non-Toxic Industry Compatible Solvent System. *Sol. RRL* (2017). doi:10.1002/solr.201700091

96. Deutsche Solar & BINE Information Service. Recycling photovoltaic modules. 1–4 (2009).

97. International Renewable Energy Agency. *The Socio-economic Benefits of Solar and Wind Energy*. (2014).

98. International Renewable Energy Agency. *Renewable Energy Benefits : Leveraging Local Industries 12th Meeting of the IRENA Council*. (2016).

99. Goe, M. & Gaustad, G. Strengthening the case for recycling photovoltaics : An energy payback analysis. *Appl. Energy* **120,** 41–48 (2014).

100. Tao, J. & Yu, S. Review on feasible recycling pathways and technologies of solar pho- tovoltaic modules. *Sol. Energy Mater. Sol. Cells* **141,** 108–124 (2015).

101. Dias, P., Javimczik, S., Benevit, M., Veit, H. & Bernardes, A. M. Recycling WEEE : Extraction and concentration of silver from waste crystalline silicon photovoltaic modules. *Waste Manag.* **57,** 220–225 (2016).

102. Søndergaard, R. R., Espinosa, N., Jørgensen, M. & Krebs, F. C. Efficient decommissioning and recycling of polymer solar cells : justification for use of silver †. *Energy Environ. Sci.* **7,** 1006–1012 (2014).

103. 3M. 3M Scotchshield Backsheet Films for PV Modules Product Brochure.

104. Rimez, B. *et al.* The thermal degradation of poly (vinyl acetate) and poly (ethylene- co -vinyl

acetate), Part I : Experimental study of the degradation mechanism. *Polym. Degrad. Stab.* **93,** 800–810 (2008).

105. National Renewable Energy Laboratory. Best Research-Cell Efficiencies. (2017).

106. Saliba, M., Matsui, T., Seo, J.-Y., Domanski, K. & Correa-Baena, J.-P. Cesium-containing triple cation perovskite solar cells: improved stability, reproducibility and high efficien. *Energy Environ. Sci.* **9,** 1989–1997 (2016).

107. Lotsch, B. V. New light on an old story: Perovskites go solar. *Angew. Chemie - Int. Ed.* **53,** 635–637 (2014).

108. Wang, D., Wright, M., Elumalai, N. K. & Uddin, A. Stability of perovskite solar cells. *Sol. Energy Mater. Sol. Cells* **147,** 255–275 (2016).

109. Shahbazi, M. & Wang, H. Progress in research on the stability of organometal perovskite solar cells. *Sol. Energy* **123,** 74–87 (2016).

110. Liu, Z., Sun, B., Shi, T. & Liao, G. Enhanced photovoltaic performance and stability of carbon counter electrode based perovskite solar cells encapsulated by PDMS. *J. Mater. Chem. A Mater. energy Sustain.* **4,** 10700–10709 (2016).

111. Kim, H., Seo, J. & Park, N. Material and Device Stability in Perovskite Solar Cells. *ChemSusChem* **9,** 2528–2540 (2016).

112. Berhe, T. A. *et al.* Organometal halide perovskite solar cells: degradation and stability. *Energy Environ. Sci.* **9,** 323–356 (2016).

113. Huang, L. *et al.* Efficient electron-transport layer-free planar perovskite solar cells via recycling the FTO/glass substrates from degraded devices. *Sol. Energy Mater. Sol. Cells* **152,** 118–124 (2016).

114. Zhang, F., Liu, X., Yi, C., Bi, D. & Luo, J. Dopant-Free Donor (D)– p – D – p – D Conjugated Hole-Transport Materials for Efficient and Stable Perovskite Solar Cells. *ChemSusChem* **9,** 2578–2585 (2016).

115. Salado, M. *et al.* Extending the Lifetime of Perovskite Solar Cells using a Perfluorinated Dopant. *ChemSusChem* **9,** 2708–2714 (2016).

116. Singh, T., Singh, J. & Miyasaka, T. Role of Metal Oxide Electron-Transport Layer Modification on the Stability of High Performing Perovskite Solar Cells. *ChemSusChem* **9,** 2559–2566 (2016).

117. Saliba, M. *et al.* Incorporation of rubidium cations into perovskite solar cells improves photovoltaic performance. *Science (80-.).* **345,** (2016).

118. Guo, F. *et al.* Extending the environmental lifetime of unpackaged perovskite solar cells through interfacial design †. *J. Mater. Chem. A Mater. energy Sustain.* **4,** 11604–11610 (2016).

119. Baranwal, A. K., Kanaya, S., Peiris, T. A. N., Mizuta, G. & Nishina, T. 100 8 C Thermal Stability of Printable Perovskite Solar Cells Using Porous Carbon Counter Electrodes. 2604–2608 (2016). doi:10.1002/cssc.201600933

120. Dong, Q. *et al.* Encapsulation of Perovskite Solar Cells for High Humidity Conditions. *ChemSusChem* **9,** 2597–2603 (2016).

121. Matteocci, F. *et al.* Encapsulation for long-term stability enhancement of perovskite solar cells cr. *Nano Energy* **30,** 162–172 (2016).

122. Weerasinghe, H. C., Dkhissi, Y., Scully, A. D., Caruso, R. A. & Cheng, Y. Encapsulation for improving the lifetime of flexible perovskite solar cells. *Nano Energy* **18,** 118–125 (2015).

123. Kaltenbrunner, M. *et al.* Flexible high power-per-weight perovskite solar cells with chromium oxide–metal contacts for improved stability in air. *Nat. Mater.* (2015). doi:10.1038/NMAT4388

124. Liu, C., Fan, J., Li, H., Zhang, C. & Mai, Y. Highly Efficient Perovskite Solar Cells with Substantial Reduction of Lead Content. *Sci. Rep.* 1–8 (2016). doi:10.1038/srep35705

125. Qiu, X. *et al.* From unstable CsSnI3 to air-stable Cs2SnI6 : A lead-free perovskite solar cell light absorber with bandgap of 1.48 eV and high absorption coefficient. *Sol. Energy Mater. Sol. Cells* **159,** 227–234 (2017).

126. Liao, W. *et al.* Fabrication of Efficient Low-Bandgap Perovskite Solar Cells by Combining Formamidinium Tin Iodide with Methylammonium Lead Iodide. *J. Am. Chem. Soc.* **138,** 12360–12363 (2016).

127. Lee, S. J., Shin, S. S., Kim, Y. C., Kim, D. & Seok, S. Il. Fabrication of Efficient Formamidinium Tin Iodide Perovskite Solar Cells through SnF2 − Pyrazine Complex. *J. Am. Chem. Soc.* **138,** 3974–3977 (2016).

128. Babayigit, A., Ethirajan, A., Muller, M. & Conings, B. Toxicity of organometal halide perovskite solar cells. *Nat. Publ. Gr.* **15,** 247–251 (2016).

129. Zhang, M. *et al.* Recent advances in low-toxic lead-free metal halide perovskite materials for solar cell application. *Asia-Pacific J. Chem. Eng.* **11,** 392–398 (2016).

130. Singh, T., Kulkarni, A., Ikegami, M. & Miyasaka, T. Effect of Electron Transporting Layer on Bismuth-Based Lead-Free Perovskite (CH3NH3)3 Bi2I9 for Photovoltaic Applications. *Appl. Mater. Interfaces* **8,** 14542–14547 (2016).

131. Park, B. *et al.* Bismuth Based Hybrid Perovskites A3Bi2I9(A:Methylammonium or Cesium) for Solar Cell Application. *Adv. Mater.* **27,** 6806–6813 (2015).

132. Burschka, J. *et al.* Sequential deposition as a route to high-performance perovskite-sensitized solar cells. *Nature* **499,** 316–319 (2013).

133. Ball, J. M., Lee, M. M., Hey, A. & Snaith, H. J. Low-temperature processed meso-superstructured to thin-film perovskite solar cells. *Energy Environ. Sci.* **6,** 1739 (2013).

134. Wei, Z. *et al.* Cost-efficient Clamping Solar Cells Using Candle Soot for Hole Extraction from Ambipolar Perovskite. *Energy Environ. Sci.* Ahead of Print (2014). doi:10.1039/C4EE01983K

135. Yang, W. S. *et al.* High-performance photovoltaic perovskite layers fabricated through intramolecular exchange. *Science.* science.aaa9272 (2015). doi:10.1126/science.aaa9272

136. Bhachu, D. S. *et al.* Scalable route to CH3NH3PbI3 perovskite thin films by aerosol assisted chemical vapour deposition. *J. Mater. Chem. A* **3,** 9071–9073 (2015).

137. Yu, C.-L. TiO2 Thick Film Printing Paste for DSSC. (2011).

138. Wolf, S. De, Niesen, B. & Ballif, C. Efficient Monolithic Perovskite/Silicon Tandem Solar Cell with

Cell Area >1 cm 2. *J. Phys. Chem. Lett.* **7,** 161–166 (2015).

139. Mailoa, J. P. *et al.* A 2-terminal perovskite/silicon multijunction solar cell enabled by a silicon tunnel junction. *Appl. Phys. Lett.* **106,** (2015).

140. Werner, J. *et al.* Efficient Near-Infrared-Transparent Perovskite Solar Cells Enabling Direct Comparison of 4 - Terminal and Monolithic Perovskite/Silicon Tandem Cells. *ACS Energy Lett.* **1,** 474–480 (2016).

141. Park, M. *et al.* Mechanically Recoverable and Highly Effi cient Perovskite Solar Cells : Investigation of Intrinsic Flexibility of Organic – Inorganic Perovskite. *Adv. Energy Mater.* **5,** 1–11 (2015).

142. Docampo, P., Ball, J. M., Darwich, M., Eperon, G. E. & Snaith, H. J. Efficient organometal trihalide perovskite planar-heterojunction solar cells on flexible polymer substrates. *Nat. Commun.* **4,** 2761 (2013).

143. Li, Y. *et al.* High-efficiency robust perovskite solar cells on ultrathin flexible substrates. *Nat. Commun.* 1–10 (2016). doi:10.1038/ncomms10214

144. Giacomo, F. Di, Fakharuddin, A. & Brown, T. M. Progress, challenges and perspectives in flexible perovskite solar cells. *Energy Environ. Sci.* **9,** 3007–3035 (2016).

145. Burrows, K. & Fthenakis, V. Glass needs for a growing photovoltaics industry. *Sol. Energy Mater. Sol. Cells* **132,** 455–459 (2015).

146. Penn State College of Agricultural Sciences extension. Lead in Residential Soils : Sources , Testing , and Reducing Exposure.

147. World Health Organization. *EXPOSURE TO LEAD : A MAJOR PUBLIC HEALTH CONCERN*.

148. World Health Organization. *Lead in Drinking-water Background document for development of WHO Guidelines for Drinking-water Quality*. (2011).

149. Brown, M. J. *Morbidity and Mortality Weekly Report-Blood Lead Levels in Children Aged 1-5 Years-United States 1999-2010*. **62,** (2013).

150. UNEP UNICEF. *Childhood Lead Poisoning-Information for Advocacy and Action*. (1997).

151. Kuijp, T. J. Van Der, Huang, L. & Cherry, C. R. Health hazards of China ' s lead-acid battery industry : a review of its market drivers , production processes , and health impacts. *Environ. Heal.* **12,** 1 (2013).

152. Chicago Department of public health. *HEALTHY HOMES : POLICY OPTIONS FOR PREVENTING LEAD POISONING*. (2013).

153. Richard L. Canfield, Ph.D., Charles R. Henderson, Jr., M. A. & Deborah A. Cory-Slechta, Ph.D., Christopher Cox, Ph.D., Todd A. Jusko, B.S., and Bruce P. Lanphear, M.D., M. P. . Intellectual Impairment in Children with Blood Lead Concentrations below 10ug per Deciliter. *N. Engl. J. Med.* **348,** 1517–1526 (2003).

154. Advisory Committee on Childhood Lead Poisoning Prevention Centres of Disease Control and Prevention. *Low Level Lead Exposure Harms Children : A Renewed Call for Primary Prevention Advisory Committee on Childhood Lead Poisoning Prevention*. (2012).

155. Centre of Disease Control and Prevention. CDC Response to Advisory Committee on Childhood

Lead Poisoning Prevention Recommendations in “Low Level Lead Exposure Harms Children: A Renewed Call of Primary Prevention”. (2010).

156. Dietrich, K. N., Ris, M. D., Succop, P. A., Berger, O. G. & Bornschein, R. L. Early exposure to lead and juvenile delinquency. *Neurotoxology Teratol.* **23,** 511–518 (2001).

157. Needleman, H. L., Mcfarland, C., Ness, R. B., Fienberg, S. E. & Tobin, M. J. Bone lead levels in adjudicated delinquents A case control study. *Neurotoxology Teratol.* **24,** 711–717 (2002).

158. Gottesfeld, P. & Pokhrel, A. K. Review : Lead Exposure in Battery Manufacturing and Recycling in Developing Countries and Among Children in Nearby Communities. 520–532 (2011). doi:10.1080/15459624.2011.601710

159. Were, F. H. *et al.* Air and Blood Lead Levels in Lead Acid Battery Recycling and Manufacturing Plants in Kenya. *J. Occup. Environ. Hyg.* **9,** 340–344 (2012).

160. Pourmand, A., Al-tiae, T. K. & Mazer-amirshahi, M. Perspective on lead toxicity , a comparison between the United States and Iran. **20,** 1 (2012).

161. King, B. S., Musolin, K., Ceballos, D., Brueck, S. E. & Beaucham, C. *Evaluation of Employees' Exposures to Lead, Noise, and Heat at an Automotive Lead-acid Battery Recycling Company-U.S. Department of Health and Human Services NIOSH Report No. 2012-0071-3224*. (2014).

162. The United States Geological Survey. Lead-Statistics and Information. 2016–2017 (2017).

163. Zhang, X. *et al.* Impacts of lead/zinc mining and smelting on the environment and human health in China. *Env. Monit Assess* **184,** 2261–2273 (2012).

164. United States Environmental Protection Agency Office of Resource Conservation and Recovery (5306P). *Advancing Sustainable Materials Management: Facts and Figures 2013*. (2013).

165. International Lead Association-Production. (2017). Available at: http://www.ila-lead.org/lead-facts/lead-production--statistics.

166. European Environment Agency. Heavy metal emissions. (2015).

167. US National Institutes of Health & Office of Dietary Supplements. Iodine-Fact Sheet for Health Professionals. (2011).

168. World Health Organizaiton. *Assessment of iodine deficiency disorders and monitoring their elimination A guide for programme managers 3rd Edition*. (2007).

169. Zimmermann, M. B. in *Iodine Chemistry and Applications* (ed. Kaiho, T.) 421–431 (Wiley, 2015).

170. Zimmermann, M. B. Iodine deficiency in pregnancy and the effects of maternal iodine supplementation on the offspring : a review 1 – 4. *Am. J. Clin. Nutr.* **89,** 668–672 (2009).

171. Polyak, D. E. *U.S. Geological Survey 2013 Minerals Yearbook Iodine*. (2015).

172. Gottardi, W. in *Iodine Chemistry and Applications* (ed. Kaiho, T.) 375–410 (Wiley, 2015).

173. Rokita, S. E. in *Iodine Chemistry and Applications* (ed. Kaiho, T.) 411–420 (Wiley, 2015).

174. Lauterbach, A. in *Iodine Chemistry and Applications* (ed. Kaiho, T.) 213–220 (Wiley, 2015).

175. Kaneko, N. & Kaiho, T. in *Iodine Chemistry and Applications* (ed. Kaiho, T.) 231–241 (Wiley, 2015).

176. Krukowski, S. T. in *Iodine Chemistry and Applications* 221–230 (Wiley, 2015).

177. Kaiho, T. in *Iodine Chemistry and Applications* (ed. Kaiho, T.) 243–247 (Wiley, 2015).

178. Eccheveria, A. World Iodine Association. *Expert Commentary: Iodine Recycling* (2015). Available at: http://www.worldiodineassociation.com/production/. (Accessed: 8th March 2017)

179. Polyak, D. E. *U.S. Geological Survey, Mineral Commodity Summaries Iodine*. (2015).

180. Desantis, N. & Incandela, S. US6827856 B2 Process for the recovery of copper from aqueous solutions containing iodinated organic compounds. 60006718 (2004).

181. Ezawa, H. & Otani, Y. JP2008013379(A) Method for recovering iodine from waste fluid in polarizing film production (in Japanese). (2008).

182. Shoji, S., Hihijira, H. & Kanbe, S. US Patent 7736617 Method of recovering iodine. 2010 (2010).

183. U.S. Deoartment of the Interior & U.S. Geological Survey. *MINERAL COMMODITY SUMMARIES 2016*. (2016).

184. Kadro, J. M. *et al.* Proof-of-concept for facile perovskite solar cell recycling. *Energy Environ. Sci.* **9,** 3172–3179 (2016).

185. Palik, E. D. *Handbook of optical constants of solids Volume 3*. (1998).

186. Yang, Y. *et al.* An all-carbon counter electrode for highly efficient hole-conductor-free organo-metal perovskite solar cells. *RSC Adv.* **4,** 52825–52830 (2014).

187. Mei, A. *et al.* A hole-conductor–free, fully printable mesoscopic perovskite solar cell with high stability. *Science (80-.).* **345,** 295–298 (2014).

188. Snaith, H. J. *et al.* Efficiency enhancements in solid-state hybrid solar cells via reduced charge recombination and increased light capture. *Nano Lett.* **7,** 3372–6 (2007).

189. United States Environmental Protection Agency. Method 1311 Toxicity Characteristic Leachin Procedure. 1–35

190. Ministry of Environment Japan. Notice 13/JIS K 0102:2013 method (JLT-13).

191. Directive 2012/19/EU of the European Parliament and of the Council of 4 July 2012 on waste electrical and electronic equipment (WEEE). *Off. J. Eur. Union* **L197/38,** (2012).

192. COUNCIL DECISION of 19 December 2002 establishing criteria and proceures for the acceptance of waste at landfills pursuant to Article 16 of and Annex II to Directive 1999/31/EC. *Off. J. Eur. Union* (2003).

193. Zeng, X., Gong, R., Chen, W. & Li, J. Uncovering the Recycling Potential of " New " WEEE in China. *Environ. Sci. Technol.* **50,** 1347–1358 (2016).

194. Foley&Lardner LLP (translation). Management Methods for the Restriction of the Use of Hazardous Substances in Electrical and Electronic Products Order No. 32Ministry of Industry and Information Technology National Development and Reform Commission Ministry of Science and Technology Minis. (2016).

195. Anctil, A. & Fthenakis, V. Critical metals in strategic photovoltaic technologies : abundance versus

recyclability. *Prog. Photovoltaics* **21,** 1253–1259 (2013).

196. Goe, M. & Gaustad, G. Strengthening the case for recycling photovoltaics : An energy payback analysis. *Appl. Energy* **120,** 41–48 (2014).

197. The European Commission. *COMMUNICATION FROM THE COMMISSION TO THE EUROPEAN PARLIAMENT, THE COUNCIL, THE EUROPEAN ECONOMIC AND SOCIAL COMMITTEE AND THE COMMITTEE OF THE REGIONS-Closing the loop - An EU action plan for the Circular Economy*. (2015).

198. The European Commission. *REPORT FROM THE COMMISSION TO THE EUROPEAN PARLIAMENT, THE COUNCIL, THE EUROPEAN ECONOMIC AND SOCIAL COMMITTEE AND THE COMMITTEE OF THE REGIONS on the implementation of the Circular Economy Action Plan*. (2017).

199. Zhang, L. & Ciftja, A. Recycling of solar cell silicon scraps through filtration , Part I : Experimental investigation. **92,** 1450–1461 (2008).

200. Klugmann-radziemska, E., Ostrowski, P., Drabczyk, K., Panek, P. & Szkodo, M. Experimental validation of crystalline silicon solar cells recycling by thermal and chemical methods. *Sol. Energy Mater. Sol. Cells* **94,** 2275–2282 (2010).

201. Müller, A., Wambach, K. & Alsema, E. Life Cycle Analysis of Solar Module Recycling Process. in *20th European Photovoltaic Solar Energy Conference, 6 –10 June 2005, Barcelona, Spain* (2005). doi:10.1557/PROC-0895-G03-07

202. PV Cycle. PV cycle: Breakthrough in PV module recycling. (2016). Available at: http://www.pvcycle.de/press/breakthrough-in-pv-module-recycling-2/. (Accessed: 16th March 2017)

203. Krueger, L. Overview of First Solar ' s Module Collection and Recycling Program.

204. Wade, A. First Solar ' s Long-Standing Leadership and Commitment to Recycling. (2013).

205. Zhou, Y. *et al.* Recyclable organic solar cells on cellulose nanocrystal substrates. *Scientifi* **3:1536,** 24–26 (2013).

206. Bhandari, K. P., Collier, J. M., Ellingson, R. J. & Apul, D. S. Energy payback time (EPBT) and energy return on energy invested (EROI) of solar photovoltaic systems : A systematic review and meta-analysis. *Renew. Sustain. Energy Rev.* **47,** 133–141 (2015).

207. Celik, I., Song, Z., Cimaroli, A. J., Yan, Y. & Heben, M. J. Life Cycle Assessment (LCA) of perovskite PV cells projected from lab to fab. *Sol. Energy Mater. Sol. Cells* **156,** 157–169 (2016).

208. Lunardi, M. M., Ho-baillie, A. W. Y., Moore, S., Corkish, R. & Alvarez-gaitan, J. P. A life cycle assessment of perovskite / silicon tandem solar cells. *Prog. Photovoltaics Res. Appl.* (2017). doi:10.1002/pip.2877

209. Kim, B. J. *et al.* Selective dissolution as a step towards recycling solar cells. *Nat. Commun.* **7,** 1–9 (2016).

210. Saperatec. Available at: http://www.saperatec.de/saperatec/#saperatec_saperatec. (Accessed: 20th March 2017)

211. Maier, W. F., Stöwe, K. & Sieg, S. Combinatorial and High-Throughput Materials Science. *Angew.*

Chemie Int. Ed. **46,** 6016–6067 (2007).

212. Green, M. L. *et al.* Applications of high throughput (combinatorial) methodologies to electronic , magnetic , optical , and energy-related materials. *J. Appl. Phys.* **231101,** (2013).

213. Strasser, P. *et al.* High Throughput Experimental and Theoretical Predictive Screening of Materials - A Comparative Study of Search Strategies for New Fuel Cell Anode Catalysts. *J. Mater. Chem. B* 11013–11021 (2003). doi:10.1021/jp030508z

214. Meyer, R., Sliozberg, K., Khare, C. & Schuhmann, W. High-Throughput Screening of Thin-Film Semiconductor Material Libraries II : Characterization of Fe-W -O Libraries. *ChemSusChem* **8,** 1279–1285 (2015).

215. Koinuma, H. & Takeuchi, I. Combinatorial solid-state chemistry of inorganic materials. *Nat. Mater.* **3,** 429–438 (2004).

216. Takeuchi, I., Lauterbach, J. & Fasolka, M. J. Combinatorial materials synthesis. *Mater. Today* **8,** 18–26 (2005).

217. Potyrailo, R. *et al.* Combinatorial and High-Throughput Screening of Materials Libraries : Review of State of the Art. *ACS COm* **13,** 579–633 (2011).

218. Jandeleit, B., Schaefer, D. J., Powers, T. S., Turner, H. W. & Weinberg, W. H. Combinatorial Materials Science and Catalysis. *Angew. Chemie Int. Ed.* **38,** 2494–2532 (1999).

219. Genzer, J. *Soft Matter Gradient Surfaces: Methods and Applications*. (WIley&Sons, 2012).

220. Fleischauer, M. D., Topple, J. M. & Dahn, J. R. Combinatorial Investigations of Si-M (M=Cr+Ni, Fe, Mn)Thin Film Negative Electrode Materials. *Electrochem. Solid-State Lett.* **8,** 137–140 (2005).

221. Minami, H. *et al.* Rapid synthesis and characterization of (Ca1- x Bax)3 Co4O9 thin films using combinatorial methods. *Appl. Surf. Sci.* **198,** 442–447 (2002).

222. Otani, M. *et al.* A high-throughput thermoelectric power-factor screening tool for rapid construction of thermoelectric property diagrams A high-throughput thermoelectric power-factor screening tool for rapid construction of thermoelectric property diagrams. *Appl. Phys. Lett.* **91,** (2007).

223. Majhi, K. *et al.* Co 3 O 4 Based All-Oxide PV : A Numerical Simulation Analyzed Combinatorial Material Science Study. (2016). doi:10.1021/acs.jpcc.6b01164

224. Woodhouse, M. CRITICAL REVIEW View Article Online www.rsc.org/csr | Chemical Society Reviews Combinatorial approaches for the identification and optimization of oxide semiconductors for efficient solar photoelectrolysis. *Chem Soc Rev* **38,** (2009).

225. Reddington, E. *et al.* Combinatorial Electrochemistry : A Highly Parallel , Optical Screening Method for Discovery of Better Electrocatalysts. *Science* **280,** 1–4 (1998).

226. Gebhardt, T., Music, D., Takahashi, T. & Schneider, J. M. Combinatorial thin film materials science : From alloy discovery and optimization to alloy design. *Thin Solid Films* **520,** 5491–5499 (2012).

227. Kennedy, K., Stefansky, T., Davy, G., Zackay, V. F. & Parker, E. R. Rapid Method for Determining Ternary-Alloy Phase Diagrams. *J. Appl. Phys.* **36,** 3808 (1965).

228. Anderson, A. Y. *et al.* Quantum efficiency and bandgap analysis for combinatorial photovoltaics: Sorting activity of Cu-O compounds in all-oxide device libraries. *ACS Comb. Sci.* **16,** 53–65 (2014).

229. nature publishing group. Reporting Checklist for Solar Cell Manuscripts. (2015).

230. Era, M., Taira, T. & Tsutsui, T. Preparation of Layered Perovskite Self-Organized Quantum Well by Dual Source Vapor Deposition. *Jpn. J. Appl. Phys.* **598,** 598–602 (1996).

231. Brinker, C. J. *et al.* Fundamentals of sol-ge dip coating. *Thin Solid Films* **201,** 97–108 (1991).

232. Das, S. *et al.* High-Performance Flexible Perovskite Solar Cells by Using a Combination of Ultrasonic Spray-Coating and Low Thermal Budget Photonic Curing. *ACS Photonics* **2,** 680–686 (2015).

233. Zabihi, F. & Eslamian, M. Fundamental Study on the Fabrication of Inverted Planar Perovskite Solar Cells Using Two-Step Sequential Substrate Vibration- Assisted Spray Coating (2S-SVASC). *Nanoscale Res. Lett.* (2016). doi:10.1186/s11671-016-1259-2

234. Prochowicz, D. & Zakeeruddin, S. M. Mechanosynthesis of the hybrid perovskite CH3NH3PbI3: characterization and the corresponding solar cell efficien. *J. Mater. Chem. A* **3,** 20772–20777 (2015).

235. Zhu, Z. *et al.* Solvent-Free Mechanosynthesis of Composition-Tunable Cesium Lead Halide Perovskite Quantum Dots. *J. Phys. Chem. Lett.* **8,** 1610–1614 (2017).

236. Thomson, W. Improvement in recording instruments for the electric telegraph. (1870).

237. Bag, M., Jiang, Z., Renna, L. A., Jeong, S. P. & Rotello, V. M. Rapid combinatorial screening of inkjet-printed alkyl-ammonium cations in perovskite solar cells. *Mater. Lett.* **164,** 472–475 (2016).

238. Nh, C. H. *et al.* Inkjet-Printed Photodetector Arrays Based on Hybrid Perovskite. (2017). doi:10.1021/acsami.7b01379

239. Li, S., Jiang, K., Su, M., Cui, X. & Huang, J. Inkjet printing of CH3NH3PbI3 on a mesoscopic TiO2 film for highly efficient perovskite solar cells. *J. Mater.* **3,** 9092–9097 (2015).

240. Mulla, M. A., Yow, H. N., Zhang, H., Cayre, O. J. & Biggs, S. in *Fundamentals of Inkjet Printing- The science of Inkjet and Droplets* (ed. Hoath, S. D.) 141–168 (Wiley, 2016).

241. Noel, N. K. *et al.* A low viscosity, low boiling point, clean solvent system for the rapid crystallisation of highly specular perovskite films. *Energy Environ. Sci.* **10,** 145–152 (2017).

242. Talbot, E., Bain, C., de Dier, R., Sempels, W. & Vermant, J. in *Fundamentals of Inkjet Printing- The science of Inkjet and Droplets* (ed. Hoath, S. D.) 263–268 (Wiley, 2016).